

UC Berkeley

UC Berkeley Electronic Theses and Dissertations

Title

Mechanisms of Mitotic Spindle Disassembly and Positioning in *Saccharomyces cerevisiae*

Permalink

<https://escholarship.org/uc/item/923199gx>

Author

Woodruff, Jeffrey Blake

Publication Date

2011

Peer reviewed|Thesis/dissertation

**Mechanisms of Mitotic Spindle Disassembly and Positioning in
*Saccharomyces cerevisiae***

by

Jeffrey Blake Woodruff

A dissertation submitted in partial satisfaction of the requirements for the degree of
Doctor of Philosophy
in
Molecular and Cell Biology
in the
Graduate Division
of the
University of California, Berkeley

Committee in charge:
Professor Georjana Barnes, Chair
Professor Rebecca Heald
Professor Abby Dernburg
Professor Arash Komeili

Spring 2011

Mechanisms of Mitotic Spindle Disassembly and Positioning in

Saccharomyces cerevisiae

Copyright (2011)

All rights reserved

by

Jeffrey Blake Woodruff

ABSTRACT

Mechanisms of Mitotic Spindle Disassembly and Positioning in *Saccharomyces cerevisiae*

by

Jeffrey Blake Woodruff

Doctor of Philosophy in Molecular and Cell Biology

University of California, Berkeley

Professor Georjana Barnes, Chair

When a cell divides, it must accurately replicate its genetic material and then faithfully segregate this material into the resulting daughter cells. My research addresses the latter half of this problem, focusing on how the cell regulates the function of the mitotic spindle, an elegant microtubule-based machine that attaches to replicated DNA and pulls it apart during mitosis. Here, I present two studies that investigate how the cell disassembles the mitotic spindle at the end of mitosis and how the cell positions the mitotic spindle prior to mitotic completion.

I combined genetic analysis with live-cell fluorescence microscopy to identify the subprocesses driving spindle disassembly as well as the proteins that perform these subprocesses. Our results suggest that mechanistically distinct pathways largely governed by the anaphase-promoting complex, Aurora B kinase, and kinesin-8 cooperate to drive spindle disassembly in budding yeast. We also describe the roles of novel disassembly factors such as the spindle protein She1 and the 7-protein Alternative Replication Factor C complex. Together, these pathways disengage the mitotic spindle halves, inhibit spindle microtubule growth, and promote sustained spindle microtubule depolymerization. Strikingly, combined inhibition of pairs of disassembly pathways yielded cells with hyper-stable spindle remnants, which caused dramatic defects in cell cycle progression, thus establishing that regulated and rapid spindle disassembly is crucial for cell proliferation.

To better understand the mechanisms of spindle positioning, I examined how the dynein-driven spindle-positioning pathway in budding yeast is silenced. My work suggests that dynein activity is regulated through interaction with the multi-subunit dynactin complex at anaphase and identifies a new cellular factor, She1, which controls this interaction. Dynactin is a well-known dynein activator, and, in budding yeast, the complete complex is required for dynein-dependent spindle movement. I found that localization of the dynactin complex is cell cycle-regulated, such that dynactin is recruited to astral microtubules, via interaction with dynein, primarily during anaphase. Additionally, we discovered that the protein She1 is a cell cycle-regulated inhibitor of dynein activity. Without She1, dynein activity extends beyond anaphase and, as a result, mis-positions the mitotic spindle. Strikingly, loss of She1 also permits recruitment of the dynactin complex to astral microtubules throughout the cell cycle. These results suggest that in wild-type cells, She1 restricts dynein activity to anaphase by preventing the interaction between dynein and the complete dynactin complex.

TABLE OF CONTENTS

| | |
|--|-----|
| List of figures | ii |
| List of tables | iii |
| Abbreviations | iv |
| Acknowledgements | v |
| | |
| CHAPTER 1: General Introduction | 1 |
| Overview | 2 |
| | |
| CHAPTER 2: Mitotic spindle disassembly occurs via distinct subprocesses driven by the Anaphase-Promoting Complex, Aurora B kinase, and kinesin-8 | 5 |
| Introduction | 6 |
| Results | 8 |
| Discussion | 30 |
| Summary | 35 |
| Materials and Methods | 36 |
| | |
| CHAPTER 3: Dynein-driven mitotic spindle positioning is restricted to anaphase by She1 inhibition of dynactin recruitment | 40 |
| Introduction | 41 |
| Results | 42 |
| Discussion | 60 |
| Summary | 63 |
| Materials and Methods | 64 |
| | |
| CHAPTER 4: Additional analysis of She1 | 68 |
| Introduction | 69 |
| Results | 70 |
| Discussion | 75 |
| Materials and Methods | 76 |
| | |
| CHAPTER 5: Conclusions and future directions | 79 |
| | |
| References | 83 |

LIST OF FIGURES

| | |
|---|----|
| Figure 2.1. Spindle morphology in cells compromised for Kip3 and APC ^{Cdh1} activity | 9 |
| Figure 2.2. The combined activities of APC ^{Cdh1} and Kip3 are required to depolymerize interpolar MTs completely | 11 |
| Figure 2.3. Cytokinetic ring contraction breaks the mitotic spindle when normal disassembly mechanisms are impaired | 14 |
| Figure 2.4. Synthetic lethal screens identify additional genes important for spindle disassembly | 16 |
| Figure 2.5. Pair-wise comparison of published synthetic genetic interactions shared between <i>CDH1</i> , <i>KIP3</i> , and <i>SHE1</i> | 17 |
| Figure 2.6. Dynamics of interpolar MT depolymerization in spindle disassembly mutants | 19 |
| Figure 2.7. The MEN and the A-RFC complex regulate Ipl1-mediated removal of Bim1 from the spindle midzone | 22 |
| Figure 2.8. Ipl1 and Mcm21 mediate spindle disassembly by regulating She1 activity | 24 |
| Figure 2.9. Analysis of She1 | 26 |
| Figure 2.10. Kip3 and Ipl1 operate in separate pathways during spindle disassembly | 29 |
| Figure 2.11. Multiple pathways regulating distinct subprocesses drive spindle disassembly | 31 |
| Figure 2.12. Ipl1-3GFP localization during late anaphase in <i>dbf2Δ</i> cells | 32 |
| Figure 3.1. She1p is a microtubule and bud-neck-associated protein required to inhibit dynein activity prior to anaphase | 43 |
| Figure 3.2. She1p is required to repress dynein activity at the end of anaphase | 46 |
| Figure 3.3. Ectopic dynein activity in <i>she1Δ</i> cells can cause unequal distribution of spindle poles at the end of mitosis | 47 |
| Figure 3.4. Loss of She1 has a modest impact on dynein localization | 50 |
| Figure 3.5. She1p affects the cell cycle-dependent localization of the dynactin components Nip100 (p150 ^{glued}) and Arp1 | 51 |
| Figure 3.6. Expression levels of tagged dynactin subunits | 54 |
| Figure 3.7. She1p affects the cell cycle-dependent recruitment of Jnm1p (dynamitin) and Ldb18p (p24) to astral MTs | 56 |
| Figure 3.8. Dynactin exists in complete and incomplete complexes that are spatially distinct | 58 |
| Figure 4.1. She1 is necessary for proper kinetochore alignment in metaphase | 72 |
| Figure 4.2. Analysis of She1 interacting partners by mass spectrometry | 73 |
| Figure 4.3. GST-She1 binds MTs and modulates their dynamics in vitro | 74 |

LIST OF TABLES

| | |
|---|----|
| Table 2.1. Depolymerization kinetics of spindle halves after onset of spindle disassembly | 13 |
| Table 2.2. Yeast Strains used in this study | 38 |
| Table 3.1. aMT dynamics and lengths in wild-type and <i>she1Δ</i> cells | 48 |
| Table 3.2. Yeast strains and plasmids used in this study | 66 |
| Table 4.1. Yeast strains and plasmids used in this study | 78 |

ABBREVIATIONS

MT: microtubule

aMT: astral microtubule

SPB: spindle pole body

Chr III: chromosome III

td-tomato: tandem dimer tomato

ipMT: inter polar microtubule

MEN: mitotic exit network

APC: Anaphase-Promoting Complex

TAP: tandem-affinity-purification

ACKNOWLEDGEMENTS

Over the past years, I've encountered so many people who have helped me in both my scientific career and my personal life. This body of work could not have developed without their generosity and patience. First, I would like to thank my graduate advisors Georjana and David for giving me the opportunity to work in such an interesting field. Moreover, I would like to thank them for teaching me how to ask interesting scientific questions and for teaching me how to present my work in the clearest and most compelling manner possible.

I must also give many thanks to my parents Tom and Brenda for their tireless efforts in raising me and teaching me the value of persistence in the face of adversity and encouraging me to be the best I can possibly be.

Many thanks go out to my fellow lab members throughout the years who helped me develop my ideas and assisted me with my experiments. Special thanks go to Yidi for teaching me how to generate publication quality data and write a paper, and to Voytek for honing my microscopy skills.

Additional advisors have been instrumental in my thesis, providing me with resources and helpful advice, including Rebecca Heald, Abby Dernburg, Doug Koshland, Stefan Westermann, Liam Holt, and Arash Komeili. My scientific mentors of the past, Gail and Marty, both took a chance on me and gave me a job in their labs even though I was a naïve undergraduate with little research experience. And, finally, I must thank Dr. Alan Cline for instilling in me the importance of attitude, the value of seeing myself for who I am, and the fact that good people need the help of others to become great.

CHAPTER 1: General Introduction

OVERVIEW

Successful cell proliferation demands equal apportionment of genetic material during each round of cell division from the mother cell to the two daughter cells. Eukaryotes have evolved an elegant microtubule-based machine, termed the mitotic spindle, to perform this task. Although the size and complexity of mitotic spindles differ between species, several key features are conserved. In all cases, mitotic spindles are organized into bipolar arrays comprising two spindle poles from which emanate three types of microtubules (MTs). Kinetochore microtubules (kMTs) connect the spindle poles to chromosomes via kinetochores, which are proteinaceous complexes that assemble on centromeric regions of the chromosome. Interpolar microtubules (ipMTs) extending from opposite poles overlap and are linked together to connect the two spindle poles and provide rigidity to the overall spindle structure. Lastly, astral microtubules (aMTs) extend toward the cell cortex, allowing the spindle to determine its position relative to the cell boundary (Glotzer, 2009). All three MTs classes share the same polarity: the slow-growing minus ends are anchored at the spindle poles, while highly-dynamic plus ends extend outward (McIntosh and Euteneuer, 1984). In addition, numerous motor and non-motor proteins associate with these spindle MTs to regulate spindle function.

The spindle as a dynamic structure

The mitotic spindle is an incredibly dynamic structure, being assembled *de novo*, elongated, and summarily disassembled during each round of cell division. Of these three processes, regulation of spindle assembly has received the greatest attention and is described classically by two models (for a comprehensive review, see Walczak and Heald, 2008). In the first model, termed “search and capture”, centrosome-nucleated MTs extend and retract until they are captured and stabilized by kinetochores. The second model, termed “self assembly”, posits that chromosomes themselves can nucleate MTs and organize them into bipolar arrays. These two mechanisms are by no means mutually exclusive, as chromosome-nucleated MTs have been shown to connect with centrosome-nucleated MTs to enhance the efficiency of kinetochore capture in budding yeast (Kitamura et al., 2010). Additionally, recent data suggest that there exists another spindle assembly pathway driven by gamma-TuRC complexes residing on spindle MTs (Janson et al., 2005; Uehara et al., 2009). But, this pathway seems to be species-specific has not yet been identified in budding yeast.

After the spindle is assembled and all sister chromatid pairs are aligned and properly attached by kMTs in a bipolar manner, the chromatids are pulled apart in an active process driven by depolymerization of kMTs, poleward-directed motor proteins, and in some organisms, kMT flux. Then, the coordinated activities of MT-growth factors that lengthen ipMTs and motor proteins that cross-link and push apart anti-parallel ipMTs elongate the spindle, thus separating the chromosomes even further (for a review, see Goshima and Scholey, 2010).

Compared with spindle assembly, chromosome segregation, and spindle elongation, very little is known about the process of spindle disassembly. This is surprising, considering that disassembly is a conserved feature of all mitotic spindles and is necessary for cell cycle progression into G1 and subsequent establishment of the

interphase MT array (Cao et al., 2003; Woodruff et al., 2010). Thus, study of spindle disassembly is essential for understanding spindle function and mitosis. In addition, given the elaborate structure of the spindle, and the fact that the spindle never reforms after disassembly (Maddox and Salmon, 2000; Woodruff et al., 2010), analyzing spindle disassembly will further our understanding of how cells break down complex organelles and make irreversible changes.

Current outlook on spindle disassembly

Spindle disassembly occurs late in the cell cycle and is a defining feature for the completion of mitosis. In all eukaryotes, dephosphorylation of cyclin-dependent kinase substrates and destruction of anaphase-promoting complex substrates govern progression through late mitosis, and thus are necessary to initiate spindle disassembly (for a review, see Sullivan and Morgan, 2007). In budding yeast, a cortical surveillance system, termed the Mitotic Exit Network, activates these two mechanisms (Visintin and Amon, 2001).

Downstream of the Mitotic Exit Network, a comprehensive model to explain the process of spindle disassembly had yet to be presented prior to this work. Insufficient insight into this process is likely a result of the limited methodology used to identify the subprocesses and molecular players involved. The majority of spindle disassembly studies were driven by the assumption that if a gene important for spindle disassembly were disabled, the spindle would persist longer after anaphase B onset, allowing the spindle to grow longer than the cell and adopt a distinctive “hook” shape at the end of anaphase. In this manner, the anaphase-promoting complex, the Aurora B kinase, the kinesin-8 motor Kip3, and the kinetochore protein Mcm21 were implicated in spindle disassembly (Juang et al., 1997; Woodbury and Morgan, 2007; Buvelot, 2003; Vizeacoumar 2010). Although these studies identified some key players, they did not deeply explore the mechanisms of these players and their overall contributions to spindle disassembly.

A landmark study of spindle dynamics by Maddox and Salmon (2000) illustrated the power of live-cell microscopy to dissect the mechanisms driving spindle disassembly. Using yeast expressing GFP-tubulin as a spindle marker, the authors monitored spindle MT dynamics after disassembly onset, and, importantly, created reference marks on the ipMTs through photobleaching. Two significant observations were made: 1) spindle halves separate early during disassembly, 2) ipMTs shorten through depolymerization of plus ends, not through flux or severing. These results suggested that spindle disassembly is an approximate reversal of the assembly process. How these activities are coordinated, both relative to each other and the cell cycle, as well as which cellular factors perform these activities remained to be determined. Chapter 2 describes an investigation of spindle disassembly that combines genetic screens with live-cell microscopy to identify spindle disassembly factors and describe their roles during this process.

Spindle positioning and chromosome segregation

During mitosis in all eukaryotic cells, the spindle is positioned in a specific location and orientation. This can either be in the exact center, to ensure equal cell division, or asymmetrically, to ensure that daughter cells differ in size and/or inheritance

of cytosolic factors that can affect cell fate, as is the case during embryogenesis. Several mechanisms have been proposed to account for spindle movements, but none are universally employed across all taxa. Rather, the utilization of a particular mechanism seems to be related to the size of the cell. For example, in *S. pombe* which are relatively small (10 μm in length), aMTs push against the cortex to center the spindle (Tran et al., 2001). In the larger *C. elegans* single cell embryo (45 μm in length), the spindle is centered by cortical motors that pull on aMTs (Grill et al., 2003). Yet, in the *X. laevis* egg, which is considerably larger (1,200 μm in diameter), both of these mechanisms are physically improbable, so it has been proposed that aMTs are pulled by a network of minus-end-directed motors associated with cytoplasmic components, such as organelles or actin filaments (Reinsch and and Gonczy, 1998; Wuhr, et al., 2009).

Spindle positioning in budding yeast

Spindle positioning is best understood in budding yeast, *S. cerevisiae*, which employs cortical motors to pull on aMTs, similar to the mechanism used in *C. elegans*. Two partially overlapping pathways operate at different cell cycle stages to place the spindle near the bud neck and parallel to the long axis of the cell. Prior to anaphase, aMTs emanating from the spindle poles, themselves connected via ipMTs and bilaterally attached chromosomes, are pulled toward the bud by binding a type V Myosin (Kar9) that walks along polarized actin filaments (Hwang et al., 2003; Kusch et al., 2003; Lee et al., 2003). Then, during anaphase, aMTs are pulled along the cortex by minus-end-directed dynein motors (Adames et al., 2000; Lee et al., 2003; Carvalho et al., 2004). In both pathways, directional movement of the spindle is ensured by polarized activation of dynein and Kar9 via polarity cues localized at the bud cortex and the bud neck (Grava et al., 2006). While much has been uncovered about the activation of these pathways, comparatively little has been revealed concerning how these pathways are turned off after the spindle has been properly positioned. Although overlooked, the process of pathway inactivation is nevertheless important. For example, if dynein is not silenced at the end of anaphase in budding yeast, the spindle poles are pulled too far around the cortex. Often, the spindle pole that should reside in the bud travels into the mother cell, creating one cell with two spindle poles and one cell with no spindle pole (Woodruff et. al, 2009). Aneuploidy results in this case, since chromosomes are closely associated with spindle poles during anaphase in budding yeast (Jin et al., 2000). Thus, inactivation of spindle positioning pathways is essential for faithful chromosome segregation. Chapter 3 describes an investigation of dynein-mediated spindle positioning in budding yeast, specifically addressing the question of how dynein is inactivated at specific times during the cell cycle.

CHAPTER 2:
**Mitotic spindle disassembly occurs via distinct
subprocesses driven by the Anaphase-Promoting Complex,
Aurora B kinase, and kinesin-8**

INTRODUCTION

The mitotic spindle comprises three sets of microtubules (MTs) that emanate from microtubule-organizing centers: astral MTs, which radiate toward the cell cortex; kinetochore MTs, which attach to chromosomes; and, interpolar MTs (ipMTs), which interdigitate to form the central spindle bridge (for review see Glotzer, 2009). The size and integrity of the mitotic spindle are maintained by a vast array of MT-binding proteins that regulate MT dynamics (e.g. XMAP215, CLASP, EB1) or cross-link the anti-parallel ipMTs (e.g., Prc1, BimC motors) (Walczak and Heald, 2008). During each cell cycle, the mitotic spindle is efficiently assembled to achieve DNA segregation and then disassembled.

Live-cell fluorescence microscopy of budding yeast expressing the spindle marker GFP-Tub1 showed that spindle disassembly is characterized by depolymerization of the ipMTs from their plus ends and separation of the spindle halves. Once the spindle halves have separated, the ipMTs are no longer detectable after ~2 min (Maddox et al., 2000). Thus, disassembly of the mitotic spindle is irreversible and swift. Moreover, these events are precisely coordinated during the cell cycle and occur only after chromosomes have cleared the plane of division but before cytokinesis (VerPlank and Li, 2005). This precise timing is governed in part by the Mitotic Exit Network (MEN) which ultimately stimulates activity of Cdc14, a phosphatase that opposes Cdk1. Dephosphorylation of Cdk1 targets is critical for mitotic exit, but the connection between this process and spindle disassembly is poorly understood (for review, see Sullivan and Morgan, 2007). Therefore, identifying the downstream targets of the MEN and their contributions to spindle midzone dissolution and spindle MT depolymerization are crucial for understanding spindle disassembly.

Other than MEN components, few proteins have been implicated in mediating spindle disassembly. One factor that has been implicated is the Anaphase-Promoting Complex (APC), an E3 ubiquitin ligase critical for mitotic progression (for review, see Peters, 2002). During mitotic exit, the APC, in association with the co-factor Cdh1 (APC^{Cdh1}), degrades an array of spindle-stabilizing proteins, including the BimC homolog Cin8 (Hildebrandt and Hoyt, 2001), the Prc1 homolog Ase1 (Juang et al., 1997), and Fin1 (Woodbury and Morgan, 2007). Other factors implicated in spindle disassembly include Kip3, a plus-end-targeted MT depolymerase of the kinesin-8 family, and the Ipl1 kinase, the Aurora B homolog in yeast (Buvelot et al., 2003). Since Kip3 actively depolymerizes MTs *in vitro* and also regulates astral MT length *in vivo*, it has been speculated that Kip3 may accelerate ipMT shrinkage to help disassemble the spindle (Varga et al., 2006; Gupta et al., 2006). Ipl1 phosphorylates the MT-stabilizing protein Bim1 (yeast EB1) and promotes its dissociation from MTs *in vitro*, suggesting a possible mechanism by which Ipl1 mediates spindle disassembly *in vivo* (Zimniak et al., 2009). Bim1 is most likely not the sole target of Ipl1 during mitotic exit, considering that Ipl1 phosphorylates many kinetochore, spindle, and chromatin-associated proteins (e.g., the Dam1 and Ndc80 complexes, Ase1, histone H3; Cheeseman et al., 2002; Kotwaliwale et al., 2007; Hsu et al., 2000). To more clearly define the role of Ipl1 during spindle disassembly, it is therefore crucial to test if Bim1 phosphorylation drives spindle disassembly *in vivo*, as well as to investigate the involvement of additional Ipl1 targets. Another unexplored issue is the relationship between Ipl1, Kip3 and the APC during

spindle disassembly. Whether these proteins operate together in a single pathway or independently in multiple pathways and how their activities are coordinated are unclear.

I conducted a large-scale analysis of spindle disassembly in budding yeast. In addition to establishing a genetic method for identifying novel proteins important for spindle disassembly, I performed real-time analysis of spindle disassembly and assessed the effects of mutations in nine proteins critical for this process. Using these methods, I described distinct phenotypes that distinguish these mutants and inferred the normal contributions of these proteins to spindle disassembly.

RESULTS

The Anaphase-Promoting Complex and Kip3 cooperate in mitotic spindle disassembly via distinct mechanisms

The enzymatic activities of the APC^{Cdh1} and Kip3 are dramatically different, suggesting that they play distinct roles in spindle disassembly. To test this idea, I followed mitotic spindle elongation and disassembly using time-lapse fluorescence microscopy in cells expressing the microtubule marker GFP-Tub1. I found that depletion of Cdh1 or Kip3 had different effects on spindle morphology. Late anaphase spindles in *cdh1Δ* or *kip3Δ* cells were hyper-extended relative to spindles in wild-type cells, indicative of a delay in spindle disassembly. However, spindles were consistently longer and more often fishhook-shaped in *cdh1Δ* mutants relative to *kip3Δ* mutants (70% vs. 15% fishhook spindles, max spindle length = $7.59 \pm 1.6 \mu\text{m}$ vs. $6.78 \pm 1.0 \mu\text{m}$ [mean \pm S.D.], respectively; $n = 20$) (Figure 2.1A).

To analyze spindle disassembly in greater depth, I followed ipMT depolymerization after the spindle halves separated in late anaphase. In wild-type cells, ipMTs quickly depolymerized (shrinkage rate, $R(\text{hs}) = 0.069 \pm 0.006 \mu\text{m} \cdot \text{s}^{-1}$; mean \pm S.E.M.) and rarely displayed recovery events ($F(\text{rec}) = 0.0050 \text{ s}^{-1}$) (Figure 2.2A; Table 2.1). In contrast, *cdh1Δ* cells displayed hyper-stable spindle halves that changed very little in length after separation ($R(\text{hs}) = 0.013 \pm 0.004 \mu\text{m} \cdot \text{s}^{-1}$; Figure 2.2B). Persistence time of these hyper-stable spindle halves fit a bimodal distribution: ~80% disassembled in under 15 min, whereas ~20% persisted longer than 55 min (Figure 2.2E; $n = 30$). Intriguingly, in every case, only one spindle half per cell remained hyper-stable. The other spindle half always depolymerized with only slightly slower kinetics relative to wild-type ($R(\text{hs}) = 0.051 \pm 0.007 \mu\text{m} \cdot \text{s}^{-1}$; $F(\text{rec}) = 0.0054 \text{ s}^{-1}$) (Figure 2.2B, Table 2.1; see diagram in Figure 2.1C). These data imply that APC^{Cdh1} enhances ipMT depolymerization, likely through removal and degradation of midzone-stabilizing proteins. In support of this hypothesis, the midzone proteins Ase1-4GFP and Cin8-4GFP continued to decorate the mitotic spindle even after spindle breakage in *cdh1Δ* cells, but not in wild-type cells (Figure 2.1B). In *cdh1Δ* cells, the spindle broke apart in a region outside of the midzone, leaving only one of the spindle halves decorated with midzone-localized Ase1-4GFP or Cin8-4GFP. Consistently, the decorated spindle halves were hyper-stable (unpublished data). These results strongly suggest that the hyper-stable half-spindle structures seen in *cdh1Δ* cells result from failure to remove stabilizing proteins like Ase1 and Cin8 from the spindle midzone and degrade them.

In contrast, spindle halves in *kip3Δ* cells alternated between shrinkage and growth, suggesting that Kip3 is necessary for sustained ipMT depolymerization during spindle disassembly (Figure 2.2C). Consistently, the frequency of spindle half recovery was two-fold higher in *kip3Δ* cells ($F(\text{rec}) = 0.0102 \text{ s}^{-1}$) relative to wild-type or *cdh1Δ* cells (Table 2.1). I never observed hyper-stable spindle halves in *kip3Δ* mutant cells ($n = 39$). These differences in spindle morphology and dynamics suggest that Kip3 and APC^{Cdh1} play different roles during spindle disassembly.

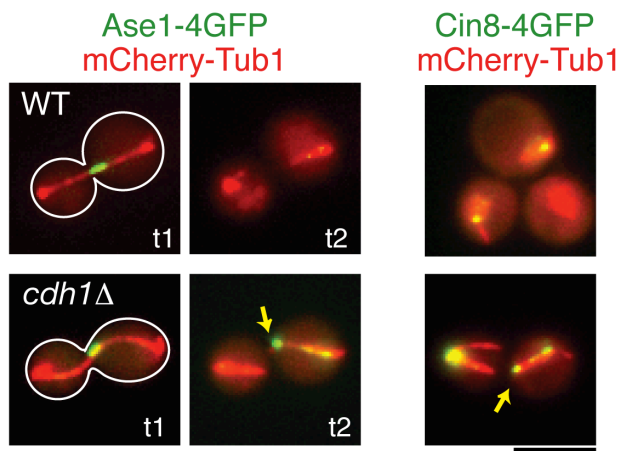
If APC^{Cdh1} and Kip3 operate via different mechanisms, I would expect combinatorial depletion of Cdh1 and Kip3 to produce synergistic defects in spindle

Figure 2.1

A

| | % fishhook spindles | Avg. max spindle length(μm) | sample number (n) |
|---|---------------------|--|-------------------|
| Wild-type | 5 | 6.00 ± 0.4 | 20 |
| <i>cdh1</i> Δ | 70 | 7.59 ± 1.6 | 20 |
| <i>kip3</i> Δ | 15 | 6.78 ± 1.0 | 20 |
| <i>cdh1</i> Δ <i>kip3</i> Δ | 95 | 9.00 ± 1.7 | 20 |

B



C

cdh1 Δ , *doc1* Δ , or *dbf2* Δ mutant

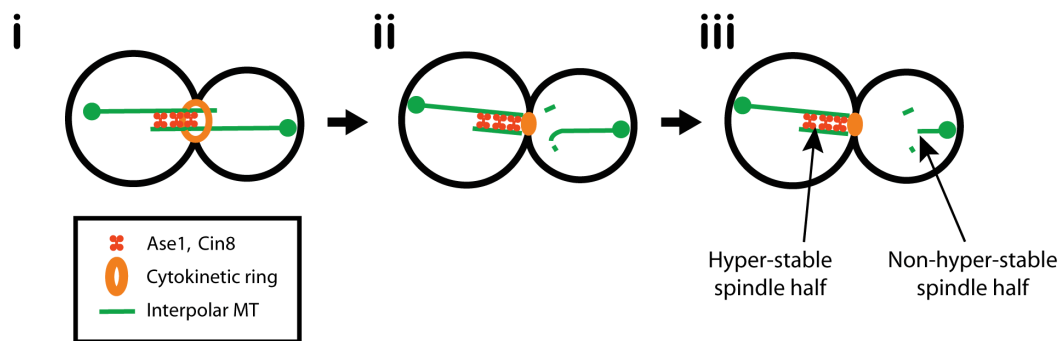


Figure 2.1. Spindle morphology in cells compromised for Kip3 and APC^{Cdh1} activity. (A) Cells expressing GFP-Tub1 were monitored during spindle disassembly by time-lapse fluorescence microscopy. For 20 events, the morphology and length of the spindle were measured just prior to disassembly. (B) Co-localization of Ase1-4GFP or Cin8-4GFP with mCherry-Tub1 in wild-type and *cdh1Δ* cells. Yellow arrows indicate Ase1-4GFP or Cin8-4GFP decoration at the end of a recently separated spindle half. This spindle half was hyper-stable (not shown). Scale bar, 5 μm. (C) Diagram of spindle disassembly in *cdh1Δ*, *doc1Δ*, and *dbf2Δ* cells. (Ci) The mitotic spindle does not disassemble prior to cytokinetic ring contraction. (Cii) Contraction of the actinomyosin ring breaks the spindle outside of the midzone. (Ciii) The spindle half decorated with Ase1, Cin8, and, presumably, other midzone proteins is hyper-stable and can persist for >100 min. The spindle half not decorated with midzone proteins depolymerizes more quickly.

Figure 2.2

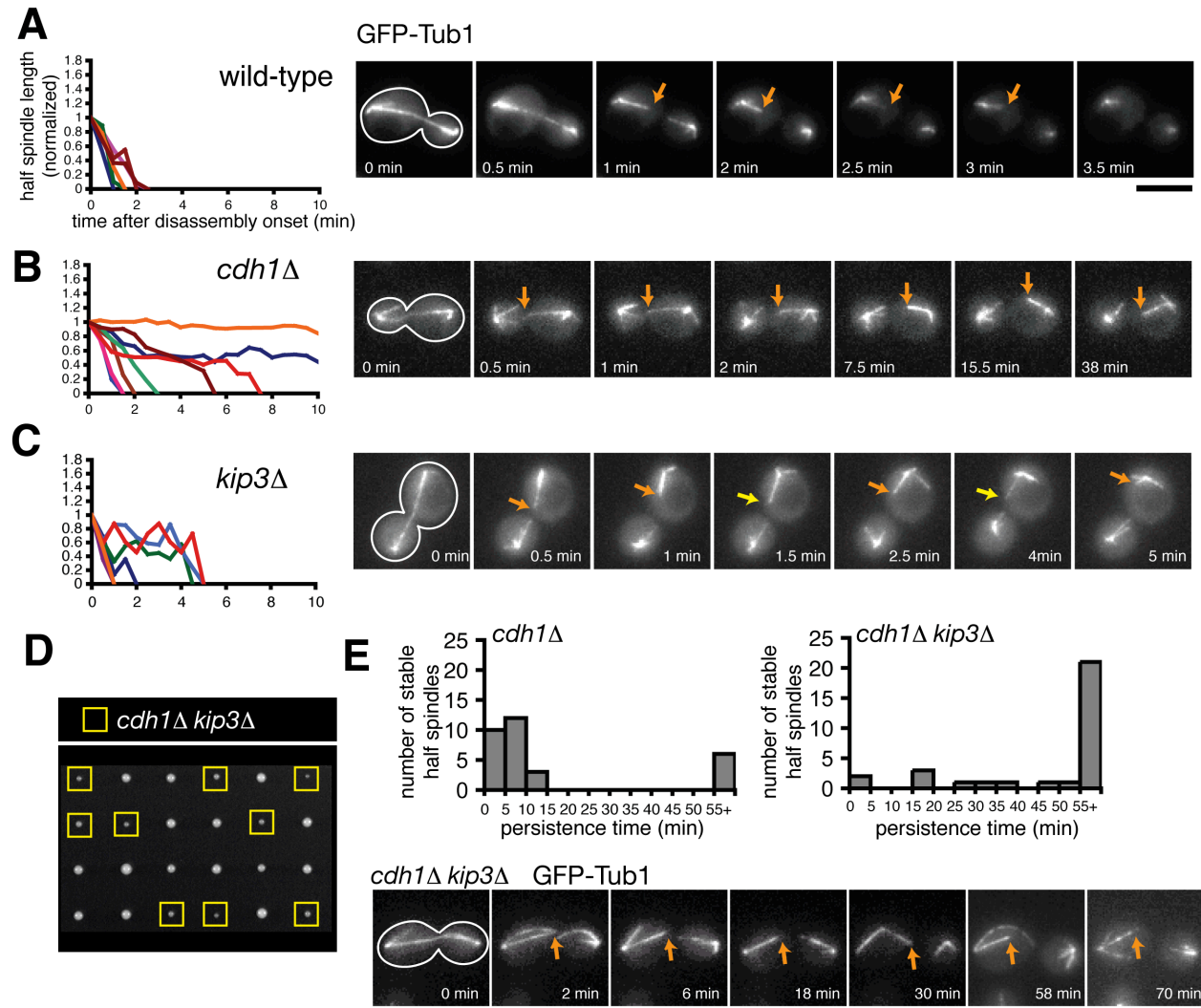


Figure 2.2. The combined activities of APC^{Cdh1} and Kip3 are required to depolymerize inter-polar MTs completely. (A-C) Time-lapse fluorescence images of wild-type, *cdh1Δ*, and *kip3Δ* cells expressing GFP-Tub1 during mitotic exit. Cell shape is outlined in white. Scale bars, 5 μ m. Orange arrows track shrinking spindle halves, whereas the yellow arrow indicates a growing spindle half. Graphs on the left represent the normalized lengths of depolymerizing spindle halves after the spindle had broken. Each line represents an individual spindle half that was selected at random. For the *cdh1Δ* mutant, the shrinkage of four non-hyperstable and four hyperstable spindle halves is charted. (D) Tetrad dissection of spores resulting from a cross between *kip3Δ* and *cdh1Δ* mutants. Offspring possessing both mutations are indicated with a yellow box. (E) Histograms representing the persistence times of hyper-stable spindle halves observed after spindle breakage in *cdh1Δ* and *cdh1Δ kip3Δ* mutants (n = 30 for both). Below the histograms is a series of fluorescence images depicting a *cdh1Δ kip3Δ* cell after spindle breakage where the hyper-stable half spindle persisted for at least 70 min.

disassembly and possibly cell proliferation. Indeed, tetrad analysis revealed a synthetic genetic interaction between *kip3Δ* and *cdh1Δ* null alleles (Figure 2.2D). Furthermore, spindles in *cdh1Δ kip3Δ* double mutants were longer (max spindle length = 9.00 ± 1.7 μm , $n = 20$) and more often fishhook-shaped (95%) than in either single mutant (Figure 2.1A). Addition of the *kip3Δ* mutation also prolonged the persistence time of the hyperstable half spindles seen in *cdh1Δ* cells. In *cdh1Δ kip3Δ* cells, only ~6% of stable spindles halves disassembled in under 15 min, whereas ~70% lasted longer than 55 min (Figure 2.2E). These results indicate that Kip3 is necessary to disassemble the persistent half-spindle structures left when APC^{Cdh1} activity is compromised.

I was surprised that spindles broke apart in *cdh1Δ kip3Δ* double mutants, since inactivation of the MEN, which is upstream of spindle disassembly, arrests cells in late anaphase with intact spindles (Visintin and Amon, 2001). Since the MEN initiates cytokinesis in addition to spindle disassembly (Luca et al., 2001), I considered the possibility that actinomyosin ring contraction might shear the mitotic spindle when spindle disassembly is inhibited. To test this hypothesis, I simultaneously visualized spindles and cytokinetic rings in cells expressing GFP-Tub1 and the actinomyosin ring marker Myo1-GFP. In $90 \pm 5\%$ (mean \pm S.D.; $n = 3$ experiments, 20 events per experiment) of wild-type cells, the mitotic spindle disassembled prior to cytokinetic ring contraction, indicating that cytokinesis is not required for spindle disassembly (Figure 2.3A; VerPlank and Li, 2005). However, in 100% of *cdh1Δ* cells and $82 \pm 10.4\%$ of *kip3Δ* cells ($n = 3$ experiments), the spindle disassembled only after the cytokinetic ring contracted (Figure 2.3A). In addition, I noticed that the initial location of spindle-half separation during spindle disassembly was widely distributed within wild-type cells, suggesting lack of a connection between cytokinetic ring contraction and spindle breakdown (Figure 2.3B). However, spindle breakage occurred exclusively at the bud neck in *kip3Δ* and *cdh1Δ* mutants. When *cdh1Δ* and *kip3Δ* cells were treated with 250 μM latrunculin A, a potent inhibitor of actinomyosin ring contraction (Asycough et al., 1997), spindle breakage was no longer restricted to the bud neck region, similar to wild-type cells (Figure 2.3B). These results show that in cells lacking Kip3 or APC^{Cdh1}, the spindle breaks as a result of cytokinetic ring contraction. Thus, it is likely that cytokinesis is not ordinarily required for spindle disassembly, but can break the spindle when disassembly is delayed. Even after the spindle breaks apart in this cytokinesis-dependent manner, Kip3 and APC^{Cdh1} activities are still required to fully disassemble the mitotic spindle halves.

Synthetic lethal screens identify novel spindle disassembly factors

Because *kip3Δ* and *cdh1Δ* null alleles showed a synthetic genetic interaction, I hypothesized that other mutants displaying synthetic genetic interactions with these alleles might also be defective in spindle disassembly. Therefore, I searched published synthetic interactions for *KIP3* and *CDH1* (Costanzo et al., 2010). Among the interesting genes identified was *SHE1*, which encodes a spindle and bud-neck-localized protein that I studied during an investigation of spindle positioning presented in the next chapter. Importantly, She1 had no previously known role in spindle disassembly (Wong et al., 2007; Woodruff et al., 2009). I found that spindles in cells lacking She1 frequently disassembled after cytokinetic ring contraction ($61.7 \pm 11.5\%$, $n = 3$ experiments; Figure 2.4E), similar to the phenotype seen in *kip3Δ* and *cdh1Δ* mutants. These results

Table 2.1

| | | | Recovery frequency F(rec) (s⁻¹) | Shrinkage rate R(hs) (μm • s⁻¹) | n | p-value |
|-----------------------|---------------|------------------|---|---|---------------|----------------|
| 23° C | wild-type | | 0.0050 | 0.069 ± 0.006 | 42 | N/A |
| | <i>cdh1Δ</i> | Non-hyper stable | 0.0054 | 0.051 ± 0.007 | 21 | 0.085 |
| | | Hyper-stable | 0.0046 | 0.013 ± 0.004 | 16 | < 0.001 |
| | <i>doc1Δ</i> | Non-hyper stable | 0.0064 | 0.044 ± 0.006 | 25 | 0.013 |
| | | Hyper-stable | 0.0016 | 0.004 ± 0.002 | 16 | < 0.001 |
| | <i>dbf2Δ</i> | Non-hyper stable | 0.0079 | 0.029 ± 0.004 | 19 | < 0.001 |
| | | Hyper-stable | 0.002 | 0.012 ± 0.002 | 16 | < 0.001 |
| | <i>kip3Δ</i> | | 0.0102 | 0.044 ± 0.004 | 39 | 0.002 |
| | <i>dcc1Δ</i> | | 0.0078 | 0.043 ± 0.004 | 40 | 0.003 |
| | <i>ctf8Δ</i> | | 0.0082 | 0.041 ± 0.005 | 39 | 0.008 |
| | <i>she1Δ</i> | | 0.0053 | 0.048 ± 0.004 | 45 | 0.008 |
| | <i>mcm21Δ</i> | | 0.0059 | 0.060 ± 0.005 | 42 | 0.31 |
| | 37° C | wild-type | | 0.0028 | 0.090 ± 0.007 | 40 |
| <i>ipl1-321</i> | | | 0.0045 | 0.052 ± 0.004 | 36 | < 0.001 |
| <i>kip3Δ</i> | | | 0.0125 | 0.061 ± 0.009 | 19 | 0.014 |
| <i>ipl1-321 kip3Δ</i> | | | 0.0076 | 0.042 ± 0.010 | 17 | < 0.001 |

Table 2.1. Depolymerization kinetics of spindle halves after onset of spindle disassembly. Cells with indicated genotype expressing GFP-Tub1 were imaged every 10 s and the lengths of the spindle halves were measured at each time point. A recovery event was scored each time a spindle half switched from shrinkage to growth. The shrinkage rate (R(hs)) represents the slope of the half spindle lengths when plotted versus time (mean ± S.E.M.). P-values were calculated using a Model I ANOVA test; half spindle shrinkage rates for each mutant were directly compared to the wild-type rates.

Figure 2.3

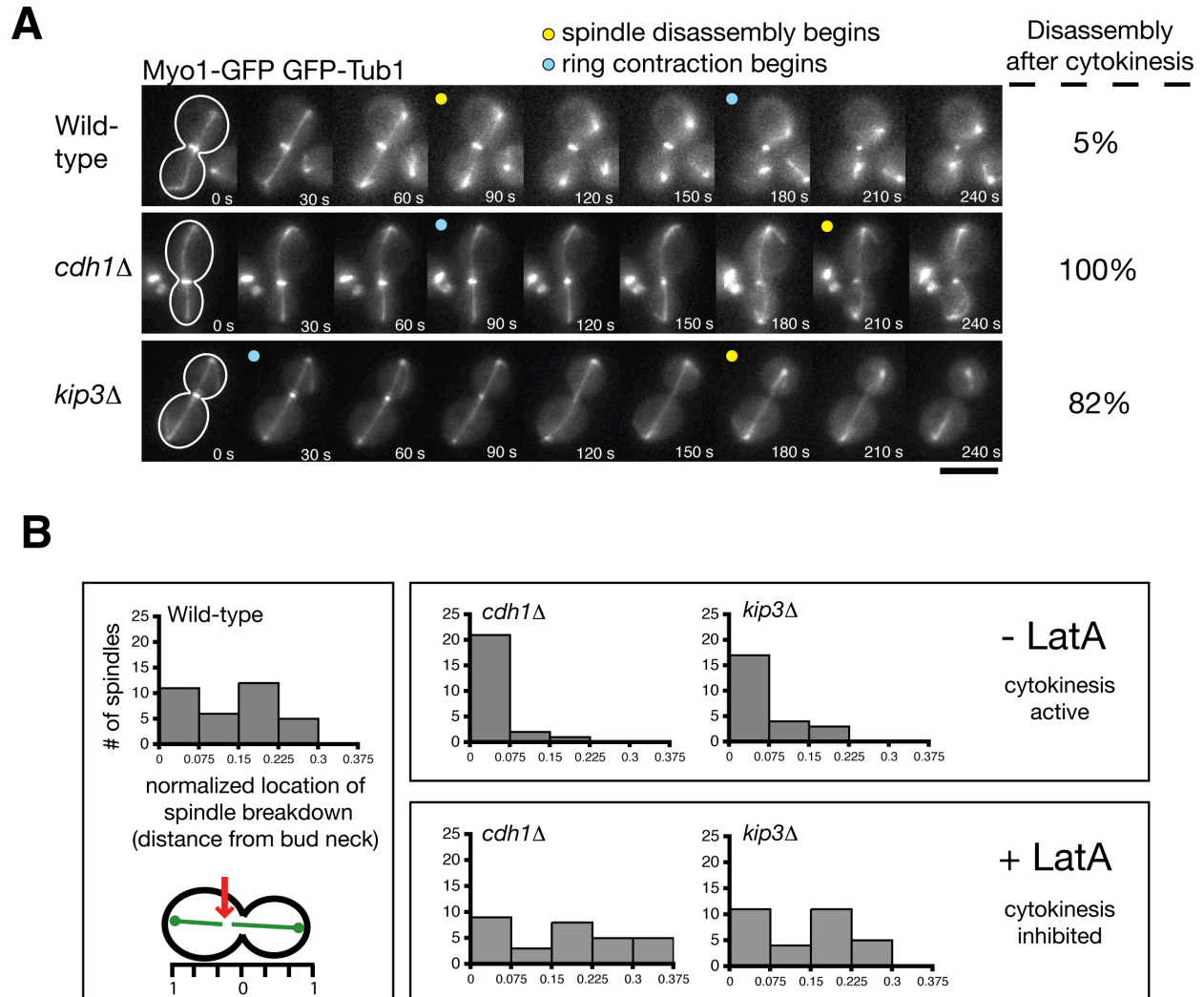


Figure 2.3. Cytokinetic ring contraction breaks the mitotic spindle when normal disassembly mechanisms are impaired. (A) Time-lapse images of cells expressing GFP-Tub1 and the cytokinetic ring marker Myo1-GFP during mitotic exit. A yellow dot indicates when the spindle breaks, whereas a blue dot indicates when the cytokinetic ring has begun contracting. The frequency of spindle disassembly events that occurred after ring contraction is indicated to the right of each image series ($n = 3$ separate experiments each analyzing 20 disassembly events for each strain; mean \pm S.D.). Note that cytokinetic ring contraction appears to break the spindle in *kip3Δ* and *cdh1Δ* cells, but not in wild-type cells. Scale bars, 5 μ m. (B) Cells were monitored as in Figure 2.2A and the location of breakdown relative to the bud neck was recorded and then normalized with the length of the cell ($n = 34, 24, 24$ for wild-type, *cdh1Δ* and *kip3Δ* strains, respectively). All numbers represent absolute values. *kip3Δ* and *cdh1Δ* cells were treated 250 with μ M latrunculin A to inhibit actinomyosin ring contraction ($n = 30$ for each strain).

demonstrate that She1 is important for spindle disassembly and validate use of synthetic lethal profiles to identify novel disassembly factors.

I found that analysis of genetic interactions shared by *CDH1*, *KIP3*, and *SHE1* provided a ~2-3 fold enrichment for genes encoding proteins with previously described mitotic or meiotic functions (Figure 2.4A; Figure 2.5). Importantly, ~44% of these proteins had been previously implicated in spindle disassembly (Vizeacoumar et al. 2010; Juang et al., 1997) (Figure 2.5). Therefore, genes showing synthetic interactions with more than one of the genes *CDH1*, *KIP3*, and *SHE1* are strong candidates for novel spindle disassembly factors. For the remainder of our study, I largely focused on such genes, listed in Figure 2.5.

In addition to further analyzing the effects of mutations in *CDH1*, *KIP3*, and *SHE1*, I also characterized the effects of mutations in six additional genes: *DOC1*, *DBF2*, *IPL1*, *MCM21*, *DCC1*, and *CTF8*. Mutant alleles of all nine genes caused delays in spindle disassembly (Figure 2.4E). Doc1 is a subunit of the APC (Hwang and Murray, 1997) and Dbf2 is a downstream component of the MEN that indirectly activates APC^{Cdh1} (Visintin et al., 1998). Ipl1 is the essential Aurora B kinase in yeast implicated previously in spindle disassembly (Buvelot et al., 2003), and Mcm21 is a component of the COMA kinetochore complex shown to affect Ipl1 localization (Vizeacoumar et al., 2010). Finally, Dcc1 and Ctf8 are components of the 7-protein alternative replication factor C (A-RFC) complex that regulates sister chromatid cohesion (Mayer et al., 2001). Like She1, Dcc1 and Ctf8 have not previously been linked to spindle disassembly.

Real-time analysis reveals distinct roles for spindle disassembly factors in regulating ipMT depolymerization

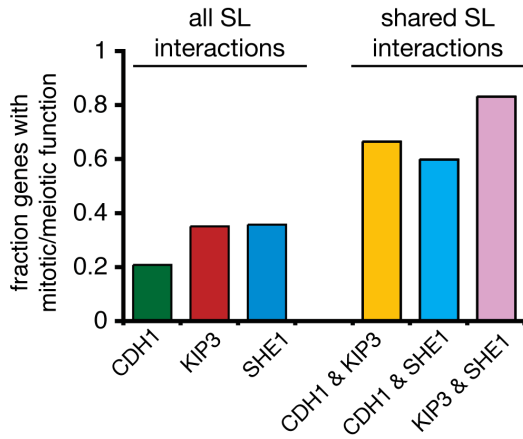
My results up to this point suggest that multiple pathways orchestrate spindle disassembly, and they identify a diverse set of proteins governing this process. As a first step toward elucidating the mechanisms underlying spindle disassembly and the complexity of the pathways controlling this process, I analyzed the effects of depleting Doc1, Dbf2, She1, Ctf8, Dcc1, Mcm21, and Ipl1 on ipMT depolymerization. I again used time-lapse fluorescence microscopy to follow shrinking ipMT plus ends after disassembly onset, similar to the experiments in Figures 1A-C.

I observed hyper-stable half spindles in *doc1Δ* and *dbf2Δ* cells ($R(\text{hs}) = 0.004 \pm 0.002$ and $0.012 \pm 0.002 \mu\text{m} \cdot \text{s}^{-1}$, respectively) similar to the phenotype I described for *cdh1Δ* cells (Table 2.1, Figure 2.6A and 4B). This result is consistent with the fact that all three mutations compromise APC^{Cdh1} activity. Surprisingly, non-hyper-stable spindle halves disassembled more slowly and underwent more recoveries in *dbf2Δ* mutants ($R(\text{hs}) = 0.029 \pm 0.004 \mu\text{m} \cdot \text{s}^{-1}$; $F(\text{rec}) = 0.0079 \text{ s}^{-1}$) than in *cdh1Δ* mutants ($R(\text{hs}) = 0.051 \pm 0.007 \mu\text{m} \cdot \text{s}^{-1}$; $F(\text{rec}) = 0.0054 \text{ s}^{-1}$) or *doc1Δ* mutants ($R(\text{hs}) = 0.044 \pm 0.006 \mu\text{m} \cdot \text{s}^{-1}$; $F(\text{rec}) = 0.0064 \text{ s}^{-1}$) (Table 1). This result suggests that Dbf2 might play a role in spindle disassembly in addition to activating APC^{Cdh1}.

I did not observe hyper-stable half spindles in *dcc1Δ*, *ctf8Δ*, *she1Δ*, *mcm21Δ*, or *ipl1-321* cells ($n > 40$ breakdown events per strain; Figure 2.6 C-H; unpublished data). Instead, *dcc1Δ* and *ctf8Δ* cells displayed spindle halves that alternated between periods of shrinkage and sustained growth, similar to the phenotype I observed in *kip3Δ* cells (Figure 2.2B). In fact, half spindle shrinkage rates and recovery frequencies were elevated 1.5-2-fold in *kip3Δ*, *dcc1Δ*, and *ctf8Δ* cells (Table 2.1). Strikingly, spindle

Figure 2.4

A



B

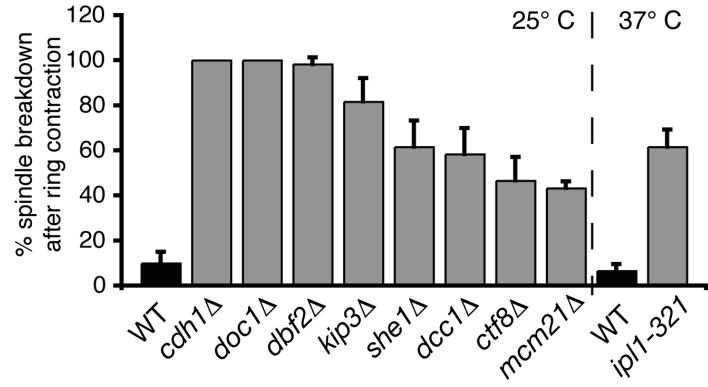


Figure 2.4. Synthetic lethal (SL) screens identify additional genes important for spindle disassembly. (A) Fraction of the genes found in the *CDH1*, *KIP3*, and *SHE1* synthetic interaction profiles that have previously described roles in mitosis or meiosis. (B) Frequency in which spindles disassembled after initiation of cytokinetic ring contraction in indicated strains ($n = 3$ experiments each analyzing 20 disassembly events for each strain; mean \pm S.D.). Analysis performed was similar to the experiments described in Figure 2A. Analysis of *ip11-321* mutants was performed at 37° C and compared with wild-type (WT) cells cultured at the same temperature.

Figure 2.5

| KIP3 & CDH1 common interactions | | SHE1 & CDH1 common interactions | | SHE1 & KIP3 common interactions | |
|---------------------------------|---|---------------------------------|---|---------------------------------|---|
| gene | description | gene | description | gene | description |
| BUB3 | Spindle checkpoint protein | CKB2 | Beta regulatory subunit of casein kinase 2 | CDH1 | Anaphase Promoting Complex subunit |
| DCC1 | Alternative Replication Factor C complex | CPR6 | Peptidyl-prolyl cis-trans isomerase | CIK1 | Kinesin-associated protein |
| ERG6 | Delta(24)-sterol C-methyltransferase | EMI1 | Transcriptional inducer of meiotic-specific transcription factors | CTF18 | Alternative Replication Factor C complex |
| SHE1 | Mitotic spindle protein | KIP3 | Kinesin-related motor protein | CTF8 | Alternative Replication Factor C complex |
| SHO1 | Transmembrane osmosensor | RPS21B | Small (40S) ribosomal subunit component | DBF2 | Ser/Thr kinase in Mitotic Exit Network |
| SLK19 | FEAR regulatory network component | SLK19 | FEAR regulatory network component | DOC1 | Anaphase Promoting Complex subunit |
| SRC1 | Inner nuclear membrane protein | SWM1 | Anaphase-promoting complex subunit | FLX1 | Protein required for transport of flavin adenine dinucleotide (FAD) |
| UME6 | Transcriptional regulator of early meiotic genes | UME6 | Transcriptional regulator of early meiotic genes | FPR4 | Histone H3 and H4 proline isomerase |
| YSC83 | Non-essential mitochondrial protein of unknown function | YLR374C | Dubious open reading frame; partially overlaps STP3/YLR375W | FYV4 | Protein of unknown function |
| | | YPL205C | Hypothetical protein; deletion of locus affects telomere length | HCM1 | Forkhead transcription factor |
| | | | | SLK19 | FEAR regulatory network component |
| | | | | UME6 | Transcriptional regulator of early meiotic genes |

XXX1 Gene with previously described mitotic/meiotic function

XXX1 Gene previously linked to spindle disassembly

Figure 2.5. Pair-wise comparison of published synthetic genetic interactions shared between *CDH1*, *KIP3*, and *SHE1*. Genes previously implicated in mitotic/meiotic processes are highlighted in green. Genes previously implicated in spindle disassembly/mitotic exit are written in red.

halves in *dcc1Δ* and *ctf8Δ* mutants occasionally grew beyond their initial length, sometimes reaching the opposing cell cortex (Figure 2.6C and 4D). These results suggest that the conserved A-RFC complex is required to inhibit ipMT growth at the end of anaphase.

Interestingly, depletion of She1 slowed half spindle shrinkage rates ($R(\text{hs}) = 0.048 \pm 0.004 \mu\text{m} \cdot \text{s}^{-1}$), but did not dramatically alter half spindle recovery frequencies ($F(\text{rec}) = 0.0053 \text{ s}^{-1}$) (Figure 2.6E; Table 2.1). On the other hand, depletion of Mcm21 dampened half spindle shrinkage rates and elevated half spindle recovery frequencies only modestly compared to wild-type cells ($R(\text{hs}) = 0.060 \pm 0.005 \mu\text{m} \cdot \text{s}^{-1}$; $F(\text{rec}) = 0.0059 \text{ s}^{-1}$) (Figure 2.6F; Table 2.1), indicating that Mcm21 plays a minimal role in regulating ipMT dynamics during spindle disassembly.

Finally, I analyzed the effects of inactivating Ipl1 on ipMT depolymerization by incubating *ipl1-321* temperature-sensitive cells at the non-permissive temperature (37° C) for 2 hr and then performing live-cell fluorescence microscopy. On average, spindle halves shrank more slowly and underwent more recoveries in *ipl1-321* cells than in wild-type cells incubated at 37° C (*ipl1-321*: $R(\text{hs}) = 0.052 \pm 0.004 \mu\text{m} \cdot \text{s}^{-1}$; $F(\text{rec}) = 0.0045 \text{ s}^{-1}$; wild-type: $R(\text{hs}) = 0.090 \pm 0.007 \mu\text{m} \cdot \text{s}^{-1}$; $F(\text{rec}) = 0.0028 \text{ s}^{-1}$) (Figure 2.6G and 4H; Table 2.1). These results suggest that Ipl1 mediates spindle disassembly by enhancing ipMT depolymerization and preventing ipMT recovery.

The data presented above indicate that regulating ipMT depolymerization and recovery are crucial for efficient spindle disassembly. Given the range of distinct phenotypes I observed, and, most importantly, that mutations in proteins operating in the same pathway produced similar phenotypes, I conclude that real-time imaging of spindle half depolymerization is a powerful method for categorizing spindle disassembly factors.

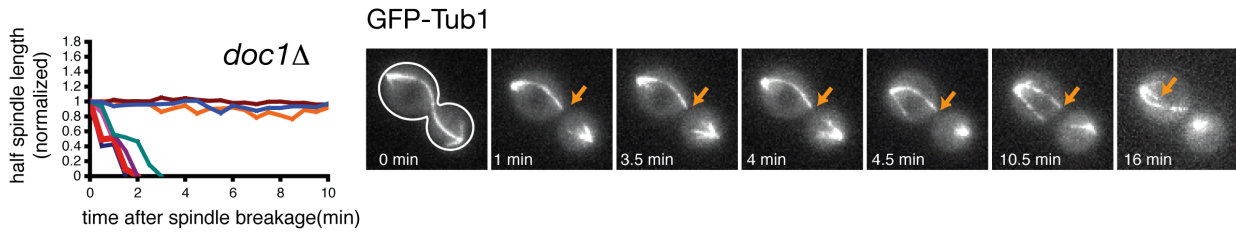
Ipl1 coordinates inhibition of the MT-growth factor Bim1 and activation of the spindle-destabilizing factor She1

Sustained ipMT depolymerization at the end of mitosis could occur either by enhancing MT shrinkage, inhibiting MT growth, or both. It is likely that Kip3, an ATP-dependent MT depolymerase, acts by the former mechanism. In contrast, our results suggest that APC^{Cdh1} accelerates depolymerization of ipMTs by removing and degrading spindle-stabilizing proteins like Ase1 and Cin8. Additional activities may be required, considering that other proteins that are not APC^{Cdh1} substrates (e.g., Bim1, Stu1, Stu2) contribute to spindle stability and length (Gardner et al., 2008, Severin et al. 2001, Yin et al., 2002). It is possible that removal of these proteins from the midzone could suppress MT growth and encourage spindle disassembly. This hypothesis is supported by previous work showing that Ipl1 phosphorylation regulates Bim1 association with MTs *in vitro* (Zimniak et al., 2009). Thus, I decided to test if Ipl1-mediated removal of Bim1 from spindle MTs facilitates spindle disassembly *in vivo*.

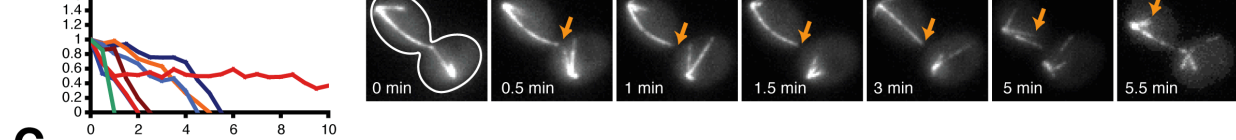
Consistent with previous findings (Zimniak et al., 2009), I observed Bim1-3GFP localization at the spindle midzone decreased dramatically as cells progressed through anaphase (Figure 2.7A), suggesting that Bim1 is unloaded from spindle MTs during spindle disassembly. This localization pattern was observed in 28/30 wild-type cells. However, in 25/30 *ipl1-321* cells, Bim1-3GFP continued to decorate the entire length of the spindle and did not concentrate to the midzone during mitotic exit, indicative of a

Figure 2.6

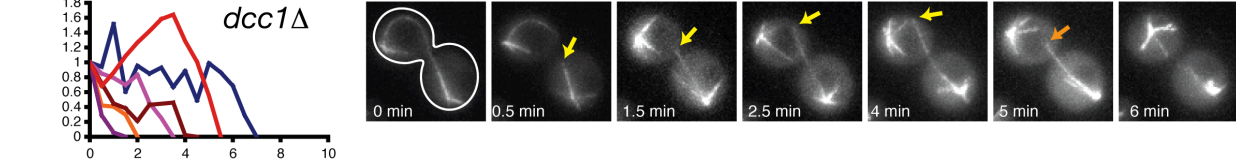
A



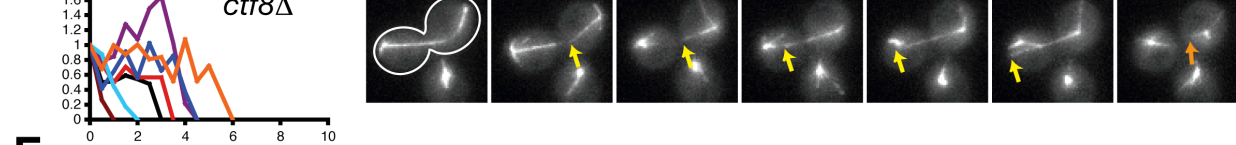
B



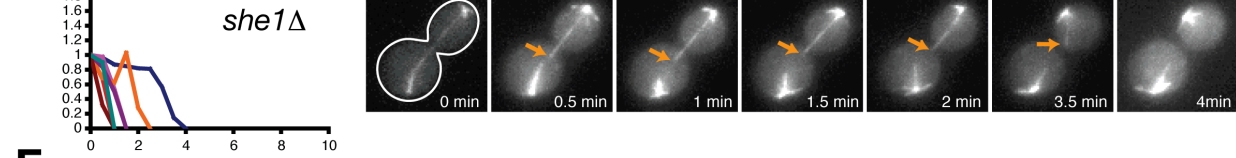
C



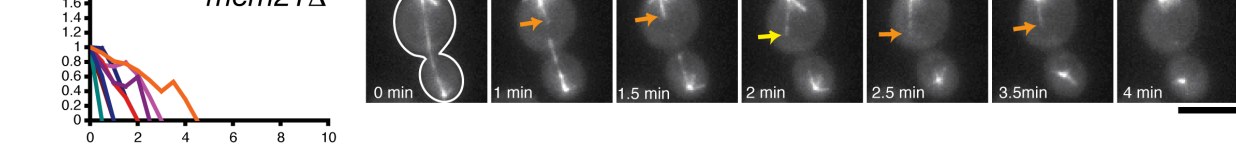
D



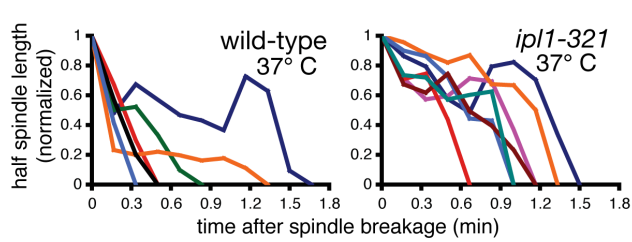
E



F



G



H

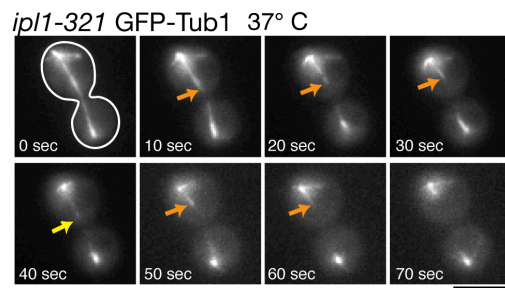


Figure 2.6. Dynamics of interpolar MT depolymerization in spindle disassembly mutants. Cells expressing the spindle marker GFP-Tub1 were analyzed by time-lapse microscopy during mitotic exit, similar to the experiments described in Figure 2.2A-C. Cells were incubated at 23° C. Cell periphery is outlined in white. Orange arrows track shrinking spindle halves, whereas yellow arrows track growing spindle halves. Line graphs on the left represent the normalized lengths of individual depolymerizing spindle halves after the spindle had broken. Scale bars, 5 μ m. (G and H) Comparison of spindle disassembly in wild-type and *ip11-321* cells incubated at 37° C.

defect in Bim1 removal (Figure 2.7A). I observed a dramatic decrease in Bim1-HA phosphorylation when either Ipl1 was inactivated or when serine/threonine to alanine mutations were made within the six Ipl1 phosphorylation sites in Bim1 (Bim1-6A-3HA; Figure 2.7B; Zimniak et al., 2009). Strikingly, cells expressing Bim1-6A displayed delays in spindle disassembly reminiscent of the phenotype seen in *ipl1-321* mutant cells (Figure 2.7C). These results strongly suggest that Ipl1 phosphorylation and consequent dissociation of Bim1 from ipMTs are required for efficient spindle disassembly.

Next, I analyzed the localization of Bim1 in other spindle disassembly mutants. I reasoned that mutations in any upstream activators of Ipl1 should also prevent Bim1 removal from the midzone. Bim1-3GFP removal from the spindle midzone occurred normally in *cdh1Δ*, *doc1Δ*, *kip3Δ*, *she1Δ*, and *mcm21Δ* mutants, but not in *dbf2Δ*, *dcc1Δ*, and *ctf8Δ* mutants (Figure 2.7D). These results suggest that Dbf2 and the A-RFC complex (Dcc1, Ctf8 and others) regulate Ipl1 phosphorylation of Bim1, and that APC^{Cdh1}, Kip3, She1, and Mcm21 do not operate upstream of Ipl1. The persistence of Bim1 on ipMTs could explain why spindle halves recover more frequently in *ipl1-321*, *dbf2Δ*, *dcc1Δ*, and *ctf8Δ* mutants than in wild-type cells (Table 2.1). That *ipl1-321* and *dbf2Δ* mutants share a similar phenotype indicates that Ipl1 phosphorylation of Bim1 occurs downstream of the MEN. Indeed, the timing of Bim1 phosphorylation is consistent with this conclusion. I synchronized *cdc15-2* cells in late anaphase and observed phosphorylated forms of Bim1-HA only after Cdc15 was reactivated (Figure 2.7E). I then asked whether the A-RFC complex indirectly activates Ipl1 by stimulating MEN activity. However, during late anaphase, while nuclear export of Cdc14-GFP was inhibited in *dbf2Δ* cells (Vizeacoumar et al., 2010), Cdc14-GFP re-localization was normal in *dcc1Δ* and *ctf8Δ* mutants (Figure 2.7F), suggesting that the A-RFC complex does not regulate the MEN. This result raises the possibility that the A-RFC complex might operate in parallel to the MEN and Ipl1 to mediate Bim1 removal. However, expression of Bim1-6D, which mimics Bim1 when fully phosphorylated by Ipl1 (Zimniak et al., 2009), partially rescued the spindle disassembly defects seen in *dcc1Δ* mutants (Figure 2.7G). Thus, the A-RFC complex might represent a novel co-factor that directly regulates the cell cycle activity and/or substrate specificity of Ipl1 while operating either downstream of or in parallel to the MEN.

It is possible that Bim1 is not the sole target of Ipl1 during mitotic exit. Likely, Ipl1 not only deactivates spindle-stabilizing factors, like Bim1, but activates spindle-destabilizing factors as well. She1 interacts with the Ipl1 complex component Sli15 (yeast INCENP homolog) in yeast-two hybrid assays, making it an excellent candidate for an Ipl1 target (Wong et al., 2007). Furthermore, She1 likely destabilizes the mitotic spindle, considering that mitotic spindles often rely on cytokinesis to initiate disassembly when She1 is mutated (Figure 2.4D). She1-13Myc migrated as multiple bands on Phos-Tag™ poly-acrylamide gels (Figure 2.8A). All but the two fastest migrating bands disappeared upon phosphatase treatment, thus the slower migrating bands are phosphorylated species (Figure 2.9A). I observed a dramatic decrease in She1-13Myc phosphorylation when either Ipl1 was inactivated or when serine/threonine to alanine mutations were made in the five Ipl1 consensus sites in She1 (She1-5A-13Myc; Figure 2.8A). Finally, spindle disassembly was delayed relative to cytokinetic ring

Figure 2.7

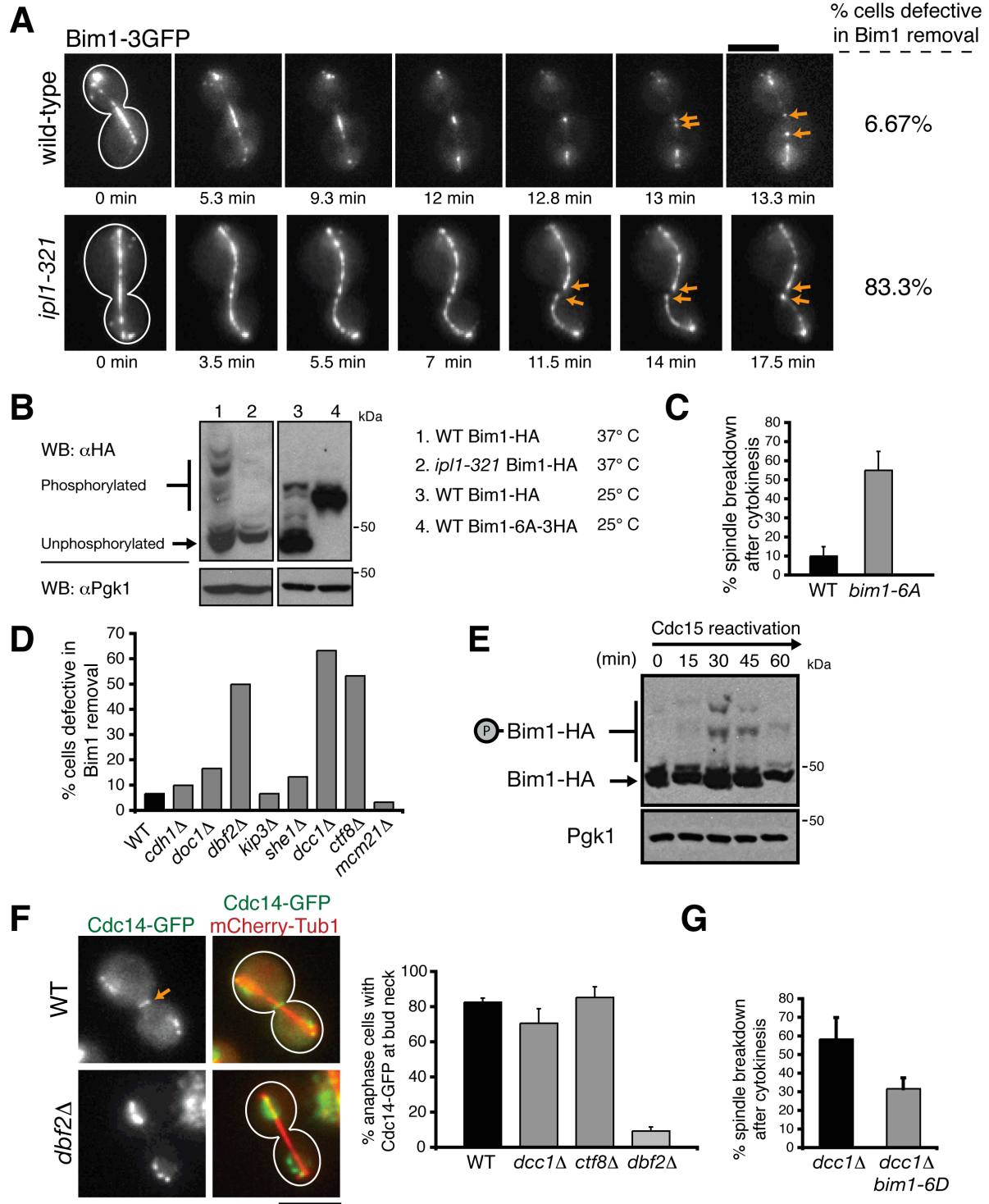


Figure 2.7. The MEN and the A-RFC complex regulate Ipl1-mediated removal of Bim1 from the spindle midzone. (A) Time-lapse fluorescence images of Bim1-3GFP localization in wild-type and *ipl1-321* cells incubated at 37° C. The orange arrows indicate Bim1-3GFP decoration of the plus-ends of spindle halves after disassembly onset. (B) Protein extracts isolated from asynchronous populations of the indicated strains were separated by SDS-PAGE supplemented with 30 μM Phos-tag™ Acrylamide. The tagged phospho-mutant version of Bim1 (Bim1-6A-3HA) contained a larger C-terminal epitope and a longer linker than Bim1-HA; thus, Bim1-6A-3HA migrates more slowly than Bim1-HA. The presence of a single Bim1-6A-3HA band indicates the absence of phosphorylation. Pgk1 was used as a loading control. (C) Frequency in which spindles disassembled after initiation of cytokinetic ring contraction in indicated cells (n = 3 experiments, 20 events per experiment; mean ± S.D.). (D) Bim1-3GFP localization just prior to spindle disassembly in indicated strains (n = 30 for each). Only *dbf2Δ*, *ctf8Δ*, and *dcc1Δ* mutants displayed pronounced defects in Bim1 removal. (E) *cdc15-2* cells expressing Bim1-HA were synchronized in late anaphase after a 3 hr incubation at 37° C. These cells were then released by lowering the temperature to 23° C, and cells were harvested every 15 min. Protein extracts were separated by SDS-PAGE supplemented with 30 μM Phos-tag™ Acrylamide. Pgk1 was used as a loading control. (F) In wild-type, *dcc1Δ*, and *ctf8Δ* cells, Cdc14-GFP was exported from the nucleus and localized to the bud neck (orange arrow) during late anaphase. However, Cdc14-GFP export was defective in *dbf2Δ* cells. (G) Expression of *bim1-6D* alleviates the spindle disassembly defects in *dcc1Δ* cells (n = 3 experiments, 20 events per experiment; mean ± S.D.). Scale bars, 5 μm.

Figure 2.8

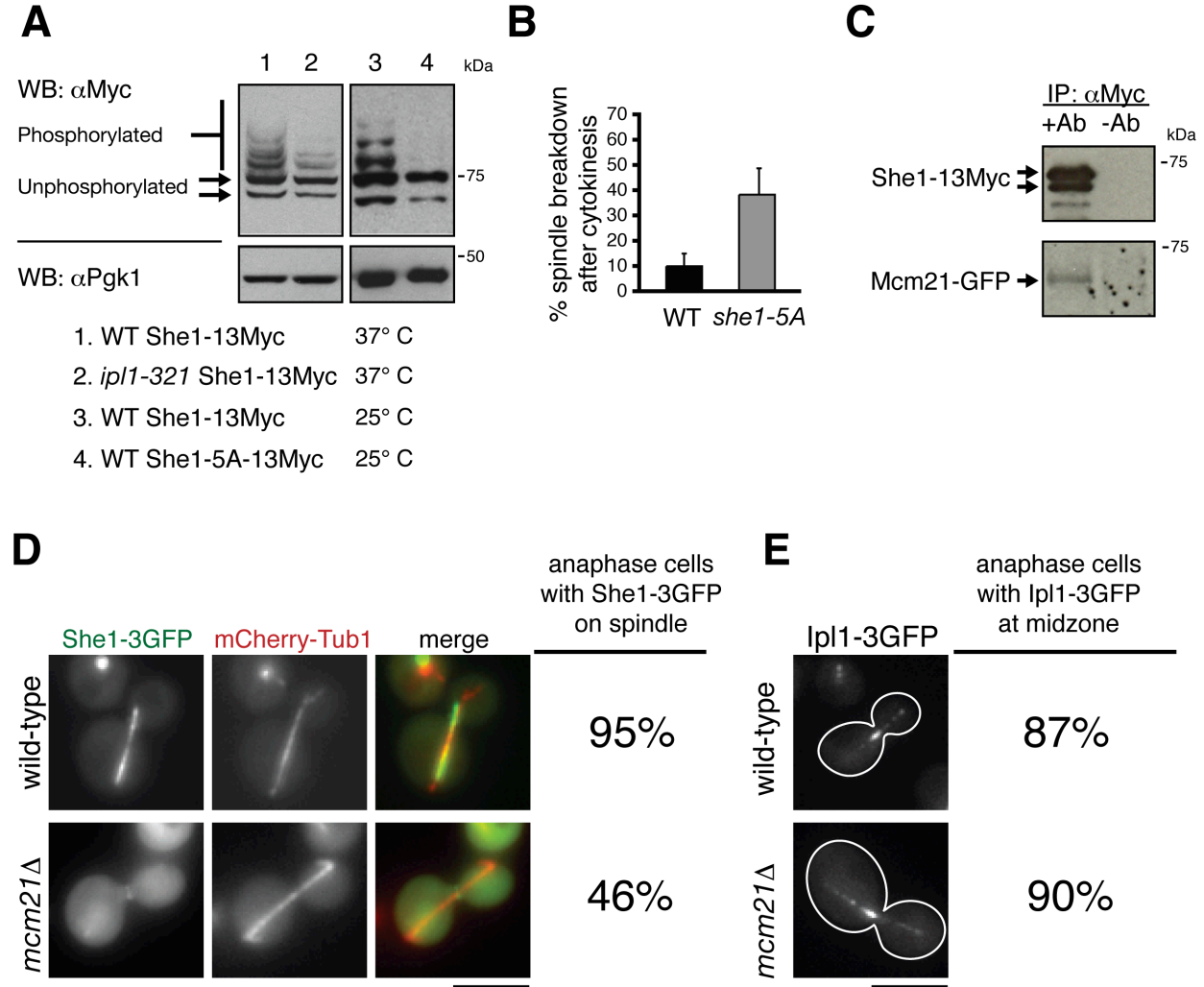


Figure 2.8. Ipl1 and Mcm21 mediate spindle disassembly by regulating She1 activity. (A) Protein extracts isolated from asynchronous populations of the indicated strains were separated by SDS-PAGE supplemented with 20 μ M Phos-tag™ Acrylamide. Detection of Pgk1 was used as a loading control. (B) Frequency in which spindles disassembled after initiation of cytokinetic ring contraction in indicated strains ($n = 3$ experiments each analyzing 20 disassembly events for each strain; mean \pm S.D.). Protein lysate from cells expressing She1-13Myc and Mcm21-GFP was passed over a column conjugated either to anti-Myc antibody (+Ab) or nothing (-Ab). Mcm21-GFP co-purified with She1-13Myc only when anti-Myc antibody was conjugated to the column. (D) She1-3GFP localization in wild-type and *mcm21* Δ cells expressing the spindle marker mCherry-Tub1 during late anaphase ($n = 80$ for both strains). (E) Ipl1-3GFP localization in wild-type and *mcm21* Δ cells during late anaphase ($n = 40$ for both strains). Scale bars, 5 μ m

contraction in cells expressing She1-5A (Figure 2.8B). These findings suggest that Ipl1 mediates spindle disassembly by directly phosphorylating She1.

Since *she1Δ* and *mcm21Δ* mutants share similar phenotypes—delays in spindle disassembly without any substantial defects in half spindle recovery frequencies, midzone protein degradation, or Bim1 localization—She1 and Mcm21 might operate in the same pathway. In support of this hypothesis, both proteins localize to the kinetochore (Figure 2.9B and S3C; Vizeacoumar et al., 2010) and Mcm21-GFP co-purified with She1-13Myc isolated from wild-type yeast extracts (Figure 2.8C). Depletion of Mcm21 reduced She1-3GFP accumulation on the spindle (Figure 2.8D). Surprisingly, in contrast with previous findings (Vizeacoumar et al., 2010), mutation of Mcm21 did not affect Ipl1-3GFP localization to the spindle midzone (Figure 2.8E). This result suggests that Mcm21 does not operate upstream of Ipl1, consistent with my observations that *mcm21Δ* and *ipl1-321* mutants have distinct spindle disassembly phenotypes (Figures 2.6 and 2.7; Table 2.1). Instead, Mcm21, and likely other components of the COMA kinetochore complex, mediate spindle disassembly by binding to She1 and recruiting it to the spindle.

Kip3 operates independently of Ipl1 to regulate spindle length and promote sustained depolymerization of ipMTs

Lastly, I considered the possibility that Ipl1 might also mediate spindle disassembly by regulating Kip3 via phosphorylation. However, I found that the spindle disassembly defects observed in *ipl1-321* cells were intensified upon additional depletion of Kip3. The frequency of spindles disassembling after cyotkinetic ring contraction, half spindle shrinkage rates, and half spindle recovery frequencies were higher in *kip3Δ ipl1-321* double mutants than in single *ipl1-321* mutants (Figure 2.10A and Table 2.1). These results suggest that Ipl1 and Kip3 perform distinct functions during spindle disassembly. When I used Phos-Tag™-SDS-PAGE to analyze protein extracts from wild-type and *ipl1-321* cells expressing Kip3-13Myc, I could not detect any difference in band migration pattern (Figure 2.10B), suggesting that Ipl1 does not phosphorylate Kip3 *in vivo*. I considered the possibility that my inability to detect Ipl1-dependent band migration shifts for Kip3-13Myc may have been due to insensitivity of the detection method. However, I obtained the same result when I affixed alternative tags to Kip3 (GFP, 3HA) and strengthened the concentration of Phos-Tag™-Acrylamide and the primary antibody used for detection by western blot (unpublished data). I still cannot completely rule out the possibility that Ipl1 phosphorylates Kip3 in a manner that does not affect the mobility of Kip3 on an acrylamide gel. Nevertheless, my conclusion that Ipl1 does not mediate spindle disassembly by phosphorylation-dependent activation of Kip3 is further supported by the fact that expression of a Kip3 construct containing serine/threonine to alanine mutations in all four putative Ipl1 consensus motifs (*kip3-4A*) did not compromise spindle disassembly (Figure 2.10C).

The exclusion of Kip3 from the APC^{Cdh1} and Ipl1 pathways, both of which seem to be activated by the MEN, raises questions about whether Kip3 activity is cell cycle regulated. I found that loss of Kip3 increased spindle length ~1.5-fold in both early and late anaphase (Figure 2.10D), suggesting that Kip3-mediated depolymerization is not restricted to late mitosis, in contrast to APC^{Cdh1}-mediated destruction of midzone proteins or Ipl1-mediated inactivation of Bim1. Thus, even though Ipl1, APC^{Cdh1}, and

Figure 2.9

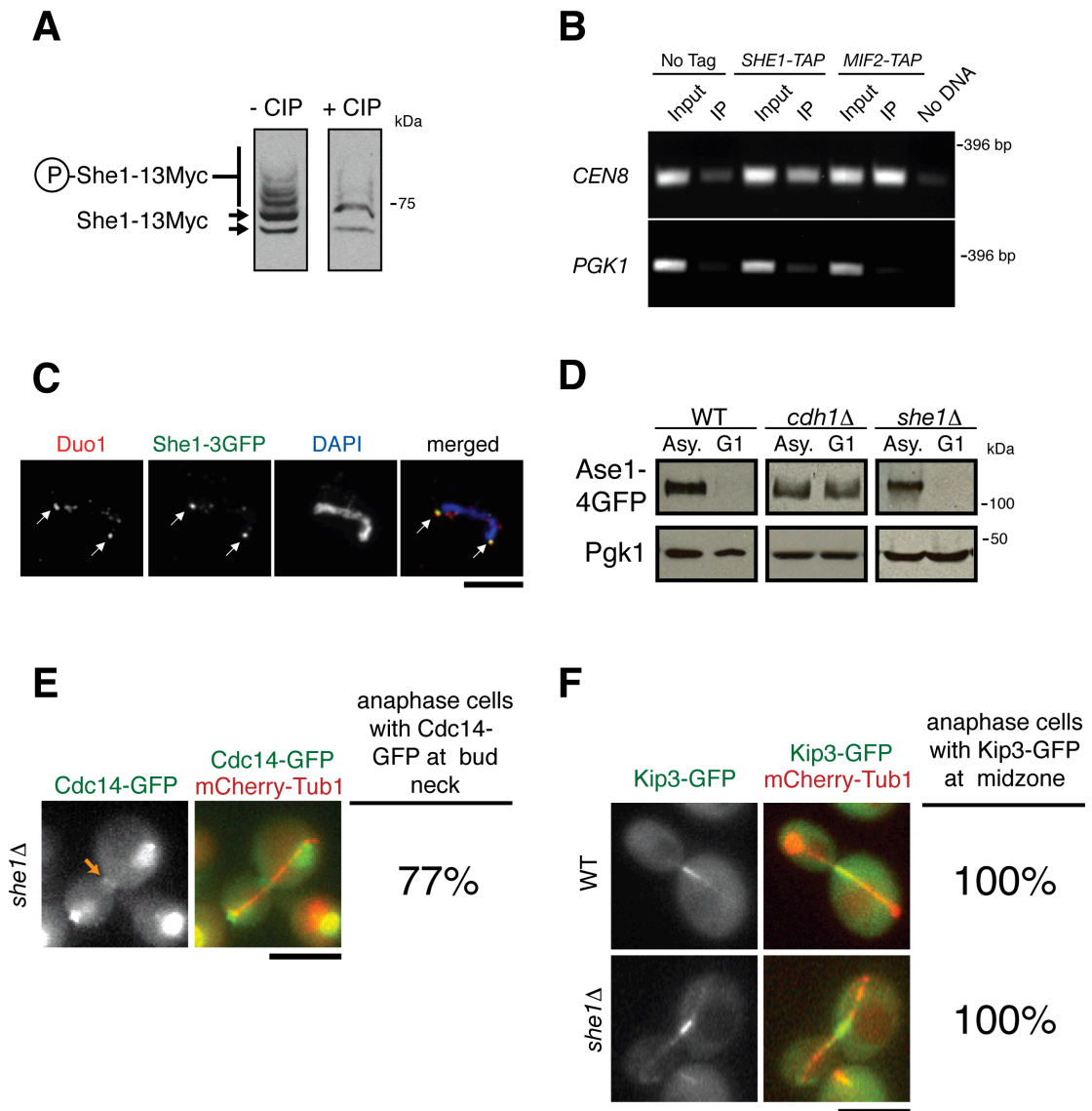


Figure 2.9. Analysis of She1. (A) Protein extracts isolated from cells expressing She1-13Myc were separated by SDS-PAGE supplemented with 20 μ M Phos-tag™ Acrylamide, then visualized by immunoblotting with anti-Myc antibody. Samples were either treated with buffer alone (-CIP) or buffer plus calf intestinal phosphatase (+CIP) for 30 min at 37° C. (B) Chromatin immunoprecipitation experiments. She1-TAP pulls down centromere-associated DNA (*CEN8*), but not a region distal to the centromere (*PGK1*). Extract from cells that did not express any tagged proteins was used as a negative control. Mif2-TAP, an established kinetochore component, was immunoprecipitated as a positive control. (C) Chromatin spread experiment. She1-3GFP co-localized with isolated DNA and Duo1, an established kinetochore component. (D) Protein extract was harvested from asynchronous (Asy.) or alpha-factor arrested (G1) cells of the indicated genotypes. In *cdh1* Δ cells, Ase1-4GFP is not degraded during G1. However, Ase1-4GFP is absent in wild-type and *she1* Δ cells at the end of G1. Pgc1 was used as a loading control. (E) Cdc14-GFP localized to the bud neck during late anaphase in 77% of *she1* Δ cells (n = 44). (F) Kip3-GFP localized to the spindle midzone during anaphase in 100% of wild-type and *she1* Δ cells (n = 25). Scale bars, 5 μ m.

Kip3 are all important for disassembling the mitotic spindle, my findings indicate that Ipl1 and APC^{Cdh1} are the major factors governing the transition from spindle growth to disassembly.

Figure 2.10

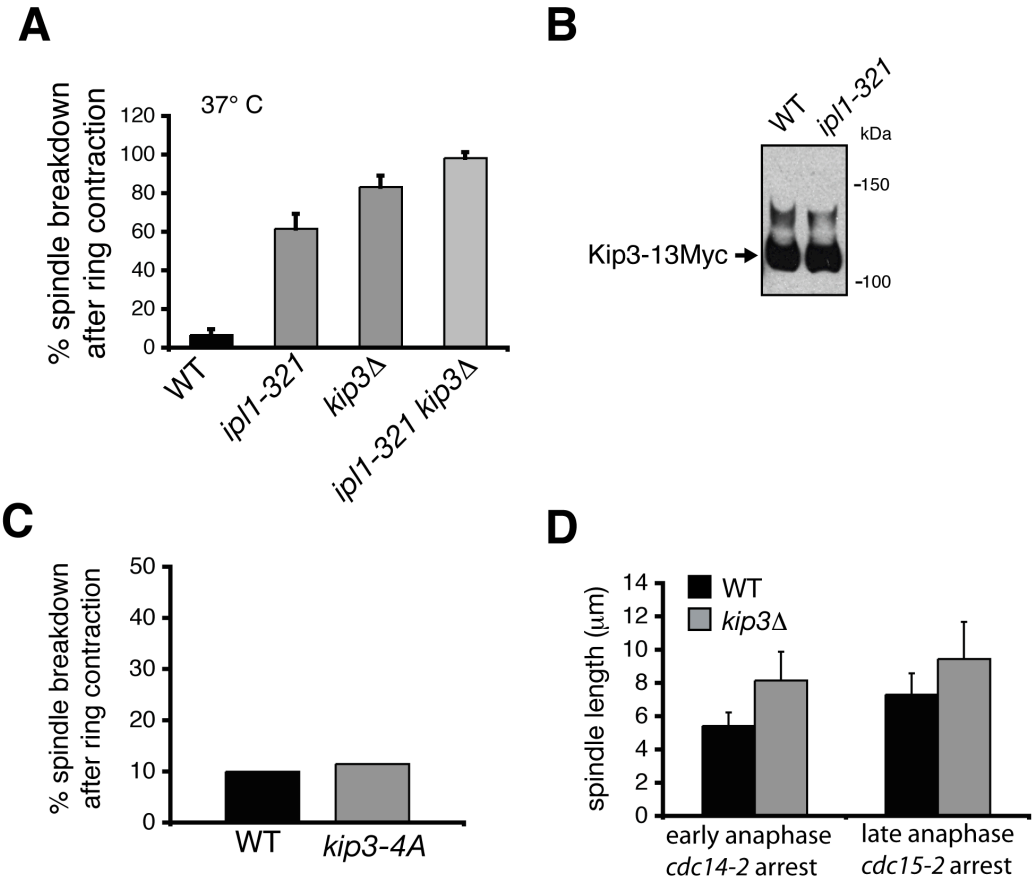


Figure 2.10. Kip3 and Ipl1 operate in separate pathways during spindle disassembly. (A) Frequency at which spindles disassembled after initiation of cytokinetic ring contraction in wild-type cells and in selected mutants ($n = 3$ separate experiments each analyzing 20 disassembly events for each strain; mean \pm S.D.). All cells were incubated at 37°C. (B) Analysis of Kip3-13Myc phosphorylation in wild-type and *ipl1-321* strains. Protein extracts were separated by SDS-PAGE supplemented with 20 μ M Phos-tag™ Acrylamide, then visualized by immunoblotting against the Myc epitope. (C) Quantification of delayed spindle disassembly in wild-type cells (WT; $n = 60$) and in cells expressing an allele of *KIP3* with all four Ipl1 consensus sites mutated (*kip3-4A*; $n = 26$). (D) Kip3 regulates mitotic spindle length throughout anaphase. Spindle length was measured in *kip3Δ* or wild-type cells expressing GFP-Tub1 arrested in early anaphase (*cdc14-2*) or late anaphase (*cdc15-2*) ($n = 60$ for each strain; mean \pm S.D.).

DISCUSSION

Prior to this work, an understanding of spindle disassembly in any organism was limited because this process has not been thoroughly analyzed in real-time to fully dissect and characterize the mechanisms involved. Previous studies have relied on two methods to assess defects in spindle disassembly: 1) static analysis of late anaphase spindle morphology, looking for the accumulation of abnormally long or bent spindles; or 2) analysis of spindle persistence after the onset of anaphase B, looking for spindles that remain intact for longer periods of time than normal (Buvelot et al., 2003; Woodbury and Morgan, 2007; Vizeacoumar et al., 2010). Although these types of measurements can identify mutants that regulate spindle dynamics and integrity, they cannot distinguish between mutants that modify the rate of spindle elongation during anaphase and those that perturb spindle disassembly during telophase, and they are inadequate for distinguishing the various steps of spindle disassembly.

In this study, I combined genetic analysis with live-cell fluorescence microscopy to identify proteins critical for spindle disassembly and to reveal their specific contributions to this process. I assessed in detail the effects of nine mutations (*cdh1Δ*, *doc1Δ*, *dbf2Δ*, *kip3Δ*, *she1Δ*, *dcc1Δ*, *ctf8Δ*, *mcm21Δ*, and *lpl1-321*) on spindle half separation, ipMT depolymerization, and removal of MT-stabilizing proteins from the spindle. The phenotypes I observed for each mutant (Figure 2.11A) support a model wherein at least three pathways, which I call the Spindle Disassembly Network, mediate spindle disassembly (Figure 2.11B).

In the first pathway, the MEN stimulates association of the APC with the late anaphase co-factor Cdh1. This holoenzyme (APC^{Cdh1}) then ubiquitinates Ase1 (yeast Prc1 homolog), Cin8 (yeast BimC homolog), and other MT-cross-linking MAPs (Hildebrandt and Hoyt, 2001; Woodbury and Morgan, 2007), thereby effecting their degradation and facilitating separation of the spindle halves.

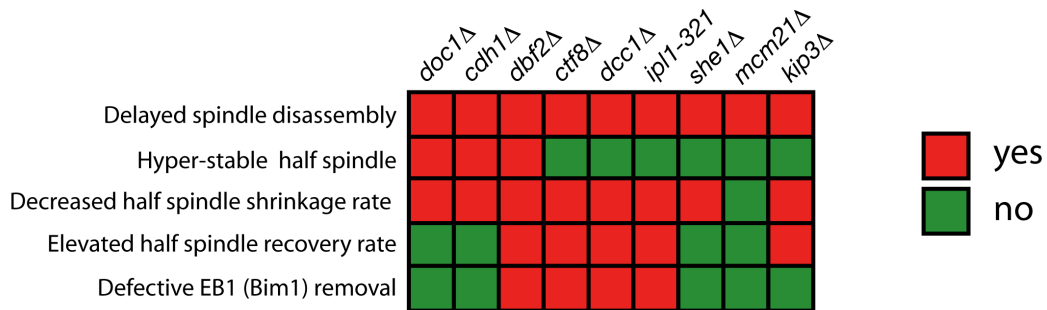
In the next pathway, the Ipl1 complex (yeast Aurora B) arrests ipMT growth by inactivating the MT-growth factor Bim1 (yeast EB1). My findings suggest that the MEN activates this pathway, but the mechanism remains to be determined. I can exclude regulation of Ipl1 localization as a possible mechanism because I observed Ipl1-3GFP decoration of the midzone in *dbf2Δ* cells (Figure 2.12). Interestingly, I also discovered that a novel factor uncovered in our screen, the highly conserved A-RFC complex (Ctf18, Dcc1, Ctf8, RFCp40, RFCp38, RFCp37, and RFCp36; Mayer et al., 2001) is necessary for Ipl1-mediated removal of Bim1. In the future, it will be important to determine how the A-RFC complex regulates Ipl1 activity.

In addition, Ipl1 destabilizes the spindle by activating She1, a novel disassembly factor identified in my screen, although the mechanism of She1 function remains to be determined. Likely, She1 does not regulate MEN, APC, or Kip3 activity, considering that Cdc14-GFP localization, Ase1-4GFP degradation, and Kip3-GFP localization are not detectably affected in *she1Δ* cells (Figure 2.9D-F). Since She1 localizes along the mitotic spindle, it is possible that She1 directly regulates MT dynamics (see Chapter 4).

Finally, my data indicate that the kinesin-8 member Kip3 operates independently of the APC^{Cdh1} and Ipl1 pathways to drive spindle MT depolymerization during spindle disassembly.

Figure 2.11

A



B

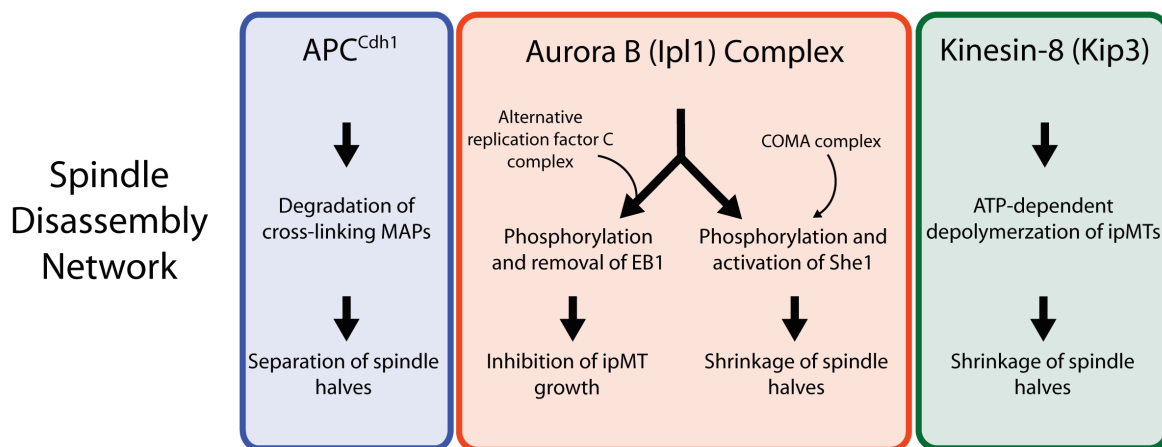


Figure 2.11. Multiple pathways regulating distinct subprocesses drive spindle disassembly. (A) Summary of phenotypic analysis for nine spindle disassembly mutants. “Decreased half spindle shrinkage rate” indicates that the average rate of half spindle shrinkage was significantly lower than the wild-type rate ($p < 0.05$; Table 2.1). Additionally, “elevated half spindle recovery rate” indicates that the spindle half recovery frequency was >1.5 -fold higher than the wild-type frequency. (B) Multiple pathways model for spindle disassembly. In the first pathway (blue box), the Anaphase-Promoting Complex loaded with the late anaphase co-factor Cdh1 (APC^{Cdh1}) degrades cross-linking MAPs (e.g. Ase1, Cin8 and others) to facilitate separation and destabilization of spindle halves. In the second pathway (red box), Aurora B (Ipl1 in yeast) phosphorylates and the spindle stabilizer EB1 (Bim1 in yeast) and the spindle destabilizer She1. The alternative replication factor C complex is needed for EB1 phosphorylation by Aurora B. The COMA kinetochore complex loads She1 onto the spindles. In the third pathway (green box), the kinesin-8 family member Kip3 actively depolymerizes spindle MTs and prevents their re-growth during mitotic exit. Inhibition of multiple pathways produces additive defects on spindle half disassembly and cell fitness.

Figure 2.12

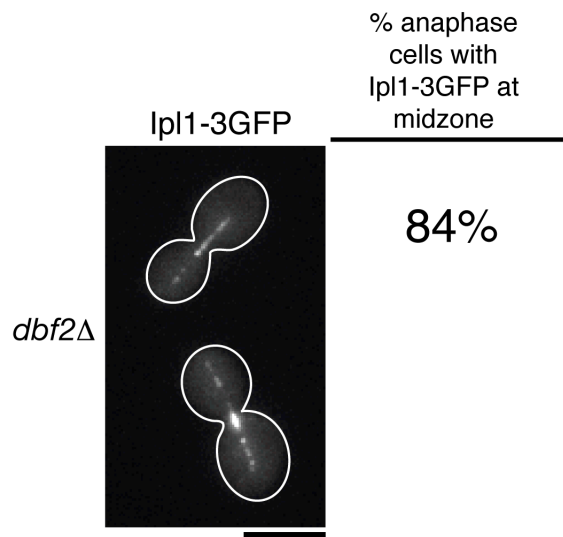


Figure 2.12. Ipl1-3GFP localization during late anaphase in *dbf2*Δ cells. Ipl1-3GFP localized along the midzone in 84% (n= 80) of *dbf2*Δ cells. Scale bar, 5 μm.

Why does spindle disassembly require coordination of multiple pathways that function via distinct mechanisms? The mitotic spindle is a highly complex structure assembled from MTs interlinked and stabilized by an assortment of MAPs. Thus, it seems logical that the diversity of stabilizing interactions must be reversed by a comparably diverse set of destabilizing mechanisms. Furthermore, the mitotic spindle is highly dynamic and is irreversibly disassembled during a brief window of time (~2 min in yeast; Maddox et al., 2000) in telophase. Deployment of multiple distinct destabilizing mechanisms may be necessary to achieve this switch-like transition. An alternative, but not mutually exclusive, explanation is that these multiple pathways may serve as a multi-tiered back-up system to ensure disassembly in the event that one pathway is compromised. This latter possibility is supported by my observation that disassembly of the hyper-stable half spindles in *cdh1Δ* cells was dramatically inhibited after additional mutation of Kip3. It is possible that Kip3-mediated depolymerization might help dissociate MT-cross-linking proteins that remain on the spindle when APC^{Cdh1} is inactive. This conclusion is further supported by the multitude of synthetic genetic interactions between null mutations that inhibit spindle disassembly (Figure 2.4; Figure 2.5).

My results demonstrate that yeast cells can accommodate the loss of one spindle disassembly pathway, but not the loss of multiple pathways, thus highlighting the importance of spindle disassembly for cell cycle progression and overall fitness. I propose that the fitness defect seen when multiple spindle disassembly pathways are inactivated results from a G1 arrest and not a failure in mitotic exit. In *kip3Δ cdh1Δ* double mutants, cytokinetic ring contraction simultaneously divided the daughter cells and separated the spindle halves, yielding G1 cells with spindle remnants that persisted for >80 min, more than 40 times longer than in wild-type cells. During this time, these *kip3Δ cdh1Δ* double mutants remained arrested in G1, while their wild-type counterparts exited from G1 and formed new spindles (unpublished data). My results suggest that cytokinesis can break the spindle when primary mechanisms are impaired, allowing entry into the next cell cycle. However, it seems that progression out of G1 is intimately linked with complete disassembly of pre-existing spindle structures. Perhaps the inability to completely depolymerize spindle MTs prevents spindle pole body duplication and/or formation of a new spindle in the next cell cycle.

Considering the high degree of conservation among APC^{Cdh1}, Aurora B, kinesin-8, and the A-RFC complex, I expect my findings to have important implications for spindle disassembly in all eukaryotes. Despite the fact that direct, real-time analysis of spindle disassembly in metazoans has yet to be performed, there is evidence that the APC, Aurora B, and kinesin-8 might participate in this process in these organisms. In human cells, APC^{Cdh1} concentrates to the central spindle and targets a variety of spindle-stabilizing proteins (e.g., Prc1, Polo kinase, TPX2) for proteasome-mediated degradation during late mitosis (Peters, 2006). Based on my results, this activity might disrupt the central spindle and facilitate separation of spindle halves in human cells. Aurora B also concentrates to the central spindle in *C. elegans* (Severson et al., 2000) and human cells (Gruneberg et al., 2004), as in yeast, but whether Aurora B facilitates removal of MT-stabilizing proteins like EB1 during telophase in these organisms remains to be seen. Finally, similar to Kip3 in yeast, the kinesin-8 members Kif18A and Klp67A have been shown to regulate spindle size in human and *Drosophila* cells,

respectively (Mayr et al., 2007; Goshima et al., 2005). Thus, it is possible that sustained MT depolymerization driven by kinesin-8 represents a universal mechanism to mediate spindle disassembly.

My goal in this study was to gain insight into how eukaryotic cells rapidly disassemble the mitotic spindle, an extremely complex structure, and to identify the proteins critical for this process. I conclude that mechanistically distinct pathways governed by APC^{Cdh1}, Aurora B, and kinesin-8 drive spindle disassembly in budding yeast. These pathways act in concert to break the proteinaceous attachments that hold overlapping ipMTs in a rigid structure, inhibit ipMT growth, and promote sustained ipMT depolymerization.

SUMMARY

The mitotic spindle is a complex and dynamic structure. Although much has been learned about how spindles assemble and mediate chromosome segregation, how spindles rapidly and irreversibly disassemble during telophase is less clear. I employed synthetic lethal screens in budding yeast to identify mutants defective in spindle disassembly. Real-time, live-cell imaging analysis of spindle disassembly was performed on nine mutants defective in this process. Results of this analysis suggest that spindle disassembly is achieved by mechanistically distinct, but functionally overlapping subprocesses: disengagement of the spindle halves, arrest of spindle elongation, and initiation of interpolar microtubule depolymerization. These subprocesses are largely governed by the Anaphase-Promoting Complex, Aurora B kinase and kinesin-8. Combinatorial inhibition of these subprocesses yielded cells with hyper-stable spindle remnants and dramatic defects in cell cycle progression, establishing that rapid spindle disassembly is crucial for cell proliferation.

MATERIALS AND METHODS

Yeast strains. The yeast strains used in this study are derivatives of S288C and are listed in Table 2.1. *doc1Δ*, *cdh1Δ*, *dbf2Δ*, *dcc1Δ*, *ctf8Δ*, *mcm21Δ* and *kip3Δ* null mutants originated from the Research Genetics Collection. The Ase1-4GFP and Cin8-4GFP strains were a generous gift from E. Schiebel (ZMBH Heidelberg, Germany). The phospho-mutant alleles *kip3-4A* (S74A, T172A, S402A, S792A) and *she1-5A* (T14A, S165A, S269A, T280A, S325A) were generated using Quikchange™ site-directed mutagenesis. Ipl1 phosphorylation sites selected for mutation matched the (R/K)X(T/S)(I/L/V/T) consensus motif (Cheeseman et. al, 2002). Plasmids containing full-length *kip3-4A* and *she1-5A* genes were then integrated at each gene's endogenous locus in *kip3Δ* and *she1Δ* strains, respectively. The *bim1-6A* and *bim1-6D* strains were a generous gift from S. Westermann (IMP Vienna, Austria), and the Kip3-GFP strain was a generous gift from K. Bloom (UNC Chapel Hill).

Fluorescence microscopy. Live-cell microscopy at room temperature was performed using an Olympus IX-71 microscope, 100X NA 1.4 objective and an Orca-ER camera (Hamamatsu, Hamamatsu City, Japan). All microscopy at 37°C was performed using an Olympus IX-81 microscope equipped with a temperature-controlled enclosure (Precision Control Weather Station), 100X NA 1.4 objective and an Orca-ER camera (Hamamatsu, Hamamatsu City, Japan). Two-color images were obtained by sequential switching between RFP and GFP filter sets. For time-lapse microscopy of shrinking half spindles, actinomyosin ring contraction, and Bim1-3GFP localization, images were collected at 10s intervals with 300 ms exposures. Each image represents a maximum intensity projection from a Z-stack containing 6 planes 0.2 μm apart. All image processing was performed using Metamorph software.

Synthetic lethal profile comparison. To examine the synthetic interactions for *SHE1*, I used the synthetic lethal and synthetic sick dataset published by Costanzo et al. (2010) and Tong et al. (2004). Although synthetic interactions between *SHE1* and *CDH1* and between *SHE1* and *DOC1* did not appear in these lists, I had previously identified such interactions through tetrad analysis. When comparing the synthetic interaction profiles of *KIP3*, *CDH1*, and *SHE1*, I used only the raw dataset with an intermediate cutoff applied ($|\epsilon| > 0.08, p\text{-value} < 0.05$) published by Costanzo et al. (2010), plus several interactions identified in my lab.

Detection of protein phosphorylation. To detect phosphorylation-dependent mobility shifts of She1-13Myc, Kip3-13Myc, and Bim1-HA, whole cell extracts were loaded onto 6-8% SDS polyacrylamide gels containing either 20 μM or 30 μM Phos-tag™ Acrylamide (FMS Laboratory, Hiroshima Univ.) and 40 μM or 60 μM MnCl₂, respectively. Membranes were then probed with 1:500 mouse anti-Myc (9E10, purified by my laboratory) or 1:1,000 mouse anti-HA (12CA5, Roche).

Immunoprecipitation. Immunoprecipitation was performed essentially as described (Woodruff et al., 2009) with the following modifications. Lysates were incubated with mouse anti-Myc antibody for one hour and then passed over protein G sepharose

beads (Amersham Biosciences) to purify She1-13Myc. The column was washed with lysis buffer and eluted with SDS loading buffer.

Chromatin Immunoprecipitation. Chromatin immunoprecipitation was conducted essentially as described previously (Kang et al., 2001), with the following modifications. Cells were fixed for 1 hr in 1% formaldehyde. Whole cell extracts were passed over IgG sepharose (Amersham Biosciences) to pull down She1-TAP and Mif2-TAP.

Chromosome Spreads. Chromosome spreads were prepared as described (Cheeseman et al., 2001). Anti-Duo1 antibody (Hofmann et al., 1998) was used at a dilution of 1:2000 to detect Duo1, and anti-GFP (rabbit, Torrey Pines) was used at a dilution of 1:2000 to detect She1-3GFP.

Table 2.2. Yeast strains used in this study

| Strain name | Mating type | genotype | source |
|-------------|---------------|---|-----------------------|
| JBY 39 | <i>MATa</i> | <i>GFP-TUB1::URA3</i> | Woodruff et al., 2009 |
| JBY 58 | <i>MATa</i> | <i>GFP-TUB1::URA3 she1Δ::LEU2</i> | Woodruff et al., 2009 |
| JBY 154 | <i>MATα</i> | <i>GFP-TUB1::URA3 cdh1Δ::KanMX6</i> | this study |
| JBY 156 | <i>MATa</i> | <i>GFP-TUB1::URA3 doc1Δ::KanMX6</i> | this study |
| JBY 145 | <i>MATa</i> | <i>GFP-TUB1::URA3 dbf2Δ::KanMX6</i> | this study |
| JBY 150 | <i>MATa</i> | <i>GFP-TUB1::URA3 kip3Δ::KanMX6</i> | this study |
| SP 17 | <i>MATa</i> | <i>GFP-TUB1::URA3 dcc1Δ::KanMX6</i> | this study |
| SP 13 | <i>MATα</i> | <i>GFP-TUB1::URA3 ctf8Δ::KanMX6</i> | this study |
| JBY 300 | <i>MATα</i> | <i>GFP-TUB1::URA3 mcm21Δ::KanMX6</i> | this study |
| JBY 222 | <i>MATa</i> | <i>GFP-TUB1::URA3 ipl1-321</i> | this study |
| JBY 293 | <i>MATa</i> | <i>GFP-TUB1::URA3 cdh1Δ::KanMX6 kip3Δ::KanMX6</i> | this study |
| JBY 204 | <i>MATa</i> | <i>MYO1-GFP::HIS3 GFP-TUB1::URA3 she1Δ::LEU2</i> | this study |
| JBY 230 | <i>MATa</i> | <i>MYO1-GFP::HIS3 GFP-TUB1::URA3 cdh1Δ::KanMX6</i> | this study |
| JBY 257 | <i>MATα</i> | <i>MYO1-GFP::HIS3 GFP-TUB1::URA3 doc1Δ::KanMX6</i> | this study |
| JBY 258 | <i>MATα</i> | <i>MYO1-GFP::HIS3 GFP-TUB1::URA3 dbf2Δ::KanMX6</i> | this study |
| JBY 205 | <i>MATα</i> | <i>MYO1-GFP::HIS3 GFP-TUB1::URA3 kip3Δ::KanMX6</i> | this study |
| JBY 206 | <i>MATα</i> | <i>MYO1-GFP::HIS3 GFP-TUB1::URA3 dcc1Δ::KanMX6</i> | this study |
| JBY 259 | <i>MATa</i> | <i>MYO1-GFP::HIS3 GFP-TUB1::URA3 ctf8Δ::KanMX6</i> | this study |
| JBY 301 | <i>MATa</i> | <i>MYO1-GFP::HIS3 GFP-TUB1::URA3 mcm21Δ::KanMX6</i> | this study |
| JBY 225 | <i>MATα</i> | <i>MYO1-GFP::HIS3 GFP-TUB1::URA3 ipl1-321</i> | this study |
| JBY 278 | <i>MATα</i> | <i>MYO1-GFP::HIS3 GFP-TUB1::URA3 bim1-6A::KanMX6</i> | Zimniak et al., 2009 |
| JBY 277 | <i>MATα</i> | <i>MYO1-GFP::HIS3 GFP-TUB1::URA3 she1-5A::URA3::she1Δ::LEU2</i> | this study |
| JBY 263 | <i>MATa</i> | <i>MYO1-GFP::HIS3 GFP-TUB1::URA3 kip3-4A::LEU2::kip3Δ::KanMX6</i> | this study |
| JBY 319 | <i>MATα</i> | <i>MYO1-GFP::HIS3 GFP-TUB1::URA3 kip3Δ::KanMX6 ipl1-321</i> | this study |
| JBY 142 | <i>MATa</i> | <i>BIM1-3GFP::HIS3 mCherry-TUB1::URA3</i> | this study |
| JBY 246 | <i>MATa</i> | <i>BIM1-3GFP::HIS3 ipl1-321</i> | this study |
| JBY 216 | <i>MATα</i> | <i>she1Δ::LEU2 BIM1-3GFP::HIS3 mCherry-TUB1::URA3</i> | this study |
| JBY 296 | <i>MATα</i> | <i>cdh1Δ::KanMX6 BIM1-3GFP::HIS3 mCherry-TUB1::URA3</i> | this study |
| JBY 175 | <i>MATa/α</i> | <i>doc1Δ::KanMX6 BIM1-3GFP::HIS3 mCherry-TUB1::URA3</i> | this study |
| JBY 273 | <i>MATa</i> | <i>dbf2Δ::KanMX6 BIM1-3GFP::HIS3 mCherry-TUB1::URA3</i> | this study |
| JBY 215 | <i>MATa</i> | <i>kip3Δ::KanMX6 BIM1-3GFP::HIS3 mCherry-TUB1::URA3</i> | this study |
| JBY 227 | <i>MATa</i> | <i>dcc1Δ::KanMX6 BIM1-3GFP::HIS3 mCherry-TUB1::URA3</i> | this study |
| JBY 299 | <i>MATα</i> | <i>ctf8Δ::KanMX6 BIM1-3GFP::HIS3 mCherry-TUB1::URA3</i> | this study |
| JBY 302 | <i>MATa</i> | <i>mcm21Δ::KanMX6 BIM1-3GFP::HIS3 mCherry-TUB1::URA3</i> | this study |
| JBY 242 | <i>MATα</i> | <i>BIM1-HA::LEU2</i> | this study |
| JBY 279 | <i>MATa</i> | <i>BIM1-HA::LEU2 ipl1-321</i> | this study |
| JBY 320 | <i>MATa</i> | <i>bim1-6A-3HA::HIS3::KanMX6</i> | this study |
| JBY 286 | <i>MATa</i> | <i>BIM1-HA::LEU2 cdc15-2</i> | this study |
| JBY 92 | <i>MATa</i> | <i>SHE1-3GFP::HIS3 mCherry-TUB1::URA3</i> | Woodruff et al., 2009 |
| JBY 317 | <i>MATa</i> | <i>SHE1-3GFP::HIS3 mCherry-TUB1::URA3 mcm21Δ::KanMX6</i> | this study |

| | | | |
|---------|---------------------------------|--|--------------------------|
| JBY 334 | <i>MATa</i> | <i>she1-5A-GFP::HIS3 mCherry-TUB1::URA3</i> | this study |
| JBY 304 | <i>MATα</i> | <i>SHE1-13MYC::HIS3</i> | this study |
| JBY 324 | <i>MATa</i> | <i>she1-5A-13MYC::HIS3::URA3:: she1Δ::LEU2</i> | this study |
| JBY 306 | <i>MATa</i> | <i>SHE1-13MYC::HIS3 ipl1-321</i> | this study |
| JBY 325 | <i>MATa</i> | <i>SHE1-13MYC::HIS3 mcm21Δ::KanMX6</i> | this study |
| JBY 325 | <i>MATa/α</i> | <i>SHE1-13MYC::HIS3/+ MCM21-GFP::KanMX6/+</i> | this study |
| JBY 309 | <i>MATa</i> | <i>KIP3-13MYC::HIS3</i> | this study |
| JBY 338 | <i>MATa</i> | <i>KIP3-13MYC::HIS3 ipl1-321</i> | this study |
| JBY 309 | <i>MATa</i> | <i>CDC14-GFP::KanMX6 mCherry-TUB1::URA3</i> | this study |
| JBY 337 | <i>MATa</i> | <i>CDC14-GFP::KanMX6 dbf2Δ::KanMX6 mCherry-TUB1::URA3</i> | this study |
| JBY 335 | <i>MATa</i> | <i>CDC14-GFP::KanMX6 dcc1Δ::KanMX6 mCherry-TUB1::URA3</i> | this study |
| JBY 336 | <i>MATα</i> | <i>CDC14-GFP::KanMX6 ctf8Δ::KanMX6 mCherry-TUB1::URA3</i> | this study |
| JBY 364 | <i>MATα</i> | <i>CDC14-GFP::KanMX6 she1Δ::KanMX6 mCherry-TUB1::URA3</i> | this study |
| JBY 329 | <i>MATa</i> | <i>IPL1-3GFP::HIS3</i> | Nakajima et al., 2009 |
| JBY 339 | <i>MATa</i> | <i>IPL1-3GFP::HIS3 mcm21Δ::KanMX6</i> | this study |
| JBY 271 | <i>MATa</i> | <i>IPL1-3GFP::HIS3 dbf2Δ::KanMX6</i> | this study |
| JBY 280 | <i>MATa</i> | <i>ASE1-4GFP::KanMX6 mCherry-TUB1::URA3 cdh1Δ::KanMX6</i> | Khmelinskii et al., 2007 |
| JBY 254 | <i>MATα</i> | <i>CIN8-4GFP::KanMX6 mCherry-TUB1::URA3</i> | Khmelinskii et al., 2007 |
| JBY 367 | <i>MATα</i> | <i>KIP3-GFP::HIS3 mCherry-TUB1::URA3 SPC42-eqFP::hphNT1</i> | this study |
| JBY 368 | <i>MATα</i> | <i>she1Δ::LEU2 KIP3-GFP::HIS3 mCherry-TUB1::URA3</i> | this study |
| JBY 365 | <i>MATa</i> | <i>dcc1Δ::KanMX6 bim1-6D::KanMX6 MYO1-GFP::HIS3 GFP-TUB1::URA3</i> | Zimniak et al., 2009 |
| | | | |

CHAPTER 3: Dynein-driven mitotic spindle positioning is restricted to anaphase by She1 inhibition of dynactin recruitment

INTRODUCTION

Proper positioning of the mitotic spindle is essential for successful cell division and requires precise coordination of motor protein activity with the cell cycle. In the budding yeast, *Saccharomyces cerevisiae*, the spindle is assembled in the mother cell and must be oriented perpendicular to the bud neck, the future site of cell division, and inserted across the bud neck before chromosome segregation occurs (Yeh et al., 2000). Two partially redundant pathways move the spindle by generating pulling forces on astral microtubules (aMTs) that emanate from the cytoplasmic face of the spindle pole bodies (SPB) (Adames et al., 2000; Shaw et al., 1997). The first pathway utilizes the adenomatous polyposis coli-related protein Kar9p and a type V myosin to orient the spindle and position it adjacent to the bud neck prior to anaphase (Hwang et al., 2003; Kusch et al., 2003; Lee et al., 2003). The second pathway utilizes dynein and its cofactors Bik1p, a CLIP-170 homolog; Kip2p, a kinesin-related protein; and the dynactin complex to position the spindle across the bud neck at anaphase onset (Adames et al., 2000; Lee et al., 2003; Carvalho et al., 2004).

In budding yeast, dynein activity is both spatially and temporally regulated to achieve correct spindle positioning within the dividing cell. Prior to mitosis, dynein is asymmetrically loaded onto the daughter-bound SPB and its associated aMTs (Grava et al., 2006; Segal et al., 2001). This localization ensures unidirectional spindle movement toward the bud and is governed by Cdk1, spindle pole components, and bud neck kinases (Grava et al., 2006). Furthermore, analysis of dynein mutants showed that 1) dynein is necessary for establishing proper spindle position during, but not prior to, anaphase; and 2) cortical aMT-sliding events mediated by dynein motor activity occur only during anaphase (Adames et al., 2000). These data indicate that dynein activity is strictly limited to anaphase.

Dynein activity appears to be cell cycle-regulated in other organisms as well. In the *C. elegans* one-cell-stage embryo, overall dynein-dependent spindle displacement and oscillation increase dramatically during metaphase and climax in anaphase. Modeling studies attribute this change in activity to a gradual increase in dynein motor processivity (Pecreaux et al., 2006), but no molecular mechanism has been revealed. In fact, how dynein-dependent spindle positioning is temporally regulated during the cell cycle has not been determined in any organism.

RESULTS

I set out to uncover determinants of dynein activity by first identifying proteins important for spindle positioning in budding yeast. I reasoned that a protein, She1, could influence spindle positioning based on its reported localization: in addition to appearing along the mitotic spindle, a 3GFP-tagged version of She1 localizes to the bud neck (Figure 3.1 A; Wong et al., 2007), a structure that establishes polarity in the cell and serves as a landmark for spindle position and cell division (Grava et al., 2006). Further analysis revealed that She1-GFP localizes along aMTs in a cell cycle-dependent manner. Greater than 40% of G1 and pre-anaphase cells displayed aMT-localized She1-GFP, whereas less than 10% of anaphase cells displayed aMT-localized She1-GFP (Figure 3.1A,B).

To test directly whether She1 plays a role in orienting the spindle, I monitored pre-anaphase spindle movements in wild-type and *she1Δ* mutant cells expressing GFP-Tub1 (α tubulin) fusion protein. Spindle movement was quantified by measuring the distance between the daughter-bound spindle pole body (dSPB) and the bud neck over time (see Figure 3.1 I for schematic). In wild-type cells, spindles stayed relatively fixed near the bud neck in the mother cell and were oriented perpendicular to the plane of division (Figure 3.1 C, D). However, in *she1Δ* cells, spindles exhibited dramatic movements. These motile spindles were lead by long aMTs that appeared to glide around the cell cortex, reminiscent of dynein-directed cortical aMT sliding normally seen during anaphase. Additionally, approximately 29% of these spindles also traveled back and forth between the mother and daughter cells (Figure 3.1 C, E). To test whether dynein activity was responsible for these dramatic spindle movements, I monitored spindle position in cells lacking both She1 and the dynein heavy chain subunit (Dyn1). Indeed, pre-anaphase spindles in the *she1Δ dyn1Δ* mutant resembled wild-type spindles, lacking any dramatic movement (Figure 3.1 F). I also noticed that *she1Δ* pre-anaphase spindles were longer than wild-type pre-anaphase spindles. Depletion of dynein in *she1Δ* cells restored pre-anaphase spindle length to normal (*she1Δ*: $1.75 \pm 0.4 \mu\text{m}$, $n = 32$; wild-type: $1.34 \pm 0.3 \mu\text{m}$, $n = 19$; *she1Δ dyn1Δ*: $1.28 \pm 0.3 \mu\text{m}$, $n = 15$), suggesting that ectopic dynein activity can “stretch” the spindle. Since dynein ordinarily is inactive prior to anaphase in budding yeast, these results suggest that She1 represses dynein activity until anaphase.

Premature spindle migration between the mother and the daughter cell has been reported in *kar9Δ* cells, raising the possibility that She1 could be an activator of the Kar9 pathway (Yeh et al., 2000). I found that spindle movements in *kar9Δ* cells (Figure 3.1 G) were not as dramatic as those in *she1Δ* cells (Figure 3.1 E), and that addition of the *she1Δ* mutation enhanced the spindle movements seen in *kar9Δ* cells (Figure 3.1 H; mean maximum displacement = $2.93 \pm 1 \mu\text{m}$ (*she1Δ*, $n = 7$), $1.66 \pm 0.8 \mu\text{m}$ (*kar9Δ*, $n = 8$), $3.63 \pm 0.6 \mu\text{m}$ (*she1Δ kar9Δ*, $n = 7$)). Also, I observed no synthetic interactions between the *she1Δ* and *dyn1Δ* alleles (unpublished data). Traditionally, null mutations in all known Kar9p pathway components show synthetic lethal/sick interactions with the *dyn1Δ* mutation (Lee et al., 2003; Grava et al., 2006). These results support the notion that She1 is not an activator of the Kar9p pathway, but rather a repressor of the dynein pathway.

Figure 3.1

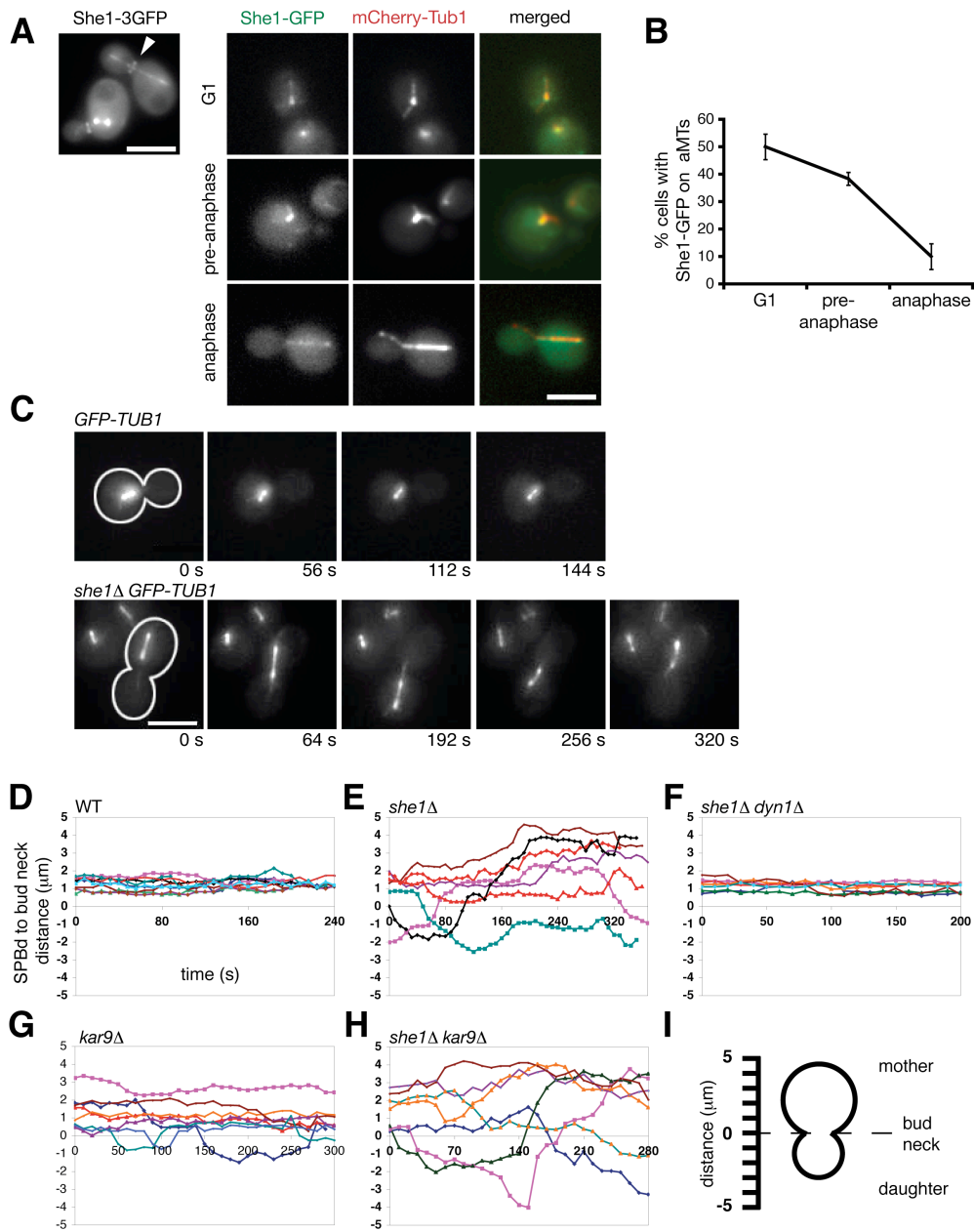


Figure 3.1. She1 is a microtubule and bud-neck-associated protein required to inhibit dynein activity prior to anaphase. (A) She1-3GFP localizes along the entire length of the mitotic spindle and at the bud neck (arrowhead). She1-GFP predominately localizes along astral microtubules in G1 and pre-anaphase cells, but not in anaphase cells. (B) Quantification of She1-GFP localization to aMTs. (C) Time-lapse images of pre-anaphase cells expressing GFP-Tub1. Cells were arrested with hydroxyurea to prevent entry into mitosis. Cell shape is outlined in white. Scale bar, 5 μm . (D-H) Graphs plotting the distances between the daughter-bound SPB (SPBd) and the bud neck over time for cells expressing GFP-Tub1. Each line represents the spindle position for an individual cell. Comparison of spindle position between wild-type (n = 9) (D), *she1* Δ (n = 7) (E), *she1* Δ *dyn1* Δ (n = 7) (F), *kar9* Δ (n = 8) (G), and *she1* Δ *kar9* Δ cells (n = 7) (H). The addition of the *dyn1* Δ mutation, but not the *kar9* Δ mutation, eliminates spindle transiting seen in *she1* Δ cells. (I) Diagram depicting the measurements represented in (D-H). Positive distances indicate that the SPBd was in the mother cell, while negative distances indicate that the SPBd was in the daughter cell.

The results above indicate that She1 inhibits dynein activity prior to anaphase. I next asked if She1 also negatively regulates dynein after anaphase. Once the cell completes anaphase, it must suppress dynein activity to permit proper spindle orientation in the next cell cycle. The absence of aMT-sliding on the cell cortex from late anaphase onward suggests that dynein suppression occurs before the next cell cycle begins (Adames et al., 2000). If She1 is necessary to inactivate dynein during late anaphase, then cortical aMT sliding events may be observed during that time in *she1Δ* cells. To test this hypothesis, I monitored GFP-Tub1-expressing cells undergoing anaphase. In all wild-type cells, the spindle entered the bud, elongated until the spindle poles reached the ends of the dividing cell, and summarily disassembled (n = 7; Figure 3.2 A). In no case did cortical MT sliding occur once the spindle poles reached the cortex. In contrast, in 16 out of 19 *she1Δ* cells, the spindle elongated properly but was then pulled around the cortex, likely by aMTs sliding along the cortex. These forces consequently bent the spindle to create a distinctive curled morphology (Figure 3.2 B and Video S4). Although the presence of aMT-sliding suggests that spindle curling is due to dynein activity, it is still possible that spindle curling is a side effect of spindle over-extension. However, in all *she1Δ dyn1Δ* cells observed, late anaphase spindles remained straight throughout extension, implicating ectopic dynein activity as the cause of spindle curling in *she1Δ* cells (n = 7; Figure 3.2 C). These results, combined with the observation that *kar9Δ* cells do not display spindle curling (data not shown), further support the conclusion that She1 is an inhibitor of dynein and not an activator of the Kar9 pathway.

Occasionally, during spindle curling in *she1Δ* cells, an aMT pulled one spindle pole far enough to penetrate the other cell, resulting in the formation of one cell with two spindle poles and one without any after cytokinesis (2 out of 16 events; Figure 3.3 A). Since chromosomes stay closely attached to the spindle pole throughout the entire cell cycle in yeast, I suspected that spindle curling could cause unequal distribution of chromosomes. I tested this possibility by arresting haploid yeast in G1 and visualizing fluorescently marked chromosome III (Chr III). Wild-type cells possessed only one Chr III (99% with one GFP “dot”), whereas *she1Δ* cells frequently possessed two Chr III’s (18% with two GFP “dots”)(Figure 3.3 B). Further analysis revealed that *she1Δ* cells correctly segregated Chr III in early anaphase, indicating that the unequal distribution of Chr III seen in G1 cells was not a result of chromosome non-disjunction (my unpublished data, not shown). These data suggest that She1 is required to inactivate dynein at the end of anaphase to ensure equal distribution of spindle poles and their associated chromosomes between the mother and daughter cell.

I next addressed how She1 affects dynein activity. The prevailing model for dynein function proposes that dynein is loaded onto aMTs, targeted to the plus ends, and then off-loaded to the cortex. Once anchored at the cortex, dynein uses its minus-end-directed motor activity to pull the attached aMT and the connected spindle toward the site of dynein anchorage (Lee et al., 2003; Li et al., 2005). Because She1 localizes along MTs, I first asked if She1 affects dynein activity indirectly by modifying aMT dynamics. However, there was no significant difference in aMT length, growth rate, or shrinkage rate between *she1Δ* and wild-type cells (Table 3.1). Next, I tested whether She1 interferes with dynein loading onto aMTs and/or recruitment to aMT plus ends. Dynein is found on aMTs throughout the cell cycle, and, although its localization to aMT

Figure 3.2

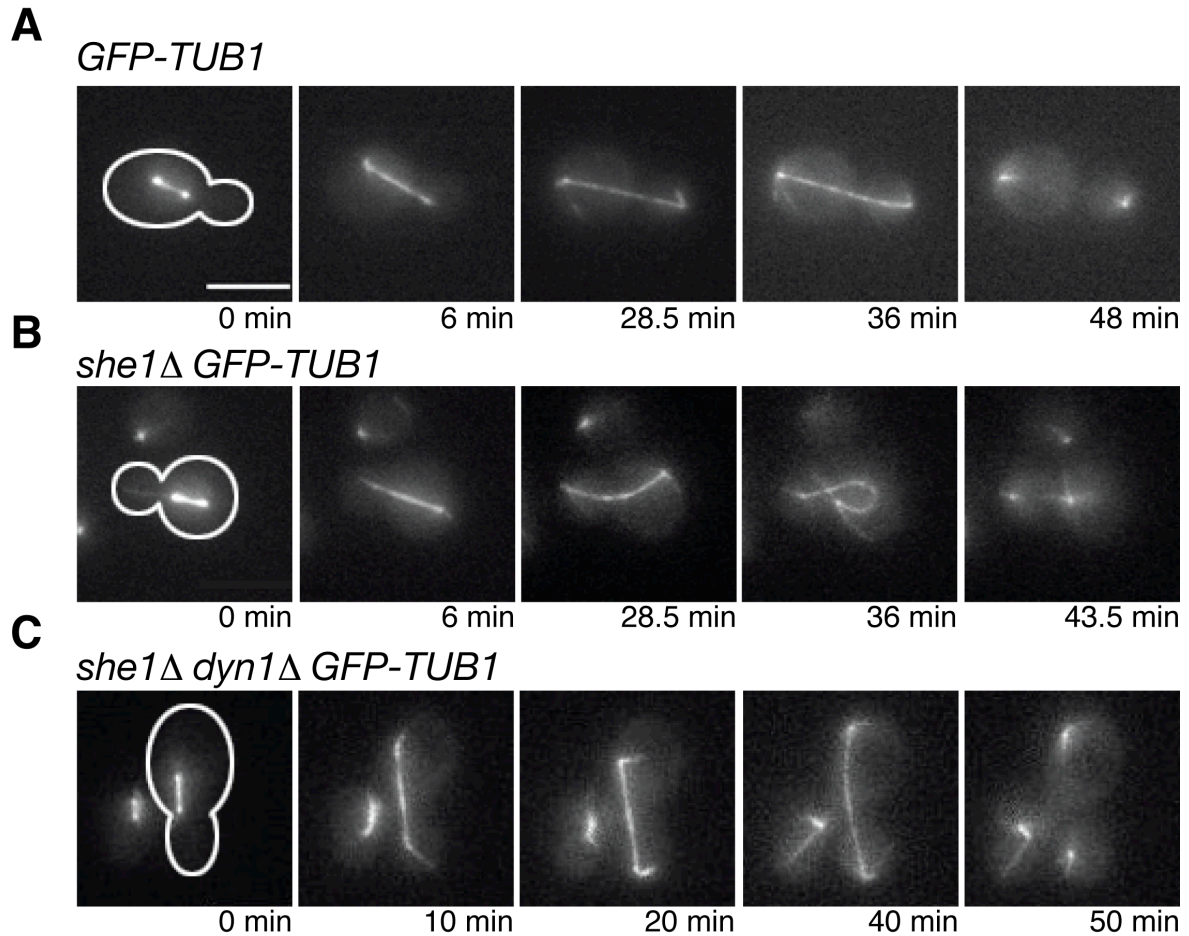


Figure 3.2. She1 is required to repress dynein activity at the end of anaphase. (A-C) Time-lapse images of wild-type, *she1Δ*, and *she1Δ dyn1Δ* anaphase cells expressing GFP-Tub1. Cell shape is outlined in white. Scale bar, 5 μ m. (A) The wild-type spindle remains straight throughout anaphase spindle elongation. (B) Without She1, the spindle poles move around the cortex of the cell and create a distinctive curled morphology. Note the long, cortical astral MT emanating from the motile spindle pole in the mother cell. (C) Addition of the *dyn1Δ* mutation eliminated the spindle curling seen in *she1Δ* cells.

Figure 3.3

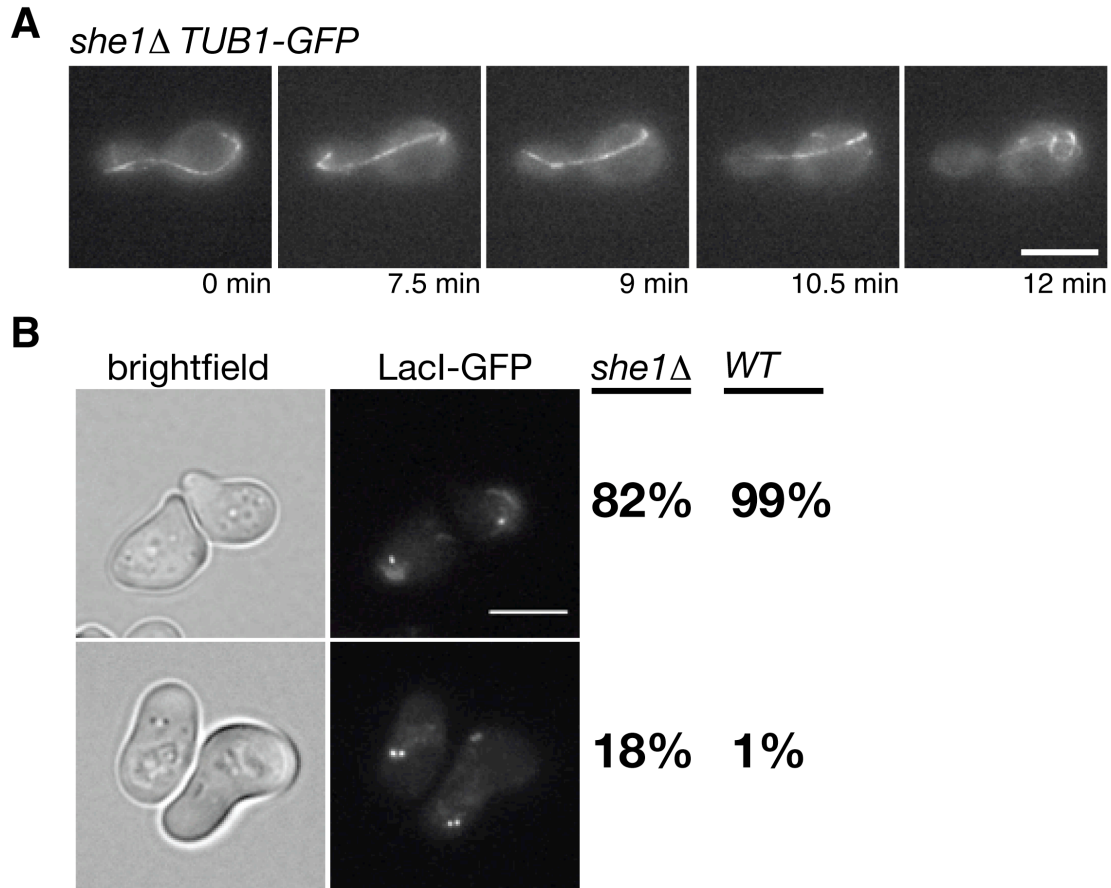


Figure 3.3. Ectopic dynein activity in *she1Δ* cells can cause unequal distribution of spindle poles at the end of mitosis. (A) Images from a time-lapse video featuring a *she1Δ GFP-TUB1* cell undergoing anaphase. One spindle pole leaves the bud and enters the mother cell. At the end of the Video, both spindle poles reside in the same cell. Scale bar, 5 μ m. (B) Analysis of Chr III distribution in wild-type and *she1Δ* cells arrested in G1 with alpha factor. Cells that have faithfully segregated their chromosomes and nuclei possess only one Chr III in G1, which appears as a single fluorescent dot per cell. *she1Δ* cells frequently display two Chr III's, indicating missegregation of chromosomes likely caused by spindle curling seen in (A). Scale bar, 4 μ m.

Table 3.1

| All values are mean \pm standard deviation with sample number (n) | | | |
|---|---------------------|---------------------------------------|----------------|
| | Wild-type | <i>she1</i>Δ | P value |
| aMT growth rate ($\mu\text{m}/\text{min}$) (G1 & pre-anaphase) | 1.37 \pm 0.5 (15) | 1.46 \pm 0.7 (13) | 0.69 |
| aMT shrinkage rate ($\mu\text{m}/\text{min}$) (G1 & pre-anaphase) | 2.54 \pm 0.9 (21) | 2.34 \pm 1.0 (20) | 0.49 |
| Metaphase aMT length (μm) (<i>cdc20</i> arrest) | 2.10 \pm 0.9 (18) | 2.00 \pm 1.1 (23) | 0.76 |
| Anaphase aMT length (μm) (<i>cdc15</i> arrest) | 3.56 \pm 1.4 (44) | 4.18 \pm 1.6 (29) | 0.11 |

Table 3.1. aMT dynamics and lengths in wild-type and *she1* Δ cells. Growth and shrinkage rates were determined by measuring the length of an aMT every 10 sec in living cells expressing GFP-Tub1. aMT lengths were determined using indirect immunofluorescent labeling of endogenous alpha tubulin in fixed cells. Haploid cells contained either a *cdc20-3* or *cdc15-2* allele and were arrested in metaphase or anaphase, respectively, by incubating at 37° C for 2 hours.

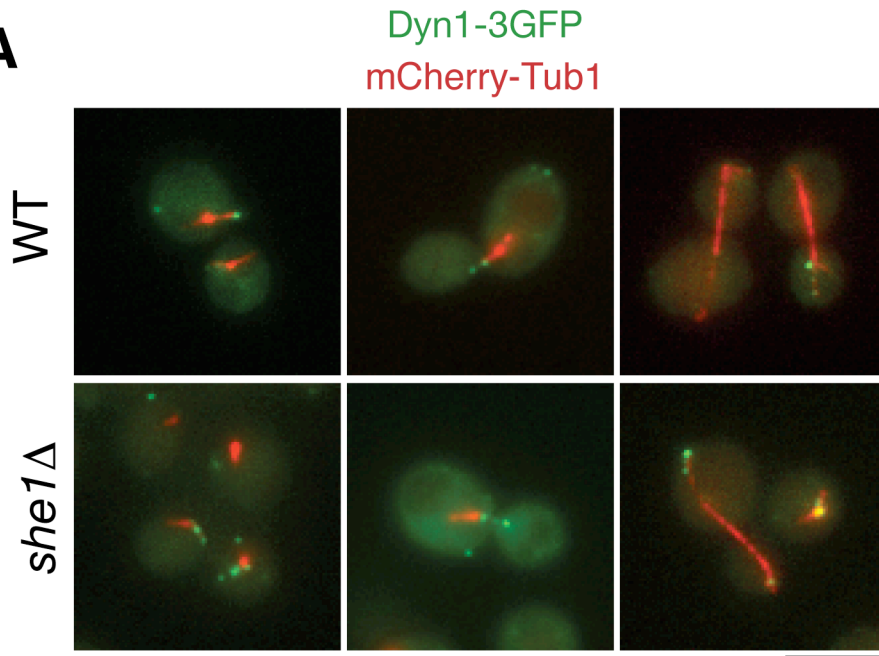
plus ends does increase as the cell enters mitosis, at least 50% of all cells retain dynein at aMT plus ends regardless of cell cycle stage (Sheeman et al., 2003). Therefore, it is unlikely that loading of dynein onto aMTs or its recruitment to the plus end contributes to the cell cycle-dependent regulation of its activity. Nevertheless, I studied the localization of dynein in wild-type and *she1Δ* cells using a 3GFP-tagged version of the dynein heavy chain (Dyn1-3GFP). Consistent with previous reports (Lee et al., 2003; Grava et al., 2006), I observed Dyn1-3GFP at SPBs, aMT plus ends, and the cell cortex in wild-type cells. This localization was unchanged in *she1Δ* cells (Figure 3.4 A). I also found that the percentage of cells with dynein localized to aMT plus ends increased slightly as the cells entered anaphase. Only a small, statistically insignificant change in the amount of plus-end-localized dynein was observed in *she1Δ* cells (G1: $67.9 \pm 8.9\%$ (wt) vs. $85.2 \pm 5.2\%$ (*she1Δ*) $p= 0.14$; pre-anaphase: $84.5 \pm 6.3\%$ vs. $87.3 \pm 0.4\%$ $p= 0.59$; anaphase: $90.3 \pm 2\%$ vs. $92.3 \pm 10.9\%$ $p= 0.82$; Figure 3.4 B). Loss of She1 induces premature dynein activity without affecting dynein localization in pre-anaphase cells, suggesting that She1 inhibits dynein activity by a mechanism other than restricting its loading onto aMTs or recruitment to aMT plus ends.

Another possibility is that She1 regulates a known enhancer of dynein motor function. One such candidate is the multi-subunit dynactin complex, which is essential for dynein activity but dispensable for dynein recruitment to aMTs in yeast (Schroer et al., 2004; Sheeman et al., 2003; Moore et al., 2008). I tested whether She1 regulates dynactin function by monitoring the localization of four prominent dynactin subunits: the p150^{glued} ortholog Nip100, the actin-related protein Arp1, the dynamitin ortholog Jnm1, and the p24 ortholog Ldb18. For visualization, I tagged the endogenous copies of each protein with 3GFP at the C terminus. Haploid cells expressing the Jnm1-3GFP, Ldb18-3GFP and Nip100-3GFP fusions displayed normal spindle positioning and were viable when Kar9 was depleted, indicating that the fusion proteins were functional. However, the Arp1-3GFP fusion was partially functional (see methods). In addition, I co-expressed each 3GFP fusion protein with the microtubule marker mCherry-Tub1. I noticed that reducing the ratio of modified tubulin to wild-type tubulin enhanced dynactin localization to concentrated foci. Hence, I studied dynactin localization in homozygous *TUB1/TUB1* diploid cells with only one copy of the *mCherry-TUB1* allele integrated at the *URA3* locus (see methods). Consistent with previous reports (Moore et al., 2008), in wild-type cells, all four dynactin subunits were found at aMT plus ends, near SPBs, and the cell cortex (Figures 3.5 and 3.6).

I found that the localization of Nip100-3GFP and Arp1-3GFP varied dramatically with the cell cycle. Nip100-3GFP and Arp1-3GFP were largely absent from SPBs or aMTs until anaphase: both proteins were found on SPBs or aMTs in ~25% of G1 and pre-anaphase cells and in ~80% of anaphase cells, representing an ~3.2-fold increase (Figure 3.5 A,C,E,F). When they did appear, Nip100-3GFP and Arp1-3GFP predominately localized to plus ends (unpublished data; Moore et al., 2008). However, in >80% of *she1Δ* cells, Nip100-3GFP and Arp1-3GFP appeared on aMTs regardless of cell cycle stage (Figure 3.5 B,D,E,F), suggesting that She1 governs the cell cycle-dependent recruitment of Nip100 and Arp1 to aMTs. I also considered the possibility that the cell cycle-dependent appearance and disappearance of Nip100 and Arp1 is regulated by changes in protein degradation or expression. However, I

Figure 3.4

A



B

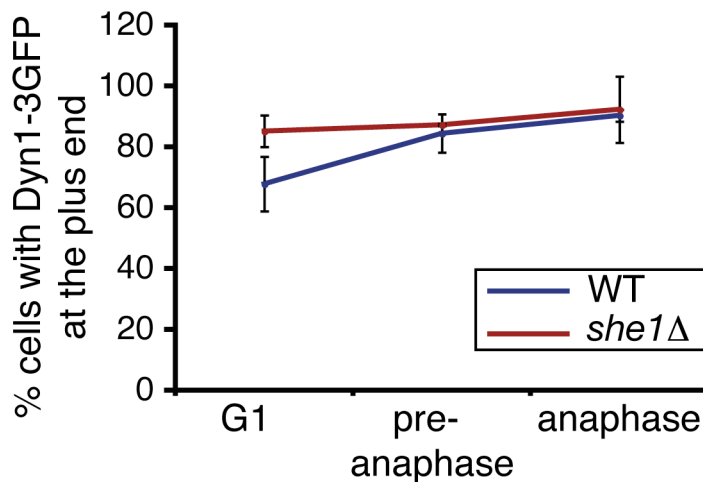


Figure 3.4. Loss of She1 has a modest impact on dynein localization. (A) Two-color images showing Dyn1-3GFP (green) and mCherry-Tub1 (red) localization in wild-type and *she1*Δ cells. Scale bar, 5 μm. (B) Percentage of cells with Dyn1-3GFP present at an astral MT plus end. Loss of She1 slightly enhances Dyn1-3GFP localization at the plus end, but the change is not statistically significant for pre-anaphase and anaphase cells.

Figure 3.5

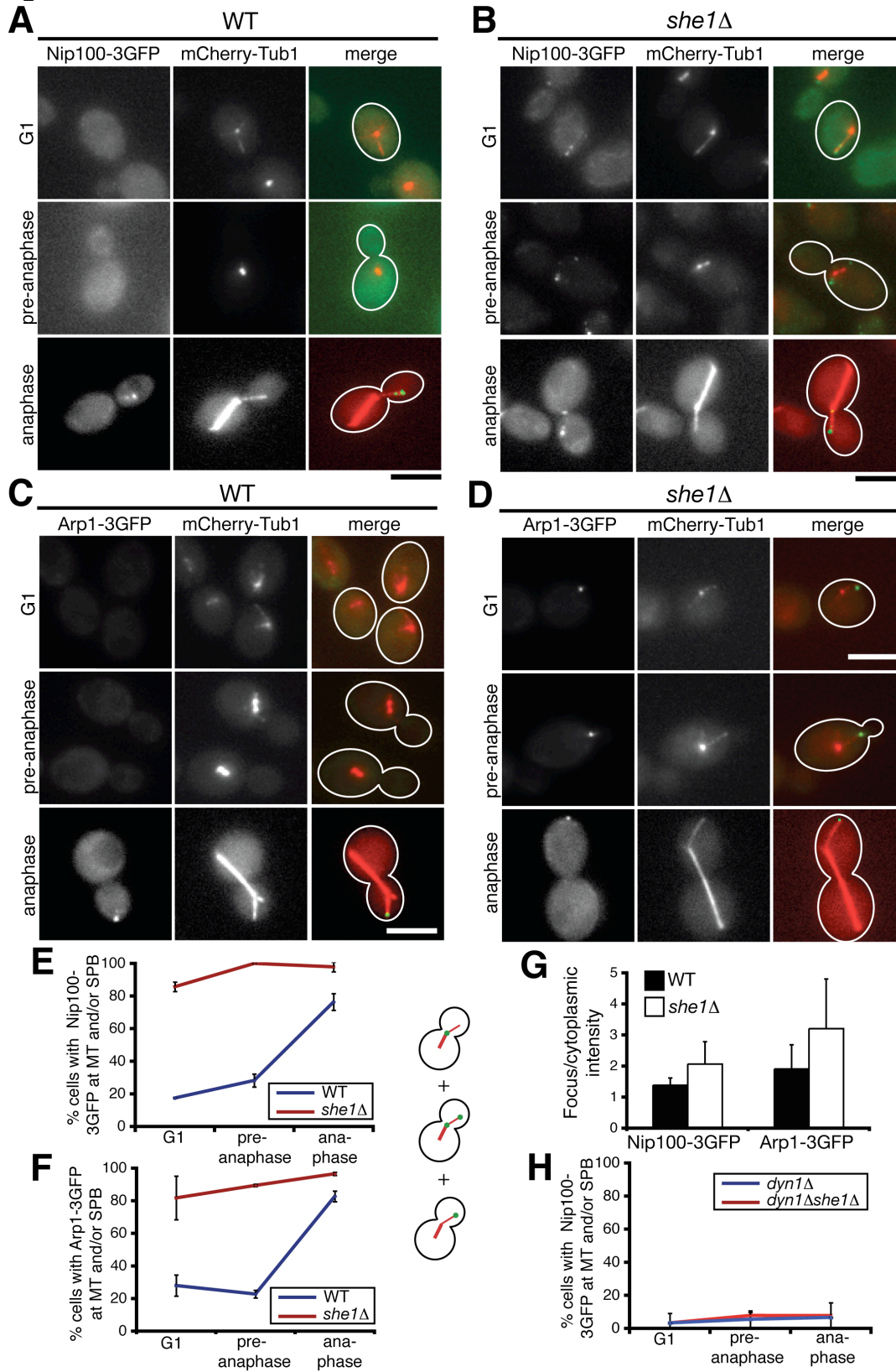


Figure 3.5. She1 affects the cell cycle-dependent localization of the dynactin components Nip100 (p150^{glued}) and Arp1. (A-B) Co-localization of Nip100-3GFP and mCherry-Tub1 in (A) wild-type and (B) *she1Δ* G1, pre-anaphase, or anaphase cells, as indicated. Nip100-3GFP foci are largely absent until anaphase in wild-type cells (A) but are present throughout the cell cycle in *she1Δ* cells (B). (C-D) Co-localization of Arp1-3GFP and mCherry-Tub1 in (C) wild-type and (D) *she1Δ* G1, pre-anaphase, or anaphase cells, as indicated. Localization of Arp1-3GFP is similar to localization of Nip100-3GFP. Scale bars, 5 μm. (E-F) The percentage of cells with Nip100-3GFP (E) or Arp1-3GFP (F) foci at aMTs and/or SPBs as a function of cell cycle stage (n > 45). (G) Ratio of the fluorescence intensity of Nip100-3GFP and Arp1-3GFP localized in foci versus the cytoplasm in wild-type and *she1Δ* cells (n = 23-30). (H) The percentage of *dyn1Δ* or *dyn1Δ she1Δ* cells with Nip100-3GFP localized to aMTs or SPBs (n = 90). Dyn1 is required for Nip100-3GFP localization to aMTs. All error bars represent standard deviation.

found that the presence of She1 had no detectable impact on Nip100 or Arp1 protein levels in asynchronous, G1, and pre-anaphase cells (Figure 3.6 A and my unpublished data, not shown). Yet, the ratio of Nip100-3GFP and Arp1-3GFP fluorescence detected in MT-associated foci vs. the cytoplasm was ~50% higher in anaphase *she1Δ* cells than in anaphase wild-type cells (Figure 3.5 G), supporting the idea that more Nip100 and Arp1 are recruited to aMTs from the cytoplasmic pool in the absence of She1. I then asked whether dynactin recruitment to aMTs occurs via direct binding to the microtubule or indirectly through dynein. I observed that Nip100-3GFP localization to SPBs and aMTs was almost entirely eliminated in both *dyn1Δ* and *dyn1Δshe1Δ* cells, suggesting that dynactin is recruited to aMTs through its interaction with dynein (Figure 3.5 H). This result is consistent with the report that a mutant version of p150^{glued} lacking its MT-binding domain still localizes to MTs in *Drosophila melanogaster* S2 cells (Kim et al., 2007). Overall, these data suggest that She1 precludes the interaction of dynein and dynactin prior to anaphase.

Interestingly, the behavior of Jnm1 and Ldb18 differed from the behavior of the other dynactin subunits. Unlike Nip100-3GFP and Arp1-3GFP, Jnm1-3GFP and Ldb18-3GFP almost always localized in foci associated with SPBs or aMTs throughout the cell cycle in wild-type cells (Fig 3.7 A,C,E,F). In G1 and pre-anaphase cells, the majority of Jnm1-3GFP and Ldb18-3GFP foci localized at or very near SPBs (Figure 3.7 A,C, my unpublished data, not shown). However, similar to Arp1-3GFP and Nip100-3GFP, the frequency of Jnm1-3GFP and Ldb18-3GFP on aMTs increased ~3.4-fold as cells entered anaphase (Figure 3.7 A,C,G,H). Again, loss of She1 eliminated the dramatic cell cycle-dependent change in Jnm1-3GFP and Ldb18-3GFP localization and enhanced the presence of both subunits on aMTs (Figure 3.7 B,D,G,H). These results suggest that She1 inhibits Jnm1 and Ldb18 recruitment to aMTs until anaphase. The difference in localization patterns of Jnm1, Ldb18, Arp1, and Nip100 suggests that the dynactin complex could exist in subcomplexes. Indeed, only ~60% of Jnm1-tdTomato foci co-localized with Nip100-3GFP foci in asynchronous wild-type cells (n = 114; Figure 3.8 A). The presence of dynactin subcomplexes is further supported by previous co-sedimentation and co-immunoprecipitation experiments that identified large pools of Jnm1 and Ldb18 unassociated with Nip100 and Arp1 (Moore et al., 2008; Amaro et al., 2008). Given these findings, and my observations that Jnm1 and Ldb18 localize to SPBs throughout the cell cycle but appear on aMTs only during anaphase, it is possible that the complete dynactin complex is assembled during anaphase from two spatially segregated subcomplexes: 1) an SPB-localized subcomplex that contains Jnm1 and Ldb18, and 2) a cytoplasmic subcomplex that contains Nip100 and Arp1. However, roughly equal amounts of Jnm1-3HA co-immunoprecipitated with Nip100-3GFP in G1, pre-anaphase, and asynchronous wild-type cells, suggesting that a complete version of the dynactin complex exists throughout the cell cycle (Figure 3.8 B). In addition, time-lapse microscopy following a cell entering anaphase showed that Jnm1 suddenly appeared at the aMT plus end, rather than being transported there from the SPB (Figure 3.8C). Furthermore, after photobleaching SPB-localized Jnm1-3GFP signal, I observed an increase in GFP fluorescence on the aMT but no recovery at the SPB (Figure 3.8 D), ruling out the possibility that aMT-localized Jnm1-3GFP foci result from transport and concentration of undetectable amounts of SPB-localized Jnm1-3GFP. The fact that I never observed recovery of fluorescence at the SPB indicates

Figure 3.6

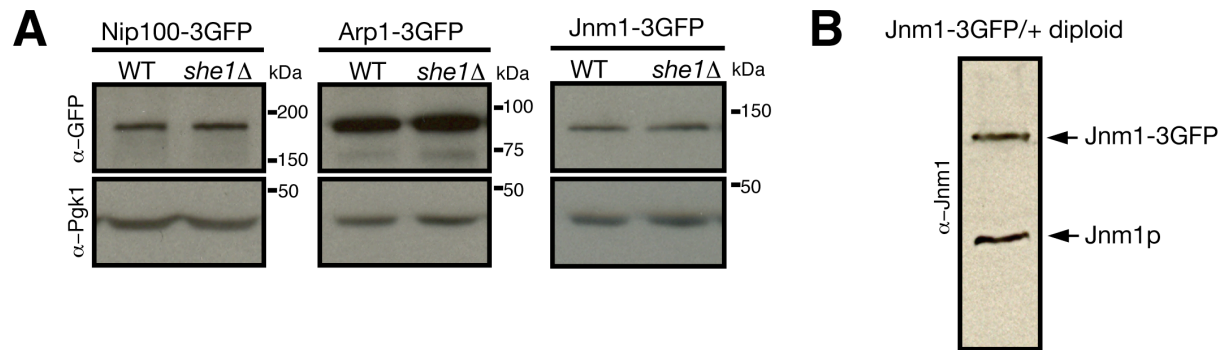


Figure 3.6. Expression levels of tagged dynactin subunits. (A) Western blots of Nip100-3GFP, Arp1-3GFP, Jnm1-3GFP and Pgk1p as a control from asynchronous wild-type or *she1Δ* whole cell extracts. (B) Whole cell extract from a JNM1-3GFP/JNM1 diploid immunoblotted with anti-Jnm1 antibody. The 3GFP tag has little effect on Jnm1 stability or expression.

that the Jnm1 localized there comprises a static structure (Figure 3.8E). Therefore, the Jnm1 that appeared on the aMT was recruited from the cytoplasm, most likely in complex with the other dynactin subunits. In total, these results suggest that the dynactin complex is present as complete and incomplete varieties, and that She1 specifically hinders recruitment of the complete version to aMTs until anaphase.

Figure 3.7

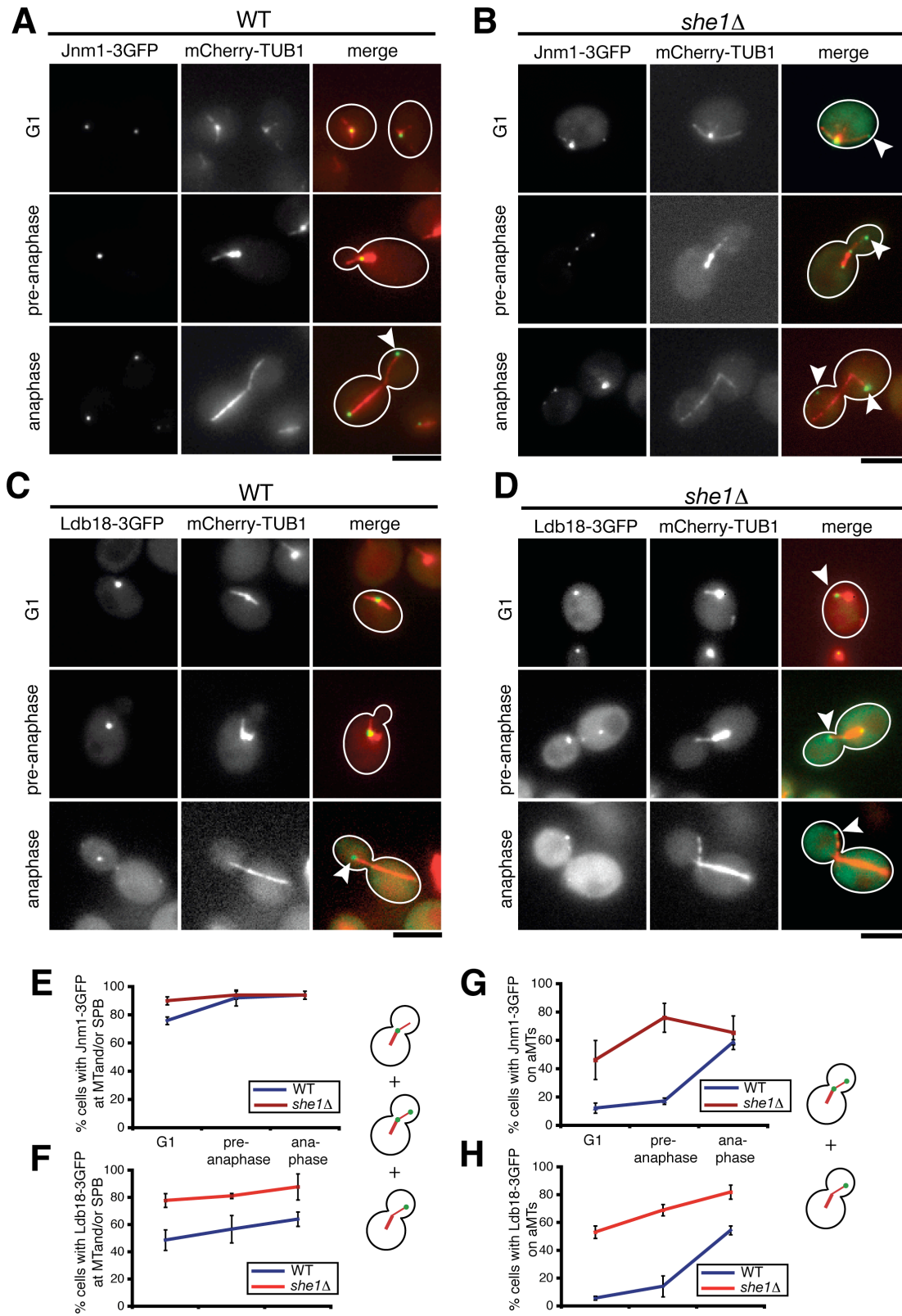


Figure 3.7. She1 affects the cell cycle-dependent recruitment of Jnm1 (dynamitin) and Ldb18 (p24) to astral MTs. (A-B) Co-localization of Jnm1-3GFP and mCherry-Tub1 in (A) wild-type and (B) *she1Δ* G1, pre-anaphase, or anaphase cells, as indicated. (C-D) Co-localization of Ldb18-3GFP and mCherry-Tub1 in (C) wild-type and (D) *she1Δ* G1, pre-anaphase, or anaphase cells, as indicated. Jnm1-3GFP and Ldb18-3GFP foci primarily localize to SPBs in G1 and pre-anaphase cells and then appear on aMTs during anaphase. White arrowheads denote Jnm1-3GFP or Ldb18-3GFP localized at an astral MT plus end. Loss of She1 permits enhanced association of Jnm1-3GFP and Ldb18-3GFP with aMTs throughout the cell cycle. Scale bars, 5 μ m. (E-F) The percentage of cells with Jnm1-3GFP (E) or Ldb18-3GFP (F) foci localized to aMTs and/or SPBs as a function of cell cycle stage. (G-H) Percentage of cells with Jnm1-3GFP (G) or Ldb18-3GFP (H) present on astral MTs (n > 50). Error bars represent standard deviation.

Figure 3.8

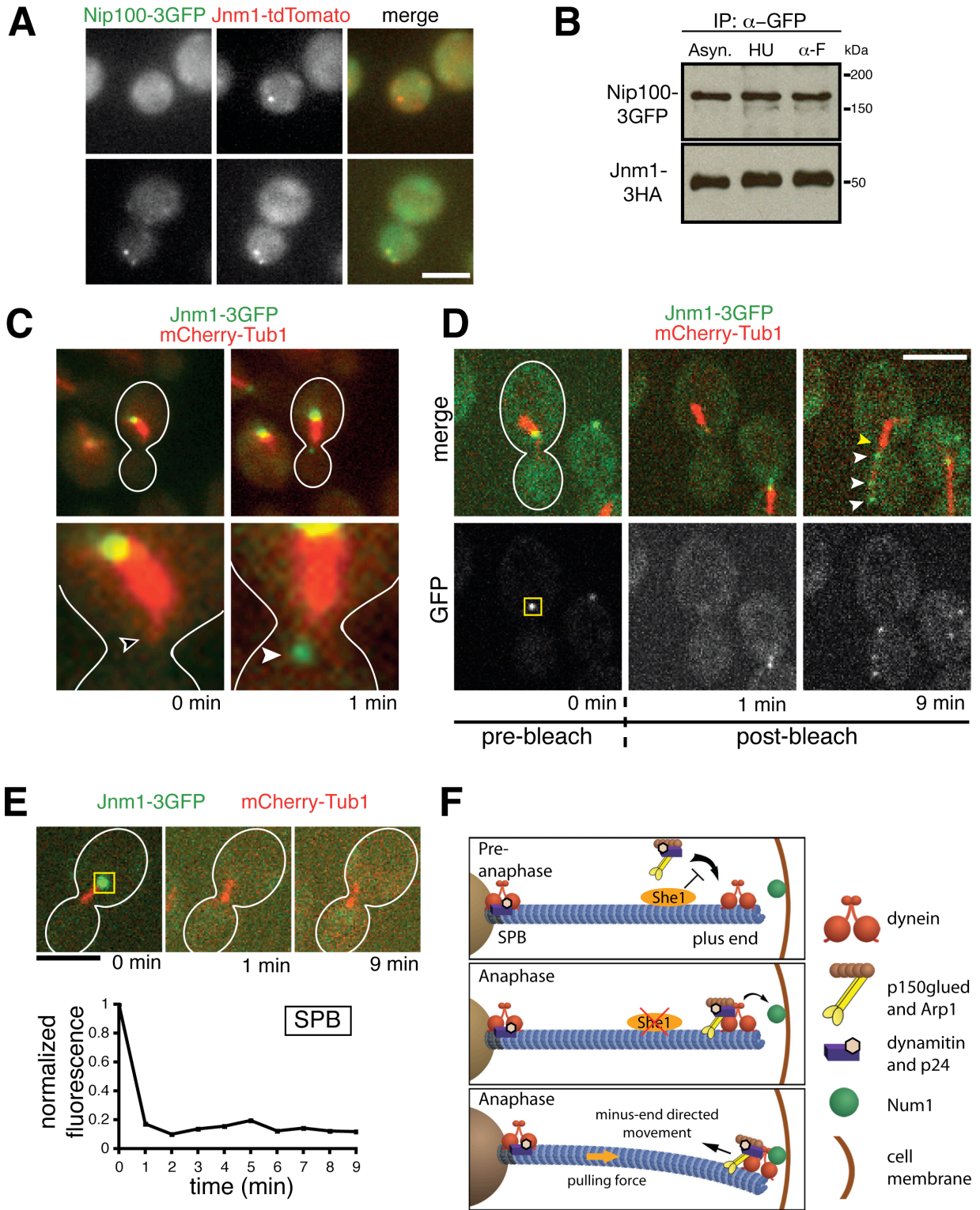


Figure 3.8. Dynactin exists in complete and incomplete complexes that are spatially distinct. (A) Approximately 60% of Jnm1-tdtomato co-localizes with Nip100-3GFP in asynchronous cells (n = 114). (B) Immunoprecipitation of Nip100-3GFP from asynchronous (Asynch), hydroxyurea-arrested (HU), and alpha factor-arrested (α -F) cells. Essentially equal amounts of Jnm1-3HA co-purify with Nip100-3GFP at different cell cycle stages, indicating that a complete dynactin complex exists throughout the cell cycle. (C) Prior to anaphase, Jnm1-3GFP localizes to the SPB but is absent from the aMT plus end (unfilled arrowhead). Near the anaphase transition, Jnm1-3GFP suddenly appeared at the plus end (filled arrowhead), rather than being transported from the SPB. Anaphase onset was indicated by rapid elongation of the mitotic spindle shortly after Jnm1-3GFP appeared on the aMT (not shown). (D) Jnm1-3GFP fluorescence at the SPB was photobleached in pre-anaphase cells. The yellow box represents the area that was photobleached at t = 0.5 min. Appearance of GFP foci (white arrowheads) occurred along the aMT as the cell entered anaphase. There was no recovery of GFP fluorescence at the SPB (yellow arrowhead). (E) The GFP fluorescence at the SPB in a different cell also did not recover following photobleaching, indicating that SPB-localized dynactin subcomplexes are very static. The yellow box represents the area that was photobleached at t = 0.5 min. Scale bars, 5 μ m. (F) A model for cell cycle control of dynein activation. She1 precludes stable association of the complete dynactin complex with dynein until anaphase.

DISCUSSION

The majority of the work detailing mitotic spindle positioning has focused on activation of the Kar9 and dynein pathways. Less studied, but equally important, is the issue of how these pathways are silenced to prevent unnecessary spindle movement. In this study, I explored the mechanisms that restrict dynein-dependent spindle positioning to anaphase in the budding yeast, *S. cerevisiae*. I obtained strong genetic evidence that She1 is an inhibitor of dynein activity *in vivo*. Also, I found that the dynactin complex is a dynamic entity whose localization is coordinated with the cell cycle. She1 regulates the localization of dynactin, preventing the complete complex from associating with aMTs, via dynein, until anaphase.

Connection between She1 and the dynactin complex

My results indicate that She1 hinders the stable interaction between dynein and dynactin by a mechanism that remains to be determined. Unfortunately, I cannot predict She1 function based on amino acid sequence, as I was unable to identify any instructive homology to previously characterized proteins. I have also purified She1p from yeast and analyzed co-purifying proteins by mass spectrometry; however, no previously known dynein pathway components were identified (my unpublished data, not shown). Nevertheless, my data support the conclusion that She1 specifically affects dynactin. Loss of She1 dramatically enhances dynactin recruitment to aMTs. The frequency of G1 and pre-anaphase cells displaying aMT-associated dynactin is approximately 4 times higher for *she1Δ* cells than for wild-type cells. This effect is not an indirect consequence of alterations in aMT dynamics or length, because She1 has no significant impact on these parameters. Also, it is unlikely that the change in dynactin localization is due to enhanced function of other MT-bound proteins needed for dynein activity. Dynein plus-end localization requires proper functioning of NudEL, CLIP170, and LIS1 (Li et al., 2005). Because She1 has little impact on dynein recruitment to aMTs or tracking to the plus ends, She1 likely does not affect the activity of NudEL, CLIP170, and LIS1.

Currently, I suspect that She1 may impact dynein-dynactin interaction indirectly through a phosphorylation-dependent mechanism. Over-expression of the protein phosphatase I co-factor Bud14 in budding yeast causes dynein-dependent spindle transiting in pre-anaphase cells (Knaus et al., 2005). This phenotype is similar to the one that I have observed in *she1Δ* cells. In addition, Vaughan et al. (2001) reported that phosphorylation of the dynein intermediate chain (DIC) disrupts binding of p150^{glued} to dynein. These studies both argue for dephosphorylation of DIC as a means to regulate dynein activity. It is enticing to speculate that She1 inhibits dynactin association with dynein by encouraging DIC phosphorylation. However, it is equally possible that other factors, including She1 itself, are phospho-targets.

Possibility of Dynactin Subcomplexes

Rate-zonal sedimentation experiments (Amaro et al., 2008; Moore et al., 2008) revealed pools of p24 (Ldb18) and dynamitin (Jnm1) that did not sediment with the other dynactin subunits, raising the possibility that dynactin subunits could form subcomplexes with discrete functions. These studies, however, did not report any major differences in dynactin subunit localization. It is possible that these studies reached this

conclusion because their analyses focused on anaphase cells, when the localization of all dynactin subunits to aMTs is most prominent. In my study, I examined cells at different cell cycle stages and noticed that dynamitin and p24 shared a localization pattern that differed from the p150^{glued} and Arp1 localization pattern. While all four subunits appeared on aMTs primarily during anaphase, dynamitin and p24 localized to SPBs throughout the cell cycle. Thus, the SPB-localized dynamitin and p24 subunits could comprise a subcomplex distinct from the aMT-localized complete dynactin complex. This possibility is consistent with findings from Moore *et al.* (2008) that dynamitin and p24 still localize to SPBs, but not aMTs, in the absence of p150^{glued}.

Due to the sensitivity of dynactin to modification of its subunits, especially dynamitin, which disrupts the complex when over-expressed (Schroer, 2004), it is possible that the SPB localization of dynamitin and p24 is an artifact caused by addition of the 3GFP tag. However, both Jnm1-3GFP and Ldb18-3GFP are functional because they rescue the nuclear migration defect characteristic of *jnm1Δ* and *ldb18Δ* null mutants (see methods). In addition, I verified that the 3GFP did not alter expression or stability of Jnm1 (Figure 3.6 B). Finally, the localization data corroborates the biochemical analysis of native Jnm1 and Ldb18 performed by Amaro *et al.* (2008) and Moore *et al.* (2008).

Cell cycle regulation of She1p activity

My data suggest that She1 activity is also regulated in a cell cycle stage-dependent manner. Activation of the anaphase promoting complex/cyclosome (APC/c) triggers movement of the anaphase spindle into the bud (Ross *et al.*, 2004). However, it is unlikely that She1 activity is silenced through APC/c-mediated degradation since She1 protein levels remain unchanged throughout anaphase (Figure 3.1 A and my unpublished data, not shown). Instead, considering that She1-GFP localization along aMTs drastically diminishes during anaphase, it is likely that She1 activity is regulated through its controlled loading and removal from aMTs. In the future, it will be worthwhile to uncover the factors that determine She1 localization.

Model for cell cycle regulation of dynein

Based on my work and previous studies, I propose that cell cycle-regulated association between dynein and dynactin controls dynein-driven spindle positioning (Figure 3.8 F). In this model, there exist at least two versions of dynactin: an incomplete version located at the SPB containing at least dynamitin (Jnm1) and p24 (Ldb18), and a complete version located in the cytoplasm containing at least dynamitin, p24, Arp1, and p150^{glued} (Nip100). Before anaphase, She1 inhibits association of the complete dynactin complex with dynein, thus rendering dynein inactive. During anaphase, removal of She1 from the aMT permits binding of the complete dynactin complex with dynein, which then stimulates dynein motor activity and primes it for off-loading onto the cell cortex. As a result, dynein pulls the spindle into the bud only during anaphase.

Coordination of spindle positioning with the cell cycle requires precise control of microtubule-bound motor proteins like dynein. This work provides a possible explanation for how dynein becomes active strictly during anaphase in budding yeast. Given that the proteins and mechanisms involved in dynein-dependent spindle

positioning are evolutionarily conserved throughout eukaryotes (Gomes et al., 2005), I expect my findings to be generally applicable.

SUMMARY

Dynein is a minus-end-directed microtubule motor important for mitotic spindle positioning. In budding yeast, dynein activity is restricted to anaphase when the nucleus enters the bud neck, yet the nature of the underlying regulatory mechanism is not known. Here, the microtubule-associated protein She1 is identified as a novel regulator of dynein activity. In *she1Δ* cells, dynein is activated throughout the cell cycle, resulting in aberrant spindle movements that mis-position the spindle. I also found that dynactin, a cofactor essential for dynein motor function, is a dynamic complex whose recruitment to astral microtubules (aMTs) increases dramatically during anaphase. Interestingly, loss of She1 eliminates the cell cycle-regulation of dynactin recruitment and permits enhanced dynactin accumulation on aMTs throughout the cell cycle. Furthermore, localization of the dynactin complex to aMTs requires dynein, suggesting that dynactin is recruited to aMTs via interaction with dynein and not the microtubule itself. Lastly, I present evidence supporting the existence of an incomplete dynactin subcomplex localized at the SPB, and a complete complex that is loaded onto aMTs from the cytoplasm. I propose that She1 restricts dynein-dependent spindle positioning to anaphase by inhibiting the association of dynein with the complete dynactin complex.

MATERIALS AND METHODS

Yeast strains and media. The yeast strains used in this study are listed in Table 3.2. The *she1* Δ null mutant was generated by PCR product-mediated gene deletion (Longtine et al., 1998). Other null mutants originated from the Research Genetics Collection. *Jnm1-3HA* and *Jnm1-tdTomato* were generated by inserting PCR-amplified *3HA::HIS3* or *tdTomato::KanMX* cassettes at the 3' end of *Jnm1* at its endogenous locus (Longtine et al., 1998, Shaner et al., 2004). For construction of 3GFP-tagged strains, ~500bp fragments of the *DYN1*, *JNM1*, *ARP1*, *LDB18*, and *NIP100* open reading frames were subcloned into the BamHI site of pYS47 (Wong et al., 2007). A (GlyAla)₃ linker was inserted between each gene and the 3GFP sequence. Each resulting plasmid was linearized and transformed into a haploid strain to integrate the fusion construct at the endogenous locus. The resulting strains showed no visible defects in spindle positioning. Furthermore, the *DYN1-3GFP*, *JNM1-3GFP*, *LDB18-3GFP*, and *NIP100-3GFP* alleles showed no synthetic growth defects in combination with a *kar9* Δ allele. However, the *ARP1-3GFP kar9* Δ strain was slightly sick. Thus, the *DYN1-3GFP*, *JNM1-3GFP*, *LDB18-3GFP* and *NIP100-3GFP* fusions were completely functional, while the *ARP1-3GFP* fusion was partially functional.

I found that the localization of *Jnm1-3GFP*, *Nip100-3GFP*, and *Arp1-3GFP* to MTs was impaired in haploid cells expressing *mCherry-Tub1* (a generous gift from E. Schiebel; Khmelinskii et al., 2007) in combination with one copy of *Tub1p*. MT-associated localization of dynactin was restored when I increased expression of wild-type alpha tubulin. Therefore, I performed all of the dynactin visualization experiments using diploid strains heterozygous for the *mCherry-TUB1* allele integrated at the *URA3* locus and homozygous for wild-type *TUB1*. (*mCherry-TUB1::URA3/ura3-52; TUB1/TUB1*).

Fluorescence microscopy. Images were obtained using an Olympus IX-71 microscope, 100X NA 1.4 objective and an Orca-ER camera (Hamamatsu, Hamamatsu City, Japan). Two-color images were obtained by sequential switching between RFP and GFP filter sets. For GFP-Tub1 time-lapse microscopy of pre-anaphase spindle movement, images were collected at 10 s intervals with 300 ms exposures. For time-lapse microscopy of spindle elongation, images were collected at 90 s intervals for 55 min. Each image represents a maximum intensity projection from a Z-stack containing 6-9 planes 0.2 μ m apart. To determine the foci/cytoplasmic ratio of *Arp1-3GFP* and *Nip100-3GFP* fluorescence, fluorescence intensity of a GFP spot (referred to as a "focus"), the adjacent cytoplasm, and background were measured using a 5 x 5 pixel area. Background intensity was subtracted from the GFP spot and cytoplasm intensity values before the ratio was calculated. All image processing was performed using Metamorph software.

Photobleaching. Photobleaching was performed using a Zeiss AxioObserver fluorescence microscope equipped with a spinning-disk confocal head (Solamere Technology Group) and a Cascade II EMCCD camera (Photometrics). Location of laser ablation was controlled using a MicroPoint system (Photonic Instruments). Areas to be photobleached were subjected to two iterations of 3 pulses from a UV laser.

Immunoblotting. To detect Jnm1-3GFP, Arp1-3GFP, and Nip100-3GFP, the upper half of the membrane (containing proteins >75 kDa) was probed with 1:2,500 anti-GFP (Torrey Pines Biolabs) and 1:5,000 anti-rabbit HRP-conjugated antibody (GE Healthcare). To detect Pgc1, the lower half of the membrane (containing proteins <75 kDa) was probed with 1:10,000 anti-Pgc1 (Molecular Probes) and 1:10,000 anti-mouse HRP-conjugated antibody (GE Healthcare). To detect Jnm1-3HA, the membrane was probed with 1:1,000 rabbit anti-HA (Covance, HA.11). To detect Jnm1, the membrane was probed with 1:1,000 rabbit anti-Jnm1p serum (a gift from Kelly Tatchell).

Immunoprecipitation. Immunoprecipitation was performed essentially as described previously (Moore et al., 2008) with the follow exceptions, Lysates were incubated with rabbit anti-GFP antibody for one hour and then passed over protein A sepharose beads (Amersham Biosciences) to purify Nip100-3GFP. The column was washed with lysis buffer and eluted with SDS loading buffer.

Table 3.2. Yeast strains and plasmids used in this study.

| Yeast strains | | | |
|---------------|---|---|---------------------|
| Strain name | | genotype | source |
| JBY 1 | <i>MATα</i> | <i>she1Δ::LEU2 leu2-3,112 lys2-801 his3Δ200 ura3-52</i> | this study |
| JBY 65 | <i>MATα</i> | <i>SPC42-mCherry::KanMX SHE1-3GFP::HIS3 leu2-3,112 lys2-801 his3Δ200 ura3-52</i> | this study |
| JBY 39 | <i>MATα</i> | <i>ura3-52::GFP-TUB1::URA3 leu2-3,112 lys2-801 his3Δ200</i> | this study |
| JBY 70 | <i>MATα</i> | <i>ura3-52::GFP-TUB1::URA3 she1Δ::LEU2 dyn1Δ::KanMX leu2-3,112 lys2-801 his3Δ200</i> | this study |
| JBY 75 | <i>MATα</i> | <i>ura3-52::GFP-TUB1::URA3 she1Δ::LEU2 kar9Δ::KanMX leu2-3,112 lys2-801 his3Δ200</i> | this study |
| JBY 89 | <i>MATα</i> | <i>DYN1-3GFP::HIS3 pHIS::mCherry-TUB1::URA3 leu2-3,112 lys2-801 his3Δ200 ura3-52</i> | this study |
| JBY 87 | <i>MATα</i> | <i>DYN1-3GFP::HIS3 pHIS::mCherry-TUB1::URA3 she1Δ::LEU2 leu2-3,112 lys2-801 his3Δ200 ura3-52</i> | this study |
| JBY 98 | <i>MATα</i> | <i>NIP100-3GFP::HIS3 she1Δ::LEU2 leu2-3,112 lys2-801 his3Δ200 ura3-52</i> | this study |
| JBY 100 | <i>MATα</i> | <i>NIP100-3GFP::HIS3 leu2-3,112 lys2-801 his3Δ200 ura3-52</i> | this study |
| JBY 102 | <i>MATα</i> | <i>ARP1-3GFP::HIS3 she1Δ::LEU2 leu2-3,112 lys2-801 his3Δ200 ura3-52</i> | this study |
| JBY 104 | <i>MATα</i> | <i>ARP1-3GFP::HIS3 leu2-3,112 lys2-801 his3Δ200 ura3-52</i> | this study |
| JBY 106 | <i>MATα</i> | <i>JNMI-3GFP::HIS3 she1Δ::LEU2 leu2-3,112 lys2-801 his3Δ200 ura3-52</i> | this study |
| JBY 108 | <i>MATα</i> | <i>JNMI-3GFP::HIS3 leu2-3,112 lys2-801 his3Δ200 ura3-52</i> | this study |
| JBY 117 | <i>MATα/α</i> | <i>ura3-52::pHIS::mCherry-TUB1::URA3/ura3-52; NIP100-3GFP::HIS3/NIP100-3GFP::HIS3; she1Δ::LEU2/she1Δ::LEU2 leu2-3,112 lys2-801 his3Δ200</i> | this study |
| JBY 118 | <i>MATα/α</i> | <i>ura3-52::pHIS::mCherry-TUB1::URA3/ura3-52; NIP100-3GFP::HIS3/NIP100-3GFP::HIS3 leu2-3,112 lys2-801 his3Δ200</i> | this study |
| JBY 119 | <i>MATα/α</i> | <i>ura3-52::pHIS::mCherry-TUB1::URA3/ura3-52; ARP1-3GFP::HIS3/ARP1-3GFP::HIS3; she1Δ::LEU2/she1Δ::LEU2 leu2-3,112 lys2-801 his3Δ200</i> | this study |
| JBY 120 | <i>MATα/α</i> | <i>ura3-52::pHIS::mCherry-TUB1::URA3/ura3-52; ARP1-3GFP::HIS3/ARP1-3GFP::HIS3 leu2-3,112 lys2-801 his3Δ200</i> | this study |
| JBY 121 | <i>MATα/α</i> | <i>ura3-52::pHIS::mCherry-TUB1::URA3/ura3-52; JNMI-3GFP::HIS3/JNMI-3GFP::HIS3; she1Δ::LEU2/she1Δ::LEU2 leu2-3,112 lys2-801 his3Δ200</i> | this study |
| JBY 122 | <i>MATα/α</i> | <i>pHIS::mCherry-TUB1::URA3/ura3-52; JNMI-3GFP::HIS3/JNMI-3GFP::HIS3</i> | this study |
| JBY 57 | <i>MATα</i> | <i>she1Δ::LEU2 ura3-52::GFP-TUB1::URA3 leu2-3,112 lys2-801 his3Δ200</i> | this study |
| JBY 10 | <i>MATα</i> | <i>she1Δ::LEU2 HIS3::pCu-LacI-GFP leu2-3,112::lacO::LEU2 leu2-3,112 lys2-801 his3Δ200 ura3-52</i> | this study |
| JBY 16 | <i>MATα</i> | <i>HIS3::pCu-LacI-GFP leu2-3,112::lacO::LEU2 leu2-3,112 lys2-801 his3Δ200 ura3-52</i> | this study |
| JBY 136 | <i>MATα</i> | <i>dyn1Δ::KanMX his3Δ1 leu2Δ0 lys2Δ0 ura3Δ0</i> | Res. Gen Collection |
| JBY 137 | <i>MATα</i> | <i>kar9Δ::KanMX his3Δ1 leu2Δ0 lys2Δ0 ura3Δ0</i> | Res. Gen Collection |
| JBY 131 | <i>MATα</i> | <i>JNMI-tdtomato::KanMX NIP100-3GFP::HIS3 LEU2 leu2-</i> | this study |

| | | | |
|-----------------|---------------|---|--------------------------|
| | | <i>3,112 lys2-801 his3Δ200 ura3-52</i> | |
| JBY 178 | <i>MATa</i> | <i>JNM1-3HA::HIS3 NIP100-3GFP::HIS3 LEU2 leu2-3,112 lys2-801 his3Δ200 ura3-52</i> | this study |
| JBY 180 | <i>MATa/α</i> | <i>dyn1Δ::KanMX/dyn1(ko)::KanMX pHIS::mCherry-TUB1::URA3/ ura3-52; NIP100-3GFP::HIS3/NIP100-3GFP::HIS3; she1Δ::LEU2/she1(KO)::LEU2</i> | this study |
| JBY 181 | <i>MATa/α</i> | <i>dyn1Δ::KanMX/dyn1Δ::KanMX pHIS::mCherry-TUB1::URA3/ ura3-52; NIP100-3GFP::HIS3/NIP100-3GFP::HIS3</i> | this study |
| JBY 184 | <i>MATa</i> | <i>SHE1-GFP::HIS3 pHIS::mCherry-TUB1::URA3 leu2-3,112 lys2-801 his3Δ200 ura3-52</i> | this study |
| JBY 213 | <i>MATa/α</i> | <i>LDB18-3GFP::HIS3/LDB18-3GFP::HIS3; pHIS::mCherry-TUB1::URA3/ ura3-52 leu2-3,112 lys2-801 his3Δ200</i> | this study |
| JBY 214 | <i>MATa/α</i> | <i>LDB18-3GFP::HIS3/LDB18-3GFP::HIS3; pHIS::mCherry-TUB1::URA3/ ura3-52; she1(KO)::LEU2/she1(KO)::LEU2 leu2-3,112 lys2-801 his3Δ200</i> | this study |
| JBY 175 | <i>MATa/α</i> | <i>pHIS::mCherry-TUB1::URA3/+; JNM1-3GFP::HIS3/+ LEU2 leu2-3,112 lys2-801 his3Δ200</i> | this study |
| Plasmids | | | |
| Plasmid name | | | source |
| pAK011 | | pRS306-mCherry-TUB1 | Khmelinskii et al., 2007 |
| pYS47 | | 3GFP::HIS3 | Wong et al., 2007 |
| | | PFA6a::tdTomato::KanMX | Shaner et al., 2004 |

CHAPTER 4: Additional analysis of She1

INTRODUCTION

In the previous chapters, I presented evidence that supports She1 as an important protein for mitosis, based on the fact that it drives spindle disassembly during telophase and regulates spindle position via silencing of the dynein pathway. The mechanisms of She1-mediated spindle destabilization and She1-mediated disruption of the dynein-dynactin complex interaction remain to be determined. Furthermore, the fact that She1 localizes to the kinetochore (Chapter 2), suggests that She1 may play an additional role in chromosome segregation. Here, to address these issues, I have analyzed She1 in more detail, specifically using epifluorescence microscopy to analyze its role at the kinetochore, mass spectrometry to identify its stable binding partners, and a variety of in vitro MT polymerization assays to assess its effects on MT dynamics.

RESULTS

To investigate the role of She1 at the kinetochore, I analyzed chromosome segregation during anaphase in *she1Δ* cells. Using DAPI to stain for DNA and Mtw1-GFP to mark kinetochores, I observed no noticeable defects in chromosome segregation during early anaphase (data not shown). Chromosomes did appear missegregated during late anaphase, but this was a result of defective spindle positioning caused by ectopic dynein activity seen in the *she1Δ* mutant (see Chapter 3). In metaphase, however, loss of She1 affected kinetochore localization. In wild-type cells, kinetochores were tightly clustered, forming a distinctive bi-lobed pattern (Figure 4.1, top panel; Tytell and Sorger, 2006). However, in *she1Δ* cells, Mtw1-GFP-labeled kinetochores often formed three or more lobes, indicating a defect in kinetochore positioning (Figure 4.1, bottom panel). These results suggest that She1 is not necessary for proper MT-kinetochore attachment and segregation during anaphase, but rather, for correct kinetochore alignment during metaphase.

To understand more clearly the roles of She1 in spindle disassembly, spindle positioning, and kinetochore alignment, I analyzed the stable binding partners of She1. A tandem affinity tagged (Cheeseman et al., 2001) version of She1 (She1-TAP) was purified from 12 L (OD(600) = 1.2) of culture and the eluate was analyzed by time-of-flight mass spectrometry (MacCoss et al., 2002). A summary of the results is detailed in Figure 4.2. I found that She1 co-purified with Mcm22, an outer kinetochore protein within the COMA/Ctf19 complex (Westermann et al., 2003), but not with any other kinetochore proteins. Combined with previous data showing that She1 binds to Mcm21, another outer kinetochore protein within the COMA/Ctf19 complex (Woodruff et al., 2010), this result strongly suggests that She1 is a novel component of the COMA/Ctf19 complex. In addition, She1 co-purified with Boi1, a bud neck-localized protein which plays a role in the NoCut pathway that regulates the timing of abscission (Norden et al., 2006). Interestingly, the remaining proteins that co-purified with She1 were either uncharacterized, or did not have any previously described role in mitosis.

My results up to this point suggest that She1 interacts with the outer kinetochore through the COMA/Ctf19 complex, but they do not indicate how She1 could regulate spindle MTs to drive spindle disassembly or control kinetochore clustering. It is possible that She1 may act independently as a MT destabilizing factor, similar to the MT depolymerase Kip3 (Varga et al., 2006). To test this hypothesis, I observed the effects of recombinant She1 on MT dynamics in vitro. GST-She1 was expressed from bacteria and then purified by affinity chromatography (glutathione column) followed by gel filtration (Superdex 200 column)(Figure 4.3A). Purified GST-She1 co-pelleted with MTs, indicating that She1 is sufficient to bind MTs. To test if She1 is sufficient to regulate MT dynamics, increasing amounts of GST-She1 were added to tubulin, then MT polymerization was induced by raising the temperature from 4° C to 37° C. Tubulin alone polymerized efficiently into MTs. However, the presence of GST-She1 inhibited bulk polymerization in a dose-dependent manner (Figure 4.3 C). I then tested the effects of recombinant GST-She1 on the length of MTs growing from purified centrosomes. MTs were visualized using rhodamine-labeled tubulin. MT growth was initiated at 30° C, at 26 μM concentration of tubulin, and in the presence of GST-She1 or bovine serum albumin (BSA). After 10 min the reactions were fixed, quenched, and analyzed visually

by microscopy. The presence of GST-She1 reduced the average MT length. (Figure 4.3 D). Taken together, these results suggest that She1 is sufficient to bind MTs and regulate their growth.

Figure 4.1

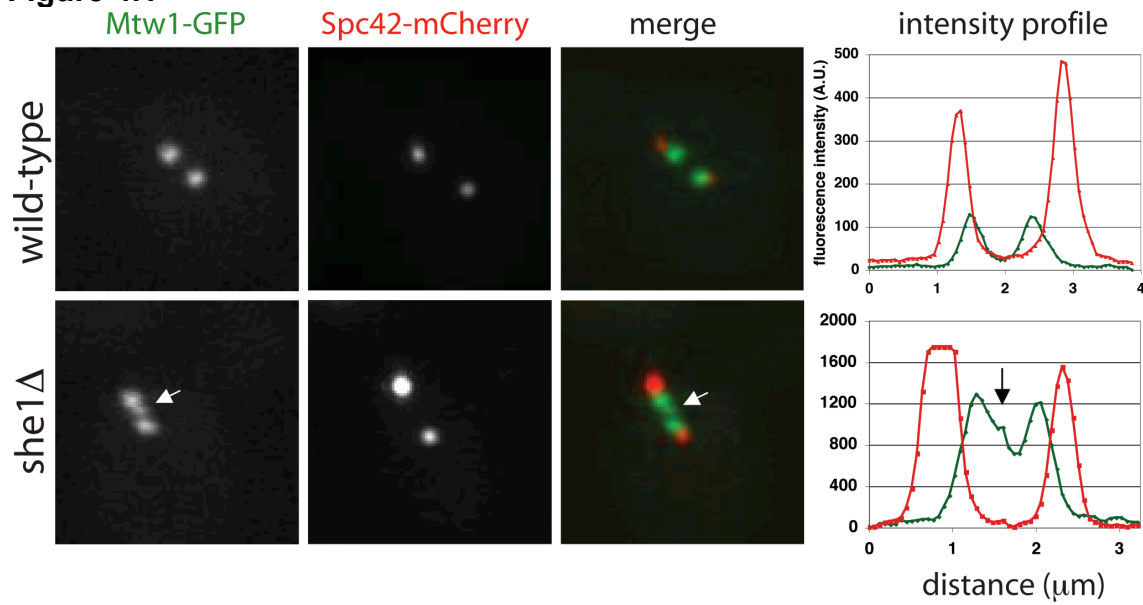


Figure 4.1. She1 is necessary for proper kinetochore alignment in metaphase. Co-localization of the kinetochore marker Mtw1-GFP and the spindle pole body marker Spc42-mCherry in wild-type or *she1Δ* cells. The white arrow indicates de-clustered kinetochores. To the right of the images are intensity profiles of the two fluorescent probes measured from one spindle pole body to the other.

Figure 4.2

| Mass Spectrometry of purified She1-TAP | | | |
|--|---------|--------------|---|
| gene | ORF | coverage (%) | description |
| SHE1 | YBL031W | 66 | spindle and bud neck protein involved in spindle disassembly and positioning |
| | YMR317W | 42 | cell wall/membrane assembly? |
| | YOL155C | 38.9 | glucosidase activity, cell wall biogenesis |
| MCM22 | YJR135C | 18.8 | component of the kinetochore; binds to centromeric DNA in a Ctf19p-dependent manner |
| MRS4 | YKR052C | 17.4 | Mitochondrial iron transporter of the mitochondrial carrier family (MCF), very similar to and functionally redundant with Mrs3p; functions under low-iron conditions; may transport other cations in addition to iron |
| BDF1 | YLR399C | 17.3 | Protein involved in transcription initiation at TATA-containing promoters; associates with the basal transcription factor TFIID; r |
| MUC1 | YIR019C | 16.8 | diploid pseudohyphal formation and haploid invasive growth, transcriptionally regulated by the MAPK pathway |
| ECM27 | YJR106W | 16.6 | cell wall/membrane assembly? |
| VPS33 | YLR396C | 15.9 | ATP-binding protein that is a subunit of the homotypic vacuole fusion and vacuole protein sorting (HOPS) complex; |
| | YIL055C | 15.9 | unknown |
| CWC2 | YDL209C | 15.6 | Protein involved in pre-mRNA splicing, component of a complex containing Cef1p; interacts with Prp19p |
| HOS4 | YIL112W | 14 | Subunit of the Set3 complex, which is a meiotic-specific repressor of sporulation specific genes that contains deacetylase activity |
| | YFR017C | 12.8 | unknown |
| SRO77 | YBL106C | 11.9 | Protein with roles in exocytosis and cation homeostasis; functions in docking and fusion of post-Golgi vesicles with plasma membrane |
| BOI1 | YBL085W | 9 | Protein implicated in polar growth, functionally redundant with Boi2p; interacts with bud-emergence protein Bem1p |

Figure 4.2. Analysis of She1 interacting partners by mass spectrometry. She1-TAP was purified from yeast cells and then analyzed by time-of-flight mass spectrometry. The names and descriptions of the proteins that co-purified with She1-TAP are described. For a given protein, the percentage of its peptide sequence that was identified is listed in the “% coverage” column.

Figure 4.3

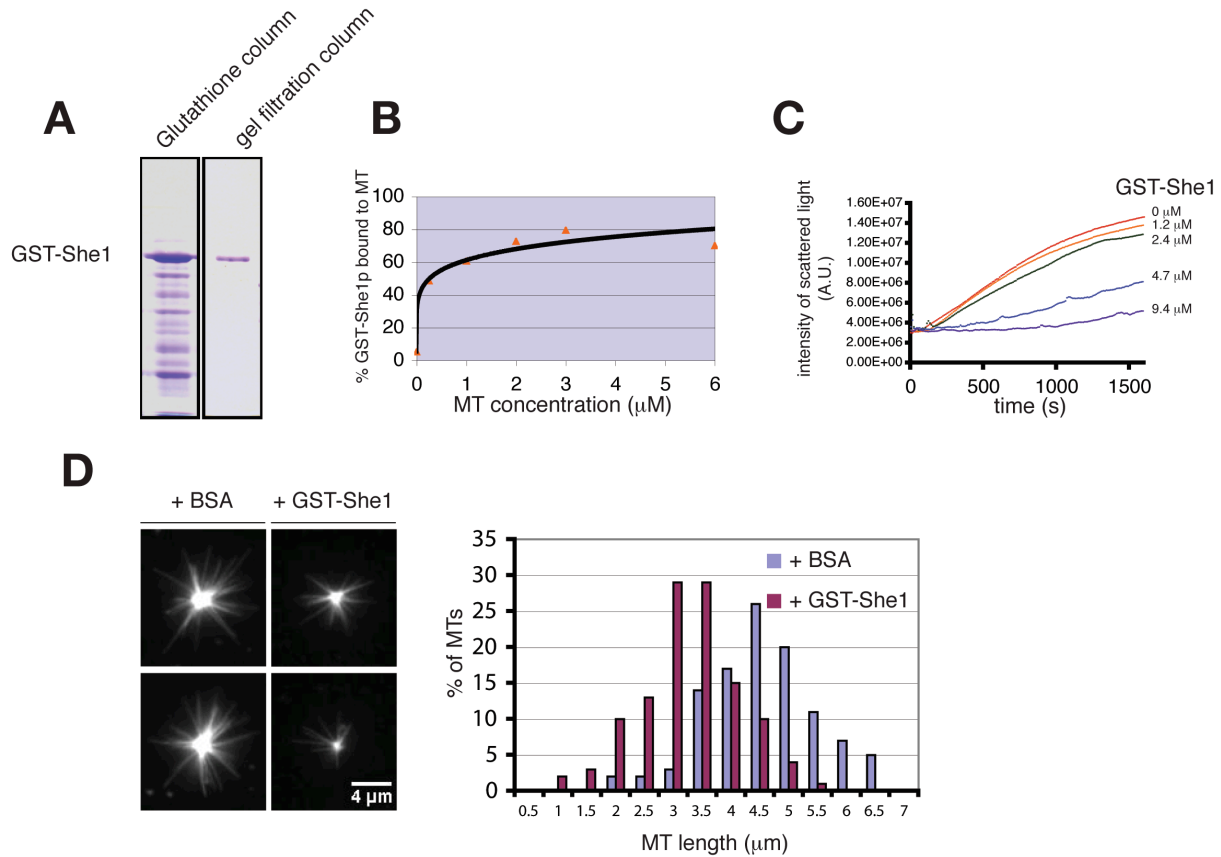


Figure 4.3. GST-She1 binds MTs and modulates their dynamics in vitro. (A) GST-She1 was expressed in bacteria and then sequentially passed over a glutathione and gel filtration column. (B) GST-She1 co-pellets with MTs. (C) GST-She1 inhibits MT polymerization in a dose-dependent manner measured by right-angle light scattering. (D) GST-She1 inhibits the growth of MTs from purified centrosomes. BSA, bovine serum albumin. To the right is a histogram indicating the lengths of the centrosome-nucleated MTs in the presence of BSA or GST-She1.

DISCUSSION

The data I have presented here, in combination with data from previous chapters, strongly suggest that She1 *per se* is a novel MT-binding protein that regulates MT dynamics. First, ipMT depolymerization is defective in *she1Δ* cells, indicating that She1 destabilizes ipMTs during spindle disassembly. Second, She1 localizes to ipMTs and aMTs in vivo, and She1 can bind MTs in vitro. Finally, addition of recombinant She1 to polymerizing MTs in vitro reduces the amount of total MT polymer and the length of MTs. How She1 restricts MT growth is still unclear. She1 could depolymerize MTs from their plus ends, similar to other depolymerizing proteins such as kinesin-8 and kinesin-13 motor proteins. Or, She1 could destabilize MTs at a location interior to the plus end, perhaps at the MT seam. Alternatively, She1 could prevent elongation of MTs, by functioning either to cap plus ends, or sequester tubulin dimers to prevent their incorporation into the growing polymer.

The MT-destabilizing activity of She1 could also explain its role in kinetochore alignment. Tytell and Sorger (2006) showed that kinetochore clustering during metaphase requires dynamic kMTs, as inhibition of a variety of motors, including the MT depolymerase Kip3, de-clustered kinetochores. My data suggest that She1 is an outer kinetochore component, that is, near the microtubules, thus placing it in a logical location to regulate MT dynamics at the kinetochore-MT interface.

However, the MT-destabilizing activity of She1 most likely does not explain its role in spindle positioning. Although She1 does localize to aMTs, depleting the cells of She1 does not affect aMT dynamics (see Chapter 3). This may be due to lack of post-translational modification needed to fully activate She1 in vivo, perhaps phosphorylation by Ipl1, the Aurora B kinase in yeast. In support of this hypothesis, mutating the five Ipl1 consensus sites in She1 phenocopied the *she1Δ* null mutation during spindle disassembly (Chapter 2, Figure 2.8). Since Ipl1 localizes strongly to ipMTs, but not to aMTs, it is possible that nuclear She1 gets phosphorylated by Ipl1 and acts as a MT destabilizer, but cytoplasmic She1 does not get phosphorylated by Ipl1 and functions in a different manner.

She1 interacts with Boi1, a bud neck-localized protein involved in the NoCut spindle/cytokinesis pathway (Norden et al., 2006). The physiological relevance of this interaction, as well as whether or not She1 is a novel component of the NoCut pathway remain to be determined. She1 may be the intermediary between the two pathways of spindle disassembly and cytokinesis, considering that NoCut activation requires Ipl1-dependent phosphorylation and that Ipl1 phosphorylates She1. In addition, She1, like Boi1, localizes to the bud neck; thus, She1 is in the proper location to regulate abscission via the NoCut pathway and spindle disassembly. It will be interesting to see if cells expressing a version of She1 that is incapable of being phosphorylated by Ipl1 (*she1-5A*, see Chapter 2) are defective for the NoCut pathway.

MATERIALS AND METHODS

Yeast Strains and plasmids. The yeast strains and plasmids used in this study are listed in Table 4.1.

Purification of She1 from yeast cells. A tandem affinity purification tag (TAP) containing a TEV protease cleavage site (ETVRFQG/S), and a ZZ tag (minimal protein A binding domain) was amplified from pKW804 (a gift from K. Weis, University of California, Berkeley) and integrated at the 3' end of *SHE1* at its endogenous locus in the genome. She1-TAP was purified from yeast and analyzed by mass spectrometry essentially as described previously (Cheeseman et al., 2001).

Purification of GST-She1 from bacteria cells. The full length *SHE1* gene was amplified by PCR from yeast genomic DNA and inserted into a PGEX-2T vector (GE Healthcare Life Sciences). During the PCR amplification, a TEV site was included in the 5' primer to insert a TEV cleavage site between the N-terminus of She1 and the GST tag. The PGEX-2T-TEV-SHE1 plasmid (JBB 4) was transformed into Codon+ BL21 bacterial cells (Stratagene). Cells were grown overnight in LB medium plus 100 µg/ml ampicillin and 50 µg/ml chloramphenicol. Expression of GST-She1 was induced after addition of 1mM IPTG for 4 hr at 25° C. Cells were harvested, washed, and resuspended in HEK-250 (50 mM HEPES, pH 7.5, 1 mM EDTA, 250 mM KCl) plus protease inhibitors (200mM PMSF + 1X protease cocktail IV (Calbiochem)). Cells were lysed using a method of 10 min incubation on ice with 0.1mg/ml lysozyme, followed by sonication for 3X10 sec. The lysis buffer was then supplemented with Triton-X100 (1% final concentration). Soluble protein lysate was separated from cellular debris by centrifugation for 10 min at 13,000 rpm. The supernatant was then passed over a glutathione-sepharose column for 1 hr, washed 3X in HEK-250 + 1% Triton-X100 + protease inhibitors (HEK-TP), then eluted with HEK-TP supplemented with 20 mM glutathione. GST-She1 that eluted from the glutathione column was pooled and dialyzed against HEN-500 (50 mM HEPES, pH 8.0, 1 mM EDTA, 500 mM NaCl, 1mM DTT, 200mM PMSF, 1X protease cocktail IV) overnight at 4° C, spun at 14,000 rpm for 10 min to remove aggregates, then passed over a Superdex 200 gel filtration column.

MT pelleting assay. Pre-spun GST-She1 or BSA was incubated with increasing amounts of taxol-stabilized tubulin were incubated in HEM buffer (25mM HEPES, pH 7.5, 1 mM MgCl₂, 1 mM EGTA, 50 mM KCl, 1mM DTT) + 1 mM GTP + 20 µM taxol + 25% glycerol for 10 min at room temperature. MTs were pelleted by ultracentrifugation at 55,000 rpm for 10 min (Beckman Coulter TLA 100 rotor) at room temperature.

Light Scattering assay. Light scattering was performed essentially as described (Westermann et al., 2005), except that MTs were polymerized in HEM buffer.

MT aster assay. Microtubules were grown from purified centrosomes (a gift from the Heald lab, UC Berkeley) at 26 µM tubulin (1:10 labeled with rhodamine tubulin) and 25 µM GST-She1 or BSA (bovine serum albumin, (Sigma Aldrich) in PEM-B buffer (80 mM PIPES, pH 7.5, 1 mM MgCl₂, 1 mM EGTA, 1mM DTT, 0.1% Brij-35) at 30° C for 10 min.

Prior to usage, protein preparations were precleared by centrifugation. Reactions were fixed with 0.75% glutaraldehyde for 3 min and subsequently quenched with 0.1% sodium borohydride. Part of the reaction was squashed under a coverslip and analyzed microscopically.

Table 4.1. Yeast strains and plasmids.

| Strain name | Mating type | Genotype (all strains are derivatives of S288C) | source |
|--------------|--------------------|--|------------|
| JBY 79 | <i>MATa</i> | <i>MTW1-GFP::HIS3 SPC42-mCherry::KanMX6 she1Δ::LEU2</i> | this study |
| JBY 80 | <i>MATa</i> | <i>MTW1-GFP::HIS3 SPC42-mCherry::KanMX6</i> | this study |
| JBY 20 | <i>MATα</i> | <i>SHE1-TAP::KanMX6 prb1-1122 pep4-3 pre1-451 trp1-1(am)</i> | this study |
| | | | |
| Plasmid name | Resistance markers | | |
| JBB 4 | ampicillin | PGEX-2T::TEV-SHE1 | this study |

CHAPTER 5: Conclusions and Future Directions

My thesis work focused on spindle disassembly and positioning, two important aspects of mitosis, but I feel that it is more exciting and worthwhile to study disassembly in the future. The field of spindle positioning is very crowded, and, consequently, much has been learned about the various mechanisms of spindle centering in a variety of eukaryotes. On the other hand, no group has taken the initiative to detail carefully and exhaustively the mechanisms of spindle disassembly. Thus, there remains a vast open field for exploration. In my work, I developed a variety of assays that identify proteins important for spindle disassembly and also yield clues on the contributions of these proteins to the disassembly process. It would be very easy to extend my project and study the additional spindle disassembly genes identified in the synthetic lethal screen described in Figure 2.5.

Additional spindle disassembly factors demand attention

There are five genes in particular that I think should be studied in greater detail: *UME6*, *CPR6*, *FPR4*, *KAR3*, and *CIK1*. Mutations in each of these genes inhibits spindle disassembly such that cytokinetic ring contraction is required to break the spindle, which is a feature shared by all previously described spindle disassembly factors (Woodruff et al., 2010; and data not shown). Ume6 is a transcriptional regulator, and Cpr6 and Fpr4 are both cis-trans proline isomerases that are presumed to regulate gene expression through histone modification. Thus, it is possible that these proteins regulate the expression of other disassembly genes. Kar3 and Cik1 form a heterodimeric minus-end-directed motor complex that depolymerizes MTs during karyogamy. Given its localization to the spindle midzone during mitosis, it is likely that the Kar3-Cik1 complex drives ipMT depolymerization during spindle disassembly.

Aurora B function during spindle disassembly

The Aurora B kinase (Ipl1 in yeast) has been shown to play a major role in spindle disassembly through the activation of the MT-destabilizing protein She1 and deactivation of the MT-growth factor EB1 (Bim1 in yeast). It is very likely that the Aurora B kinase regulates additional proteins during this process. To understand more completely the functions of Aurora B during disassembly, it is essential to uncover all of the Aurora B substrates specifically during late anaphase and telophase. This can be done through the use of stable isotope labeling in cell culture (SILAC) combined with quantitative mass spectrometry. By using cells expressing an analog-sensitive allele of Ipl1 (*ipl1-as5*) that responds to the small molecule inhibitor CZ40, Aurora B can be specifically and quickly inhibited. Expression of a non-degradable B type cyclin (*pGAL:: Δ N-CLB2*) will ensure that all cells are arrested in late anaphase, after the mitotic exit network is activated. I have confirmed that Aurora B phosphorylation of EB1 still occurs when cells are arrested in this manner.

Understanding Aurora B function during spindle disassembly also requires investigation of the upstream regulation of Aurora B. The first key question is how Aurora B is activated during mitotic exit. Phosphorylation of EB1 occurs downstream of the mitotic exit network, but it is unclear how this signaling pathway activates Aurora B. Another key question is how Aurora B specificity is achieved. For example, like other Aurora B substrates (e.g., the Dam1 complex), EB1 is in close proximity to Aurora B at the kinetochore, but phosphorylation of EB1 and Dam1 complex subunits occurs at

different cell cycle stages. Thus, a localization-independent mechanism ensures temporal specificity. The 7-protein alternative replication factor C complex (Dcc1, Ctf8, Ctf18 and others) may be the key in answering these questions. Depleting cells of Dcc1 and Ctf8 disrupts Aurora B-mediated EB1 phosphorylation and removal from spindle MTs, but does not affect the ability of Aurora B to phosphorylate its kinetochore substrates. It is possible that the alternative replication factor C complex binds to the Aurora B complex, modifying it in such a way allows access to the phosphorylation sites on EB1. Alternatively, the alternative replication factor C complex may catalyze this interaction through binding to EB1.

Mechanism of She1-mediated spindle destabilization

She1 localizes all along the mitotic spindle as well as at the bud neck and is important for driving spindle disassembly. It has no clear homology to any other identified protein in metazoans or fission yeast and no recognizable domains that could tell us about its mechanism. She1 may represent an entirely new class of MT-destabilizing protein.

I have done some preliminary analysis of recombinant GST-labeled She1 purified from bacteria. She1 can bind bovine MTs in vitro and inhibits the growth of MTs from purified mammalian centrosomes. Considering that GST can dimerize, it is possible that the GST tag is altering the function of She1 by artificially inducing GST-She1 dimers. But, these results are nevertheless interesting and they suggest that She1 alone is sufficient to destabilize or inhibit the growth of MTs. In the future, She1 should be purified with another tag that doesn't dimerize (e.g., MBP), or She1 should be purified in conditions that allow removal of the GST tag but maintain the solubility of She1. It would then be important to examine: 1) the effects of purified She1 on MT dynamicity in vitro, 2) where She1 localizes along MTs using both total internal fluorescence microscopy (TIRF) and electron microscopy, 3) the hydrodynamic properties of She1 (e.g., does it form a dimer, or a higher-order complex?), and 4) how Ipl1 phosphorylation affects the activity of She1. Finally, obtaining a high-resolution crystal structure of She1 would help explain its activity and may lead to the identification of the metazoan homolog, if one exists.

Spindle reassembly after incomplete disassembly

Yeast cells can tolerate the loss of one spindle disassembly pathway. However, when two separate spindle disassembly pathways are disabled, cell cycle progression is slowed, and consequently cell growth is severely compromised. Interestingly, the cells still manage to break down the spindle, partly through contraction of the cytokinetic ring, and, presumably, through the actions of the remaining disassembly pathway(s) (I mention three pathways in Chapter 3, but, there may be more). If the spindle is broken apart, then why are the cells so sick?

I began to answer this question by combining a *doc1Δ* null allele (which inactivates the anaphase promoting complex pathway) with a conditional allele of Kip3 (created by fusing a temperature-sensitive degron tag to the N-terminus of Kip3). This approach allows inhibition of two spindle disassembly pathways without dealing with the strong synthetic sickness that would hamper cell growth and encourage the acquisition of suppressor mutations. In *doc1Δ td-kip3* cells that were synchronized in S phase,

released, then incubated at 37° C to allow one round of defective disassembly, I observed many aberrant spindle phenotypes in the next cell cycle. Most often, spindles would collapse or display asymmetric MT staining. Providing a brief (30 min) pulse of nocodazole to artificially disassemble the spindle rescued the aberrant spindle phenotype. Taken together, these preliminary results suggest that full disassembly of the spindle is necessary for spindle reassembly in the next cell cycle. Currently it is unclear why the presence of spindle remnants prevents spindle formation, although I have recently observed that duplication of spindle pole bodies is normal in *doc1Δ td-kip3* cells, thus ruling out that possibility. Perhaps ipMT formation or cross-linking is defective. In the future, it will be important to test these hypotheses by observing these aberrant spindles by electron microscopy and testing their ability to recruit key cross-linking proteins like Ase1 and Cin8.

REFERENCES

- Adames, N.R., and J.A. Cooper. 2000. Microtubule Interactions with the Cell Cortex Causing
- Amaro, I.A., M. Costanzo, C. Boone, and T.C. Huffaker. 2008. The *Saccharomyces cerevisiae* Homolog of p24 Is Essential for Maintaining the Association of p150 Glued With the Dynactin Complex. *Genetics*. 178:703-709.
- Ayscough, K.R., J. Stryker, N. Pokala, M. Sanders, P. Crews, and D.G. Drubin. 1997. High rates of actin filament turnover in budding yeast and roles for actin in establishment and maintenance of cell polarity revealed using the actin inhibitor latrunculin-A. *J Cell Biol*. 137:399-416.
- Buvelot, S., S.Y. Tatsutani, D. Vermaak, and S. Biggins. 2003. The budding yeast Ipl1/Aurora protein kinase regulates mitotic spindle disassembly. *J Cell Biol*. 160:329-39.
- Cao, K., R. Nakajima, H.H. Meyer, and Y. Zheng. 2003. The AAA-ATPase Cdc48/p97 regulates spindle disassembly at the end of mitosis. *Cell*. 115:355-67.
- Carvalho, P., M.L. Gupta, Jr., M.A. Hoyt, and D. Pellman. 2004. Cell cycle control of kinesin-mediated transport of Bik1 (CLIP-170) regulates microtubule stability and dynein activation. *Dev Cell*. 6:815-29.
- Cheeseman, I. M., Enquist-Newman, M., Muller-Reichert, T., Drubin, D. G., and Barnes, G. 2001. Mitotic spindle integrity and kinetochore function linked by the Duo1p/Dam1p complex. *J Cell Biol* 152, 197-212.
- Cheeseman, I.M., S. Anderson, M. Jwa, E.M. Green, J. Kang, J.R. Yates, 3rd, C.S. Chan, D.G. Drubin, and G. Barnes. 2002. Phospho-regulation of kinetochore-microtubule attachments by the Aurora kinase Ipl1p. *Cell*. 111:163-72.
- Costanzo, M., A. Baryshnikova, J. Bellay, Y. Kim, E.D. Spear, C.S. Sevier, H. Ding, J.L. Koh, K. Toufighi, S. Mostafavi, J. Prinz, R.P. St Onge, B. VanderSluis, T. Makhnevych, F.J. Vizeacoumar, S. Alizadeh, S. Bahr, R.L. Brost, Y. Chen, M. Cokol, R. Deshpande, Z. Li, Z.Y. Lin, W. Liang, M. Marback, J. Paw, B.J. San Luis, E. Shuteriqi, A.H. Tong, N. van Dyk, I.M. Wallace, J.A. Whitney, M.T. Weirauch, G. Zhong, H. Zhu, W.A. Houry, M. Brudno, S. Ragibizadeh, B. Papp, C. Pal, F.P. Roth, G. Giaever, C. Nislow, O.G. Troyanskaya, H. Bussey, G.D. Bader, A.C. Gingras, Q.D. Morris, P.M. Kim, C.A. Kaiser, C.L. Myers, B.J. Andrews, and C. Boone. 2010. The genetic landscape of a cell. *Science*. 327:425-31.
- Gardner, M.K., J. Haase, K. Myhre, J.N. Molk, M. Anderson, A.P. Joglekar, E.T. O'Toole, M. Winey, E.D. Salmon, D.J. Odde, and K. Bloom. 2008. The microtubule-based motor Kar3 and plus end-binding protein Bim1 provide structural support for the anaphase spindle. *J Cell Biol*. 180:91-100.
- Glotzer, M. 2009. The 3Ms of central spindle assembly: microtubules, motors and MAPs. *Nat Rev Mol Cell Biol*. 10:9-20.
- Gomes, E.R., S. Jani, and G.G. Gundersen. 2005. Nuclear Movement Regulated by Cdc42, MRCK, Myosin, and Actin Flow Establishes MTOC Polarization in Migrating Cells. *Cell*. 121:451-463.
- Goshima, G., and J.M. Scholey. Control of mitotic spindle length. *Annu Rev Cell Dev Biol*. 26:21-57.

- Goshima, G., R. Wollman, N. Stuurman, J.M. Scholey, and R.D. Vale. 2005. Length control of the metaphase spindle. *Curr Biol.* 15:1979-88.
- Grava, S., F. Schaerer, M. Faty, P. Philippsen, and Y. Barral. 2006. Asymmetric Recruitment of Dynein to Spindle Poles and Microtubules Promotes Proper Spindle Orientation in Yeast. *Developmental Cell.* 10:425-439.
- Grill, S.W., J. Howard, E. Schaffer, E.H. Stelzer, and A.A. Hyman. 2003. The distribution of active force generators controls mitotic spindle position. *Science.* 301:518-21.
- Gruneberg, U., R. Neef, R. Honda, E.A. Nigg, and F.A. Barr. 2004. Relocation of Aurora B from centromeres to the central spindle at the metaphase to anaphase transition requires MKlp2. *J Cell Biol.* 166:167-72.
- Gupta, M.L., Jr., P. Carvalho, D.M. Roof, and D. Pellman. 2006. Plus end-specific depolymerase activity of Kip3, a kinesin-8 protein, explains its role in positioning the yeast mitotic spindle. *Nat Cell Biol.* 8:913-23.
- Hildebrandt, E.R., and M.A. Hoyt. 2001. Cell cycle-dependent degradation of the *Saccharomyces cerevisiae* spindle motor Cin8p requires APC(Cdh1) and a bipartite destruction sequence. *Mol Biol Cell.* 12:3402-16.
- Hofmann, C., Cheeseman, I. M., Goode, B. L., McDonald, K. L., Barnes, G., and Drubin, D. G. (1998). *Saccharomyces cerevisiae* Duo1p and Dam1p, novel proteins involved in mitotic spindle function. *J Cell Biol* 143, 1029-1040.
- Hsu, J.-Y., Z.-W. Sun, X. Li, M. Reuben, K. Tatchell, D.K. Bishop, J.M. Grushcow, C.J. Brame, J.A. Caldwell, D.F. Hunt, R. Lin, M.M. Smith, and C.D. Allis. 2000. Mitotic Phosphorylation of Histone H3 Is Governed by Ipl1/aurora Kinase and Glc7/PP1 Phosphatase in Budding Yeast and Nematodes. *Cell.* 102:279-291.
- Hwang, E., J. Kusch, Y. Barral, and T.C. Huffaker. 2003. Spindle orientation in *Saccharomyces cerevisiae* depends on the transport of microtubule ends along polarized actin cables. *J Cell Biol.* 161:483-8.
- Hwang, L.H., and A.W. Murray. 1997. A novel yeast screen for mitotic arrest mutants identifies DOC1, a new gene involved in cyclin proteolysis. *Mol Biol Cell.* 8:1877-87.
- Janson, M.E., T.G. Setty, A. Paoletti, and P.T. Tran. 2005. Efficient formation of bipolar microtubule bundles requires microtubule-bound gamma-tubulin complexes. *J Cell Biol.* 169:297-308.
- Jin, Q.W., J. Fuchs, and J. Loidl. 2000. Centromere clustering is a major determinant of yeast interphase nuclear organization. *J Cell Sci.* 113 (Pt 11):1903-12.
- Juang, Y.L., J. Huang, J.M. Peters, M.E. McLaughlin, C.Y. Tai, and D. Pellman. 1997. APC-mediated proteolysis of Ase1 and the morphogenesis of the mitotic spindle. *Science.* 275:1311-4.
- Kang, J., I.M. Cheeseman, G. Kallstrom, S. Velmurugan, G. Barnes, and C.S. Chan. 2001. Functional cooperation of Dam1, Ipl1, and the inner centromere protein (INCENP)-related protein Sli15 during chromosome segregation. *J Cell Biol.* 155:763-74.
- Khmelinskii, A., C. Lawrence, J. Roostalu, and E. Schiebel. 2007. Cdc14-regulated midzone assembly controls anaphase B. *J Cell Biol.* 177:981-93.
- Kim, H., S.-C. Ling, G.C. Rogers, C. Kural, P.R. Selvin, S.L. Rogers, and V.I. Gelfand. 2007. Microtubule binding by dynactin is required for microtubule organization but not cargo transport. *J. Cell Biol.* 176:641-651.

- Kitamura, E., K. Tanaka, S. Komoto, Y. Kitamura, C. Antony, and T.U. Tanaka. Kinetochores generate microtubules with distal plus ends: their roles and limited lifetime in mitosis. *Dev Cell*. 18:248-59.
- Knaus, M., E. Cameroni, I. Pedruzzi, K. Tatchell, C. De Virgilio, and M. Peter. 2005. The Bud14p-Glc7p complex functions as a cortical regulator of dynein in budding yeast. *Embo J*. 24:3000-11.
- Kotwaliwale, C.V., S.B. Frei, B.M. Stern, and S. Biggins. 2007. A pathway containing the Ipl1/aurora protein kinase and the spindle midzone protein Ase1 regulates yeast spindle assembly. *Dev Cell*. 13:433-45.
- Kramer, E.R., N. Scheuringer, A.V. Podtelejnikov, M. Mann, and J.M. Peters. 2000. Mitotic regulation of the APC activator proteins CDC20 and CDH1. *Mol Biol Cell*. 11:1555-69.
- Kusch, J., D. Liakopoulos, and Y. Barral. 2003. Spindle asymmetry: a compass for the cell. *Trends in Cell Biology*. 13:562-569.
- Lee, W.L., J.R. Oberle, and J.A. Cooper. 2003. The role of the lissencephaly protein Pac1 during nuclear migration in budding yeast. *J Cell Biol*. 160:355-64.
- Li, J., W.L. Lee, and J.A. Cooper. 2005. NudEL targets dynein to microtubule ends through LIS1. *Nat Cell Biol*. 7:686-90.
- Longtine, M.S., A. McKenzie, 3rd, D.J. Demarini, N.G. Shah, A. Wach, A. Brachat, P. Philippesen, and J.R. Pringle. 1998. Additional modules for versatile and economical PCR-based gene deletion and modification in *Saccharomyces cerevisiae*. *Yeast*. 14:953-61.
- Luca, F.C., M. Mody, C. Kurischko, D.M. Roof, T.H. Giddings, and M. Winey. 2001. *Saccharomyces cerevisiae* Mob1p is required for cytokinesis and mitotic exit. *Mol Cell Biol*. 21:6972-83.
- MacCoss, M.J., W.H. McDonald, A. Saraf, R. Sadygov, J.M. Clark, J.J. Tasto, K.L. Gould, D. Wolters, M. Washburn, A. Weiss, J.I. Clark, and J.R. Yates, 3rd. 2002. Shotgun identification of protein modifications from protein complexes and lens tissue. *Proc Natl Acad Sci U S A*. 99:7900-5.
- Maddox, P.S., K.S. Bloom, and E.D. Salmon. 2000. The polarity and dynamics of microtubule assembly in the budding yeast *Saccharomyces cerevisiae*. *Nat Cell Biol*. 2:36-41.
- Mayer, M.L., S.P. Gygi, R. Aebersold, and P. Hieter. 2001. Identification of RFC(Ctf18p, Ctf8p, Dcc1p): an alternative RFC complex required for sister chromatid cohesion in *S. cerevisiae*. *Mol Cell*. 7:959-70.
- Mayr, M.I., S. Hummer, J. Bormann, T. Gruner, S. Adio, G. Woehlke, and T.U. Mayer. 2007. The human kinesin Kif18A is a motile microtubule depolymerase essential for chromosome congression. *Curr Biol*. 17:488-98.
- Miller, R.K., and M.D. Rose. 1998. Kar9p is a novel cortical protein required for cytoplasmic microtubule orientation in yeast. *J Cell Biol*. 140:377-90.
- Moore, J.K., J. Li, and J.A. Cooper. 2008. Dynactin Function in Mitotic Spindle Positioning. *Traffic*. 9:510-527.
- Nakajima, Y., Tyers, R. G., Wong, C. C., Yates, J. R., 3rd, Drubin, D. G., and Barnes, G. (2009). Nbl1p: a Borealin/Dasra/CSC-1-like protein essential for Aurora/Ipl1 complex function and integrity in *Saccharomyces cerevisiae*. *Mol Biol Cell* 20, 1772-1784.

- Nuclear Movements in *Saccharomyces cerevisiae*. *J. Cell Biol.* 149:863-874.
- Pecreaux, J., J.-C. R[^]per, K. Kruse, F. J_ulicher, A.A. Hyman, S.W. Grill, and J. Howard. 2006. Spindle Oscillations during Asymmetric Cell Division Require a Threshold Number of Active Cortical Force Generators. *Current Biology.* 16:2111-2122.
- Peters, J.M. 2002. The anaphase-promoting complex: proteolysis in mitosis and beyond. *Mol Cell.* 9:931-43.
- Peters, J.M. 2006. The anaphase promoting complex/cyclosome: a machine designed to destroy. *Nat Rev Mol Cell Biol.* 7:644-56.
- Pinsky, B.A., C. Kung, K.M. Shokat, and S. Biggins. 2006. The Ipl1-Aurora protein kinase activates the spindle checkpoint by creating unattached kinetochores. *Nat Cell Biol.* 8:78-83.
- Reinsch, S., and P. Gonczy. 1998. Mechanisms of nuclear positioning. *J Cell Sci.* 111 (Pt 16):2283-95.
- Ross, K.E., and O. Cohen-Fix. 2004. A Role for the FEAR Pathway in Nuclear Positioning during Anaphase. *Developmental Cell.* 6:729-735.
- Schroer, T.A. 2004. DYNAMACTIN. *Annual Review of Cell and Developmental Biology.* 20:759-779.
- Segal, M., and K. Bloom. 2001. Control of spindle polarity and orientation in *Saccharomyces cerevisiae*. *Trends in Cell Biology.* 11:160-166.
- Severin, F., B. Habermann, T. Huffaker, and T. Hyman. 2001. Stu2 promotes mitotic spindle elongation in anaphase. *J Cell Biol.* 153:435-42.
- Severson, A.F., D.R. Hamill, J.C. Carter, J. Schumacher, and B. Bowerman. 2000. The aurora-related kinase AIR-2 recruits ZEN-4/CeMKLP1 to the mitotic spindle at metaphase and is required for cytokinesis. *Curr Biol.* 10:1162-71.
- Shaner, N.C., R.E. Campbell, P.A. Steinbach, B.N.G. Giepmans, A.E. Palmer, and R.Y. Tsien. 2004. Improved monomeric red, orange and yellow fluorescent proteins derived from *Discosoma* sp. red fluorescent protein. *Nat Biotech.* 22:1567-1572.
- Shaw, S.L., E. Yeh, P. Maddox, E.D. Salmon, and K. Bloom. 1997. Astral microtubule dynamics in yeast: a microtubule-based searching mechanism for spindle orientation and nuclear migration into the bud. *J Cell Biol.* 139:985-94.
- Sheeman, B., P. Carvalho, I. Sagot, J. Geiser, D. Kho, M.A. Hoyt, and D. Pellman. 2003. Determinants of *S. cerevisiae* Dynein Localization and Activation: Implications for the Mechanism of Spindle Positioning. *Current Biology.* 13:364-372.
- Sullivan, M., and D.O. Morgan. 2007. Finishing mitosis, one step at a time. *Nat Rev Mol Cell Biol.* 8:894-903.
- Tong, A.H., G. Lesage, G.D. Bader, H. Ding, H. Xu, X. Xin, J. Young, G.F. Berriz, R.L. Brost, M. Chang, Y. Chen, X. Cheng, G. Chua, H. Friesen, D.S. Goldberg, J. Haynes, C. Humphries, G. He, S. Hussein, L. Ke, N. Krogan, Z. Li, J.N. Levinson, H. Lu, P. Menard, C. Munyana, A.B. Parsons, O. Ryan, R. Tonikian, T. Roberts, A.M. Sdicu, J. Shapiro, B. Sheikh, B. Suter, S.L. Wong, L.V. Zhang, H. Zhu, C.G. Burd, S. Munro, C. Sander, J. Rine, J. Greenblatt, M. Peter, A. Bretscher, G. Bell, F.P. Roth, G.W. Brown, B. Andrews, H. Bussey, and C. Boone. 2004. Global mapping of the yeast genetic interaction network. *Science.* 303:808-13.
- Tran, P.T., L. Marsh, V. Doye, S. Inoue, and F. Chang. 2001. A mechanism for nuclear positioning in fission yeast based on microtubule pushing. *J Cell Biol.* 153:397-

411.

- Uehara, R., R.S. Nozawa, A. Tomioka, S. Petry, R.D. Vale, C. Obuse, and G. Goshima. 2009. The augmin complex plays a critical role in spindle microtubule generation for mitotic progression and cytokinesis in human cells. *Proc Natl Acad Sci U S A*. 106:6998-7003.
- Varga, V., J. Helenius, K. Tanaka, A.A. Hyman, T.U. Tanaka, and J. Howard. 2006. Yeast kinesin-8 depolymerizes microtubules in a length-dependent manner. *Nat Cell Biol*. 8:957-62.
- Vaughan, P.S., J.D. Leszyk, and K.T. Vaughan. 2001. Cytoplasmic Dynein Intermediate Chain Phosphorylation Regulates Binding to Dynactin. *J. Biol. Chem*. 276:26171-26179.
- VerPlank, L., and R. Li. 2005. Cell Cycle-regulated Trafficking of Chs2 Controls Actomyosin Ring Stability during Cytokinesis. *Mol. Biol. Cell*. 16:2529-2543.
- Visintin, R., and A. Amon. 2001. Regulation of the Mitotic Exit Protein Kinases Cdc15 and Dbf2. *Mol. Biol. Cell*. 12:2961-2974.
- Visintin, R., K. Craig, E.S. Hwang, S. Prinz, M. Tyers, and A. Amon. 1998. The phosphatase Cdc14 triggers mitotic exit by reversal of Cdk-dependent phosphorylation. *Mol Cell*. 2:709-18.
- Vizeacoumar, F.J., N. van Dyk, S.V. F, V. Cheung, J. Li, Y. Sydorsky, N. Case, Z. Li, A. Datti, C. Nislow, B. Raught, Z. Zhang, B. Frey, K. Bloom, C. Boone, and B.J. Andrews. Integrating high-throughput genetic interaction mapping and high-content screening to explore yeast spindle morphogenesis. *J Cell Biol*. 188:69-81.
- Walczak, C.E., and R. Heald. 2008. Mechanisms of mitotic spindle assembly and function. *Int Rev Cytol*. 265:111-58.
- Wong, J., Y. Nakajima, S. Westermann, C. Shang, J.-s. Kang, C. Goodner, P. Houshmand, S. Fields, C.S.M. Chan, D. Drubin, G. Barnes, and T. Hazbun. 2007. A Protein Interaction Map of the Mitotic Spindle. *Mol. Biol. Cell*. 18:3800-3809.
- Woodbury, E.L., and D.O. Morgan. 2007. Cdk and APC activities limit the spindle-stabilizing function of Fin1 to anaphase. *Nat Cell Biol*. 9:106-12.
- Woodruff, J. B., Drubin, D. G., and Barnes, G. 2009. Dynein-driven mitotic spindle positioning restricted to anaphase by She1p inhibition of dynactin recruitment. *Mol Biol Cell* 20, 3003-3011.
- Woodruff, J.B., D.G. Drubin, and G. Barnes. 2010. Mitotic spindle disassembly occurs via distinct subprocesses driven by the anaphase-promoting complex, Aurora B kinase, and kinesin-8. *J Cell Biol*. 191:795-808.
- Wuhr, M., S. Dumont, A.C. Groen, D.J. Needleman, and T.J. Mitchison. 2009. How does a millimeter-sized cell find its center? *Cell Cycle*. 8:1115-21.
- Yeh, E., C. Yang, E. Chin, P. Maddox, E.D. Salmon, D.J. Lew, and K. Bloom. 2000. Dynamic positioning of mitotic spindles in yeast: role of microtubule motors and cortical determinants. *Mol Biol Cell*. 11:3949-61.
- Zimniak, T., K. Stengl, K. Mechtler, and S. Westermann. 2009. Phosphoregulation of the budding yeast EB1 homologue Bim1p by Aurora/Ipl1p. *J Cell Biol*. 186:379-91.